ANTIPROTOZOAL AND ANTIDIABETIC ACTIVITIES OF SECONDARY METABOLITES ISOLATED FROM *Vepris glandulosa*

PRINCE ONYANGO OJUKA

A THESIS SUBMITTED IN PARTIAL FULFILLMENT OF THE REQUIREMENTS FOR THE AWARD OF THE DEGREE OF MASTER OF SCIENCE IN CHEMISTRY OF THE UNIVERSITY OF EMBU

AUGUST, 2024

DECLARATION

This thesis is my original work and has not been presented elsewhere for a degree or any other award.

Signature……. Date……

Prince Onyango Ojuka

Department of Physical Sciences

B523/1410/2020

This thesis has been submitted for examination with our approval as the University Supervisors

Signature……  ……Date……19/08/2024…….

Dr. Mark Kimani

Department of Physical Sciences

University of Embu

Signature……. Date……19/08/2024…….

Dr. James Nyabuga

Department of Biochemistry and Biotechnology

Technical University of Kenya

Signature……  ……. Date……19/08/2024……

Dr. Seth Apollo

Department of Pure and Applied Chemistry

Masinde Muliro University of Science and Technology

DEDICATION

This piece of work is dedicated to my mother, Mrs. Francisca Ojuka, for her prayers, support, and encouragement throughout this journey. My siblings, Nancy, Mouline, Manfred, and Francis, whose unwavering support and motivation have made me reach this far. In loving memory of my late dad, whose wisdom and love continue to inspire me.

ACKOWLEDGEMENT

I am deeply grateful to the Almighty God, whose grace, wisdom, and blessings have guided me throughout this study. I am grateful to the University of Embu, for the scholarship to pursue my MSc studies. I extend my heartfelt appreciation to my supervisors, Dr. Mark Kimani, Dr. James Nyariki, and Dr. Seth Apollo, for their unwavering support and guidance. Their mentorship and encouragement have been instrumental in shaping my academic and professional growth. I would also like to extend my gratitude to the Physical Sciences department, University of Embu academic staff headed by Dr. Simba Nyamato for their insightful comments, encouragement, and assistance in keeping me up-to-date with departmental, school, and Board of Postgraduate Studies requirements, which have greatly supported the execution of this study.

Special thanks are due to Dr. Charles Ochieng of Maseno University, Department of Chemistry, for his assistance in carrying out the alpha-amylase bioactivity assay, and to Mr. Patrick Mutiso (Taxonomist) of the University of Nairobi, School of Biological Sciences, for authenticating the plant material and processing the voucher specimen. I also extend my gratitude to Mr. Justus Mukavi, University of Münster, Germany, for his help with NMR and MS analyses. I would like to acknowledge the Institute of Pharmaceutical Biology and Phytochemistry, Münster, Germany, for conducting the NMR and MS experiments, and express my gratitude to Mr. Ndarawit Wilberforce for his assistance with the molecular docking studies. I am grateful to Mr. Simon Mkono, University of Embu lab technician, for his technical expertise and assistance during the early stages of this study.

I am deeply grateful to my classmates for their intellectual exchange and collaborative efforts. Their diverse perspectives and collective wisdom have enriched my understanding and contributed to the success of this work. I am grateful to my family for their unwavering support and encouragement during my study period. Without you, it would not have been possible to accomplish this work. Finally, I extend my gratitude to Maurine Kemuma, Paul Were, Caroline Chepkemoi, and all my friends. Your diligent work behind the scenes has been indispensable to the progress and completion of this study.

TABLE OF CONTENTS

LIST OF TABLES

LIST OF FIGURES

LIST OF APPENDICES

ABBREVIATIONS/SYMBOLS AND ACRONYM

^{13}C NMR	Carbon 13 Nuclear Magnetic Resonance
^{1}H NMR	Proton Nuclear Magnetic Resonance
ACTs	Artemisinin-base Combination Therapies
ADME	Absorption, Distribution, Metabolism, and Excretion
ADMET	Absorption, Distribution, Metabolism, Excretion, and Toxicity
AIDS	Acquired Immune Deficiency Syndrome
ARG	Arginine
ASN	Asparagine
ASP	Aspartic acid
BBB	Blood-brain barrier
BOILED-Egg	Brain-Or-Intestinal Estimated Permeation
CC	Column Chromatography
CD	Chagas disease
Cpd	Compound
CNS	Central nervous system
COSY	Correlated Spectroscopy
CYP	Cytochrome
CYS	Cystein
DM	Diabetes Mellitus
DNA	Deoxyribonucleic Acid
EtOAc	Ethyl acetate
FDA	Food and Drug Administration
Fsp^3	Proportion of hybridized sp3 carbon atoms
GI	Gastrointestinal
GLY	Glycine

HAT	Human African Trypanosomiasis
hERG	human Ether-à-go-go-Related Gene
HIV	Human Immunodeficiency Virus
HMBC	Heteronuclear Multiple Bond correlation
HPLC	High-Performance Liquid Chromatography
HRESI-MS	High-Resolution Electrospray Ionization Mass Spectrometry.
HSQC	Heteronuclear Single Quantum Correlation
IC50	50% inhibitory concentration
IUCN	International Union for Conservation of Nature
ID	Identification
J	Coupling constant
kcal/mol	Kilocalories per mole
L.d	*Leishmania donovani*
LEU	Leucine
Lm	Leishmaniasis
log $P_{o/w}$	N-octanol/water partition coefficient
LYS	Lysine
MeOH	Methanol
MET	Methionine
MHz	Mega Hertz
MOE	Molecular Operating Environment
MS	Mass Spectrometry
NGOs	Non-governmental organizations
NMR	Nuclear Magnetic Resonance
NOESY	Nuclear Overhauser Effect Spectroscopy

NTDs	Neglected Tropical Diseases
NTPDs	Neglected Tropical Protozoan Diseases
PAINS	Pan Assay Interference Compounds
PDB	Protein Data Bank
Pf	*Plasmodium falciparum*
*Pf*LDH	*Plasmodium falciparum* lactate dehydrogenase
P-gp	P-glycoprotein
PRO	Proline
RMSD	Root mean square deviation
RNA	Ribonucleic Acid
RPM	Revolutions Per Minute
SA	Synthetic accessibility
SER	Serine
SMILES	Simplified Molecular Input Line Entry System
SP	Sulfadoxine-pyrimethamine
T2DM	Type two Diabetes Mellitus
Tbg	*Trypanosoma brucei gambience*
Tbr	*Trypanosoma brucei rhodesiense*
T.cruzi	*Trypanosoma cruzi*
THR	Threonine
TLC	Thin Layer Chromatography
TPSA	Topological polar surface area
USA	United States of America
UV	Ultra Violet
WHO	World Health Organization

ABSTRACT

Protozoal infections, particularly malaria and neglected tropical diseases like kinetoplastid diseases affect impoverished populations in tropical regions. Similarly, diabetes mellitus is among the leading cause of global death and disability, with a significant ramification on the global economy. Amidst the diminishing effectiveness of existing treatments, the search for novel antiprotozoal and antidiabetic drugs is imperative. Plants have long been recognized as promising sources of bioactive compounds with therapeutic potential. Thus, researchers prioritize medicinal plants as critical targets for discovering novel therapeutic agents. This necessity prompted the search for the potent antiprotozoal and antidiabetic drugs from unexploited plant sources, such as *Vepris glandulosa. V. glandulosa* is endangered plant species, endemic in central Kenya. It has been utilized in folklore medicine to cure various conditions. In this study, the dried leaves of *V. glandulosa* were pulverized into a fine powder and extracted with methanol at room temperature by cold solvent percolation. Separation techniques involved liquid-liquid partitioning followed by column chromatography on silica gel as a stationary matrix, employing gradients of n-hexane and ethyl acetate for elution. The resulting fractions were further purified using finer silica gel through recurrent column chromatography, leading to the isolation of two known alkaloids: Choisyine acetate **29** and Choisyine **30**. Their structure elucidation involved a detailed analysis using Nuclear Magnetic Resonance, Mass Spectrometry and a comparison with related compounds in the existing literature. Both *in vitro* and *in silico* assays were utilized to assess the activity and toxicity of the isolated compounds. The α-amylase inhibition assay revealed noncompetitive inhibition for both compounds with IC_{50} and K_i values of 4.74±0.17 and 4.75 mM for compound **29**, and 11.29±0.44 and 12.37 mM for compound **30**, respectively. In comparison, the standard drug acarbose displayed a competitive mode of inhibition, with IC_{50} and K_i values of 11.985±0.02 and 2.24 mM. Docking scores (kcal/mol) demonstrated significant interactions with the target proteins. Compound **29** revealed a binding score of -6.42 and -6.17 while compound **30** had -6.07 and -5.38 whereas acarbose, the standard drug showed -8.03 and -8.49 for α-amylase and glucosidase, respectively. For *P. falciparum* lactate dehydrogenase (*P. falciparum*), compound **29** showed a score of -7.10, and compound **30** scored -7.20, while the standard drug chloroquine scored -6.88. In the case of dihydroorotate dehydrogenase (*L. donovani*), compound **29** had a score of -7.19, compound **30** scored -7.09, and standard drug miltefosine scored -8.01. Trypanothione reductase (*T. cruzi*), compound **29** showed a score of -8.19, compound **30** scored -7.81, and the standard drug melarsoprol, scored -6.24. For L-threonine-3-dehydrogenase (*T. brucei*), compound **29** had a score of -6.31, compound **30** scored -6.97, and the standard drug benznidazole scored -7.33. These compounds demonstrated remarkable inhibition potential comparable to, and even greater than some currently available drugs, highlighting their potential as viable alternatives in the fight against these diseases. Their physicochemical properties, pharmacokinetics and lead-likeness further justify their potential as lead candidates in drug research. Synthetic accessibility, Pan Assay Interference Structures, Brenk alerts and toxicity evaluation revealed their ease of synthesis, lack of undesirable features and low toxicity profile. The findings from this study also revealed that *V. glandulosa* contains alkaloids with the potential to inhibit diabetes and protozoa-associated biomarkers, thereby providing a scientific rationale for using the plant in Kenyan folk medicine as treatment for various health issues.

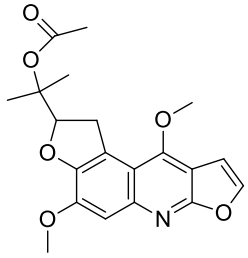

Compound **29**

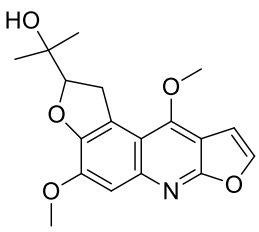

Compound **30**

CHAPTER ONE

INTRODUCTION

1.1: Background Information

The treatment of protozoal diseases such as neglected topical diseases (NTDs) and malaria as well as diabetes, a lifestyle disease, is increasingly becoming complex worldwide. NTDs are infectious diseases that mainly impact people in tropical/subtropical regions globally (Hotez et al., 2020). They are termed as "neglected" because they primarily afflict marginalized and impoverished communities. Despite their significant impact on public health and socioeconomic development, NTDs have historically received relatively little attention and funding compared to other diseases (Engels & Zhou, 2020). These diseases include various forms of cutaneous and visceral leishmaniasis, African trypanosomiasis, and Chagas disease (kinetoplastid diseases) which threaten nearly one-sixth of the global population (Capela et al., 2019). They are dangerous to human health in 149 low-income nations in tropical regions of Asia, South America, and Africa especially war-torn regions like Congo and for which new drugs are desperately required (WHO, 2010). Although these diseases predominantly affect tropical/subtropical regions, ecological and environmental modification due to natural phenomena and anthropogenic activities are increasingly influencing the onset and spread of these diseases in high-income nations (Ehrenberg *et al*., 2020; Montesino & Schmidt, 2018; WHO, 2010).

Several factors contribute to the neglect of tropical diseases. These include their association with poverty, which often results in marginalized communities lacking access to basic healthcare services and preventive measures (Hotez et al., 2020). Additionally, many NTDs primarily affect populations in remote and rural areas, making them less visible on the global health agenda. Furthermore, insufficient potent diagnostic tools, vaccines, and cost-effective treatments for many NTDs has hindered efforts to control and eliminate these diseases (Engels & Zhou, 2020). Recently, there has been growing recognition of the importance of addressing neglected tropical diseases. Global health initiatives, such as the World Health Organization's NTDs Roadmap, has aimed to raise awareness, mobilize resources, and coordinate efforts to mitigate and eliminate NTDs (Forbes et al., 2023). These initiatives have led to

significant progress in lessening the implication of several neglected diseases through mass drug administration, and improved access to healthcare services. Despite these advances, challenges remain in achieving the goals of controlling and eliminating neglected tropical diseases (Forbes et al., 2023).

Malaria, albeit not presently mentioned by the WHO list as a neglected tropical disease is included in this study due to the elevated infections cases and deaths it elicits annually attributable to the multi-drug resistance of *Plasmodium* species (Montesino *et al*., 2015). It has high mortality and morbidity throughout the globe affecting millions annually (Bello *et al*., 2017). Based on 2023 World Malaria Report by WHO, an estimated 249 million malaria cases were reported in 85 malaria-endemic nations in 2022, (Venkatesan, 2024). The majority of cases (around 95%) were reported in the Africa, with Congo, Mozambique, Nigeria and Uganda accounting nearly half of all cases (Venkatesan, 2024). The limitations of the existing anti-malarial drugs such as low efficacy, lethal toxicity, high cost as well as drug resistance associated with Kelch-13 genes have necessitated the continual hunt for safer and more effective antimalarial drugs (Al-Musayeib *et al*., 2012).

Diabetes mellitus (DM), a lifestyle disease, is also included in this study due to elevated levels of mortality and morbidity on a global scale. The prevalence of diabetes globally in 2021 was 537 million. Adults aged 20 to 79 are presently diabetic, equating to approximately 1 in every 10 individuals (Dysted et al., 2021). Projections indicate a steady increase in these numbers, with an estimated escalation to 643 million by 2030 and a staggering 783 million by 2045 (Dysted et al., 2021).

The use of plants in traditional therapeutics for preventing and managing various diseases has a long history (Mahmoud, 2020). Medicinal plants are rich in bioactive molecules, several of which have been utilized as drugs or as precursors for synthetic analogues with enhanced bioactivity (Malebo et al., 2013). Specifically, in Kenya, diverse communities turn to herbal remedies to address a range of illnesses, including protozoal diseases and diabetes, due to challenges in accessing or affording pharmaceutical treatments (Muthee et al., 2011). The use of indigenous plants' metabolites for drug development against infections is thus a well-known technique in medicine (Torres *et al*., 2014). *V. glandulosa* is among 80 species that belong to the genus *Vepris* whose various parts are applied in many African folk medicines in the

treatment of gonorrhea, they are also used as an analgesic and antipyretic (Kamatenesi-Mugisha et al., 2007). Most species in *Vepris* genus have been documented to contain bioactive compounds (cpd), for instance, *Vepris nobilis* was documented to contain anti-inflammatory activity (Omujal et al., 2020), antimicrobial (Al-Rehaily, 2001), anti-malarial in its leaves and fruits (Magadula & Erasto, 2009), anti-leishmanial and anti-trypanosomal activity in its fruits and leaves (Lacroix et al., 2012). Additionally, Kiplimo (2012) reported the diverse biological activities exhibited by several *Vepris* species native to Kenya.

Vepris glandulosa has been traditionally used as a potential medicine to cure several conditions without scientific evidence that might perhaps justify its application (Kokwaro, 1978). Despite the availability of medicinal plants like *V. glandulosa*, there is a scarcity of scientific studies documenting their usage in folk medicine. Consequently, there is insufficient established knowledge regarding its potency and safety profiles. *V. glandulosa* is believed to contain novel bioactive compounds as well as phytochemicals in its leaf and bark owing to its wide use with its antiprotozoal and antidiabetic activities overlooked. This study isolated pure compounds from the leaves of *V. glandulosa* and assessed their antiprotozoal and antidiabetic properties.

1.2: Statement of the Problem

The detrimental effects of protozoal diseases and diabetes are rising and have been intensified by inadequate drugs due to the development of resistance and lethal toxicity of present antiprotozoal and antidiabetic drugs (Agents et al., 2019; Misra et al., 2019). NTDs, malaria and diabetes have high morbidity and mortality rates, impacting approximately 2.7 billion impoverished individuals globally and costing emerging economies billions of dollars annually (Artasensi et al., 2020; Engels & Zhou, 2020; Hotez et al., 2020). Notwithstanding the positive attributes of presently accessible therapies over the years, challenges such as poor absorption, resistance, ineffectiveness, toxicity, and lengthy treatment duration persist, necessitating the discovery of new drugs (Tiwari et al., 2018). This has paralyzed the ability of some of the medications to treat these protozoal diseases since pathogens continue to mutate resulting in new strains resistant to existing antiprotozoal drugs; what doesn't kill you mutates and tries again! Additionally, the currently used antidiabetic drugs have drastically lost their therapeutic activities (Cowie et al., 2018; Montesino & Schmidt,

2018). Natural products especially from medicinal plants, historically served as the foundation of drug discovery. However, the evolution of multidrug-resistance continue to jeopardize their effectiveness and thus there is a necessity to develop a new antiprotozoal (Montesino et al., 2015). The fundamental aspect of this study is to elucidate the active compounds present in *V. glandulosa*, which has demonstrated effectiveness in traditional medicine but lacks comprehensive knowledge of its active ingredients. Thus, this study seeks to bridge this gap by isolating and characterizing the secondary metabolites of *V. glandulosa* with potential antiprotozoal and antidiabetic properties, contributing to the development of novel therapeutic interventions against herein mentioned diseases.

1.3: Justification of the Study

Plants have long been recognized as promising sources of bioactive compounds with therapeutic potential. Scientific investigations into various species of the genus *Vepris* have revealed their notable antiprotozoal and antidiabetic activities (Garcia et al., 2017). Recent studies by Ojuka et al. (2023) further support the exploration of *Vepris* genus as potential candidates for drug discovery. Despite this promising evidence, metabolites derived from *V. glandulosa*, which could hold significant antiprotozoal and antidiabetic properties, remain largely unexplored. This study aims not only to fill this gap but also to provide direct benefits to society by offering a cost-effective treatment alternative for populations facing economic hardship. Additionally, the investigation contributes to improving the understanding and quality of traditional medicine by scientifically validating the medicinal use of *V. glandulosa* in Kenyan folk medicine. Furthermore, the discovery of antiprotozoal and antidiabetic compounds from *V. glandulosa* would enhance the prospects of self-medication, particularly in remote or inaccessible areas where access to healthcare facilities is limited. Therefore, a phytochemical inquiry of *V. glandulosa* with the target of isolating and characterizing antiprotozoal and antidiabetic compounds to further justify the genus conservation and its application in disease treatment has been pursued. The antiprotozoal and antidiabetic compounds will contribute to the development of novel therapeutic interventions against protozoal infections and diabetes.

1.4: Null Hypotheses

1. Secondary metabolites from *V. glandulosa* cannot be isolated and characterized through classical means.
2. *Vepris glandulosa* secondary metabolites do not exhibit *in silico* antiprotozoal activities.
3. *Vepris glandulosa* secondary metabolites do not exhibit significant antidiabetic activities.
4. *Vepris glandulosa* secondary metabolites do not exhibit favorable physicochemical and ADMET properties.

1.5: Objectives

1.5.1: General Objectives

To investigate the antiprotozoal and antidiabetic activities of secondary metabolites isolated from *V. glandulosa*

1.5.2: Specific Objectives

1. To isolate and characterize secondary metabolites from *V. glandulosa*.
2. To determine *in silico* antiprotozoal activities of *V. glandulosa* secondary metabolites.
3. To determine *in silico* and *in vitro* antidiabetic activities of *V. glandulosa* secondary metabolites.
4. To determine *in silico* physicochemical and ADMET properties of *V. glandulosa* secondary metabolites.

CHAPTER TWO

LITERATURE REVIEW

2.1: Parasitic Protozoan Diseases

The protozoan diseases are a global clinical concern and a world challenge since they are dangerous to human health with over a million fatalities yearly (Lozano et al., 2012). Such diseases jeopardize the health of millions of individuals globally and are linked with massive morbidity and huge influence on the economy (Fletcher et al., 2012; WHO, 2010). Even though it is obvious that the protozoan diseases significance is more acute in (sub)tropics globally, most temperate regions of the world such as North America as well as the Asian Pacific region are also at risk of being impacted by protozoan diseases (Andrews et al., 2014). The notable consequences of protozoan diseases have been worsened by inadequate licensed vaccines (Andrews et al., 2014). Therapy, in addition to prophylaxis, has consequently relied on drugs, which have become less effective due to resistance, compelling the search for replacements (Nagle et al., 2014). The most common human infections caused by protozoan parasites include, but are not limited to malaria and, kinetoplastid diseases (such as African trypanosomiasis, Leishmaniasis and, Chagas disease) (Andrews et al., 2014).

2.1.1: Human African Trypanosomiasis (HAT)

It is a NTD that is responsible for disastrous epidemics in the 20th century (Franco et al., 2020). It is caused by the genus Trypanosoma parasites and it is a fatal illness threatening the lives of millions of people, especially in Africa (Montesino & Schmidt, 2018). It is caused by parasites; Trypanosoma brucei rhodesiense (Tbr) which is a zoonotic and mainly exist in East and Central Africa (Tempone et al., 2021) and Trypanosoma brucei gambience (Tbg) which is anthroponotic and dispersed in West and Central Africa) (Tempone et al., 2021). These species are conveyed by tsetse fly. The aforementioned two parasites are etiological agents of HAT that are endemic in sub-Saharan countries (Franco et al., 2020), with its global consequence estimated at 0.3 million annually. Another species of Trypanosoma is Trypanosoma brucei brucei which is responsible for livestock diseases; Nagana (Torres et al., 2014) which results in huge economic losses in the affected countries (Alsan, 2015). The presently accessible diagnostic tests, and treatment of trypanosomiasis, require skilled personnel and mostly hospitalization which cannot be accessed by many affected individuals

living in remote areas (Aksoy et al., 2017). In addition, the currently used drugs have serious side effects, thus new effective and cheap treatment of HAT is urgently required (Franco et al., 2020). The progressive campaign championed by World Health Organization (WHO), Non-Governmental Organizations (NGOs) as well as public and private partnerships to combat HAT, distributed drugs in the affected countries and brought about a massive decline in the worldwide HAT prevalence to below 3000 cases by 2015 (Aksoy et al., 2017). Despite vast studies into trypanosome biology, the toolbox for diagnosis and the therapy of HAT is negligible and marred with difficulty (Franco et al., 2020). The therapy of HAT varies depending on the phase of the illness and the specific species of parasite causing the infection. Several drugs have traditionally been employed for treatment, including suramin, melarsoprol, fexinidazole, nifurtimox, eflornithine, and pentamidine (Capela et al., 2019). However, these medications are associated with limited efficacy, adverse side effects, toxicity and challenges in availability, highlighting the urgent need for research and development aimed at discovering new and improved treatments for African trypanosomiasis (Tempone et al., 2021). Research efforts are focused on developing safer and more potent drugs with little side effects and broader activity against different strains of the parasite. Additionally, strategies for disease prevention, vector control, and improved healthcare infrastructure are essential for the control and elimination of HAT.

2.1.2: Leishmaniasis

Leishmaniasis is a complex infection of tropical regions worldwide (Ponte-Sucre *et al*., 2017) caused by 20 species of genus *Leishmania* conveyed by sandflies. WHO considers leishmaniasis as one of the worldwide causes of death by infectious diseases (Alemayehu & Alemayehu, 2017). It is manifested in two forms, cutaneous (most common) and visceral leishmaniasis which is the most fatal with 1.3 million cases yearly leading to 20,000-30,000 deaths (Lenk *et al*., 2018; Montesino *et al*., 2015). It is also approximated that there were 50,000-90,000 cases in 2019 and was heavily skewed toward adult males (Dahal *et al*., 2021). Despite the improvement in terms of diagnostic programs and a reduction in treatment prices, mortality, and morbidity due to leishmaniasis, is still a recognized health concern (Montesino & Schmidt, 2018). Insufficient vaccine against *Leishmania* and escalated resistance of the pathogens to

present drugs necessitates the urgent search and discovery of new treatment. Medicinal plants have been scientifically explored as potential antileishmanial, even so, none of the scrutinized compounds appear to have been made to a clinical investigation (Singh *et al*., 2014). *Leishmania* also appears as an opportunistic parasite in immunosuppressed individuals (Ponte-Sucre *et al*., 2017) for instance, it has been documented that HIV/AIDS has significantly led to escalated cases of leishmaniasis in the endemic regions (Lindoso *et al*., 2014). The present-day therapy for leishmaniasis is chemotherapy; nonetheless, it has various challenges like toxicity, low efficacy in endemic areas and drug misuse (Torres *et al*., 2014). Despite the attempts to get new therapies against leishmaniasis, the therapy of leishmaniasis remains the use of sodium stibogluconate and meglumine antimoniate (pentavalent antimonial) (Ponte-Sucre *et al*., 2017) which were discovered 60 years ago and have various side effects like diarrhea, nausea, cardiotoxicity as well as skin rashes (Bello et al., 2017). Moreover, resistance to these drugs is still a 21st-century challenge (Ponte-Sucre *et al*., 2017; Fletcher *et al*., 2012) and is linked with elevated death rates particularly in HIV co-infected patients (Torres *et al*., 2014). Therefore, the development of a new drug from secondary metabolites of *V. glandulosa* becomes a necessity.

2.1.3: Malaria

Amidst protozoal infections, malaria has encountered the most scientific research-based attention owing to the widespread complexion and devastating consequences on human (Tempone et al., 2021). Although malaria is not among the WHO list of NTDs, it is a neglected infection in most areas of the globe, in which individuals live in malaria penetrated areas and poor socio-economic environment with limited access to health services and sufficient medication (Montesino et al., 2015). Malaria is a global health issue with about 3 billion individuals in 97 countries at peril (World malaria report 2019, 2019). Currently, it has an approximated 249 million people affected and an estimated 600,000 deaths annually. Shockingly, 78% of these deaths happen in children below the age of five (Venkatesan, 2024). Despite its existence in the tropics, the clinical consequence is enormous with the bulk of the global parasitized people in Asia and 90% of demise happen in Africa, mainly in children (World malaria report 2019, 2019). Treated insecticide net, timely diagnosis, and artemisinin-base

combination therapies (ACTs), as well as chemo-prevention, are the main strategies to control malarial infection (Ashley & Phyo, 2018).

Recently, there have been prolonged calls for controlling and eventual elimination of malaria, as a result, the malaria vaccine (RTS, S/AS01) received indisputable acclamation, however, it was associated with various challenges especially drug resistance (Chaniad et al., 2021). The application of ACTs as an antimalarial drug dates back to the early 1900s when the malaria infection in Asia was worst; chloroquine, sulfadoxine-pyrimethamine (SP), and mefloquine had been availed consecutively but had perished to drug resistance (Ashley & Phyo, 2018) which necessitated the such for effective antimalarial drugs. The drug resistance that was observed in chloroquine and pyrimethamine in the early 1960s (Verlinden et al., 2016) triggered antimalarial drug search and development, with main enterprise in the USA (leading to mefloquine) and China (yielding artemisinin) (Verlinden et al., 2016). Previous research has documented the promising anti-malarial potential of certain medicinal plants. For instance, quinine derived from the Cinchona plant and artemisinin extracted from Artemisia annua have been highlighted for their efficacy in combating malaria (Tagboto & Townson, 2001). However, these drugs have limitations, and a majority have succumbed to drug resistance, necessitating the hunt for new antimalarial drugs.

Chloroquine and pyrimethamine resistance spread to Africa resulting in an elevated number in children mortality (Snow et al., 2001). This calamity renewed the force to control malaria and huge financial resources were availed. There was also a realization that advanced therapies were required as well as innovative perspective was desperately needed to stimulate drug development (Ashley & Phyo, 2018). This initiative led to the discovery of a new medicine artemether-lumefantrine (Coartem Novartis) approved by the USA FDA (Premji, 2009), nevertheless, there are increased reports of resistance of Plasmodium species to this drug (Price et al., 2014) necessitating further hunt for new effective drugs. Various supplementary drugs have been assessed and made available but have fallen to resistance and proved ineffective (John et al., 2010) . Thus, malaria cases and related demises have more than doubled in the past 15 years and the aim of global eradication is being targeted (Ashley & Phyo, 2018; World malaria report 2019, 2019). Hence there is a necessity to discover a new drug to combat malarial infection.

2.1.4: Chagas Disease (CD)

This is a protozoan infection that is most common in Latin America thus also known as Human America Trypanosomiasis (Gascon *et al*., 2010). CD is a serious global clinical concern and a new world challenge and due to migration, it is an appearing infection in formerly non-endemic states (Pérez-Molina & Molina, 2018; Coura & Viñas, 2010; Gascon *et al*., 2010). It is caused by *Trypanosoma cruzi* (Wang *et al*., 2021) which is both zoonotic and anthroponotic (Tempone *et al*., 2021). Chagas disease exhibit as the first acute phase which is transmitted orally (Prata A., 2001) and then accompanied by the chronic stage. Currently, there are no vaccines for Chagas disease, however, the two available therapeutics benznidazole together with nifurtimox are used to treat the disease (Andrews *et al*., 2014). The disease affects the lives of millions of individuals in Mexico, Latin America and the USA (Pinazo *et al*., 2013).

Approximately 8 to 10 million people are infected annually (WHO, 2010). These therapies are effective if given immediately upon infection, however, there are incidences of treatment failure (Muñoz-Calderón *et al*., 2013; Pinto *et al*., 2013) as well as resistant parasites (Mougabure-Cueto & Picollo, 2015). Furthermore, the two drugs have adverse side effects in many patients especially in expectant women (Jackson *et al*., 2010). Due to the above-mentioned limitations of current therapies as well as the deficiency of the current therapy alternatives, there is an urgent necessity for drug development research.

2.2: Antiprotozoal Resistance

Protozoal infections refer to illnesses caused by single-celled microorganisms known as protozoa (Chanda, 2021). Protozoans are microscopic, unicellular eukaryotic organisms that are either free-living or parasitic. They normally multiply in humans with enhanced survival within the host, which results in exacerbation in the pathogenicity (Bello *et al*., 2017). Numerous species of protozoa have been identified, most of which are free-living organisms. These protozoa have internal structures and conduct complex metabolic processes (Capela et al., 2019). Their developmental stages typically include feeding trophozoites, which can be either intracellular or extracellular (Siciliano & Alano, 2015). Conveyance methods among hosts include direct contact, fecal-oral routes, vector-borne transmission, and predator-prey

interactions. Protozoa also have dormant cyst stages that allow them to endure harsh conditions devoid of oxygen, water, or nutrients for extended periods (Antonovics et al., 2017). The armamentarium of antiprotozoal therapies is not extensive, and their potency is increasingly compromised by the evolution of resistance. Notable example is the widespread resistance to chloroquine in malaria (Capela et al., 2019).

The rise and proliferation of drug resistance and the absence of effective vaccines present significant challenges in controlling protozoan infections. In addition, most research on drug resistance in protozoa has been carried out on laboratory strains under circumstances that do not mirror the usual parasite-host interaction (Monzote & Siddiq, 2011). The necessity for advanced antiprotozoal drugs triggers a global investigation and needs an innovative approach to a viable invention and development of novel compounds. To curb this threatening menace, innovative ways to come up with antiprotozoals that are more active need to be proposed.

2.3: Diabetes mellitus (DM)

DM is a complex metabolic condition marked by abnormal levels of glucose in the bloodstream, known as hyperglycemia, which is linked to increased rates of mortality and morbidity globally (Artasensi et al., 2020). The report by the International Diabetes Federation (IDF) highlights that more than 537 million adults are currently diabetic; thus, out of every ten persons, one is a diabetic. Statistical projections predict that these numbers will continue to rise, with an anticipated elevation to 643 million by 2030 and 783 million in 2045. The prevalence is unevenly distributed: a majority of diabetic individuals live in low- and middle-income countries (Dysted et al., 2021).

In terms of mortality, diabetes was found to contribute notably to 6% of global mortality. It is estimated that there were 7 million deaths in 2021 alone, equivalent to one demise in every five seconds (Dysted et al., 2021). Furthermore, the economic impact of diabetes cannot be overlooked as it accounted for at least USD 966 billion in health costs in 2021, which is nearly 316% higher than in the last 15 years (Dysted et al., 2021). In addition, 541 million individuals are diagnosed with Impaired Glucose Tolerance (IGT), which makes them highly prone to developing Type 2 Diabetes Mellitus (T2DM). These statistics emphasize the necessity of developing integrated approaches toward preventing and managing diabetes and its socioeconomic

implications for healthcare systems worldwide (Suryasa et al., 2021). This condition's development stems from several reasons, such as impaired insulin release, insulin resistance, or a combination of both processes (Cowie et al., 2018). These factors may be triggered by several environmental and genetic conditions, including lifestyle changes, age, predisposition, and familial diabetes history (Tomic et al., 2022). Although the search for universal pharmacologic therapy remains ongoing, there have been considerable efforts in managing patients with DM through effective glycemic control and prevention of associated complications (Kimani et al., 2023). These strategies include the use of insulin and various classes of antidiabetic drugs. These work by different mechanisms, such as enhancing insulin secretion, boosting insulin sensitivity, reducing insulin resistance, or inhibiting intestinal glucose absorption (Galicia-Garcia et al., 2020).

Nevertheless, some of these drugs, primarily those that act on glucose absorption like miglitol and acarbose, are associated with gastrointestinal side effects, including diarrhea and bloating, due to their effects on various glucosidases (Kimani et al., 2023). Despite these challenges, metformin is an ideal and promising drug for DM management; although, caution is warranted for patients with kidney and liver damage (Suryasa et al., 2021). Due to the side effects of currently available drugs, researchers are keen on exploring natural and plant-based sources of α-glucosidase and α-amylase inhibitors that possess significant therapeutic benefits (Kumar et al., 2020). Herbal medicines and natural products have been used for years mainly due to their safety, accessibility, and potentially fewer side effects than synthetic drugs. This has led to an increased focus on phytotherapy as plants are promising as potential therapeutics for DM (Kimani et al., 2023). Nevertheless, discovering new natural products with therapeutic properties to control T2DM is a relatively complicated exercise due to insufficient structural mechanistic studies in these phytopharmaceuticals (Alam et al., 2014). Bridging this knowledge gap is critical in achieving the full therapeutic roles of natural remedies against DM and improving patient outcomes. This necessity led to the identification of new antidiabetic compounds, which prompted this study.

2.4: Use of Natural Products in Medicine

Natural products have proven to be a rich reservoir of active ingredients for drug discovery (Harvey et al., 2015), with most commercial therapies derived from natural

sources (Al, 2008). These medicinal properties stem from bioactive compounds found within natural products thus, researchers prioritize plant metabolites as critical targets for discovering novel therapeutic agents (Wambua, 2020). Extensive scientific investigations have unveiled active compounds against protozoa and diabetes in medicinal plants worldwide (Harvey et al., 2015; Kimani et al., 2023), renewing interest in traditional medicinal plants for pharmaceutical exploration. Consequently, researchers are isolating new anti-infective agents from various natural sources (Bello et al., 2017). Metabolites, as significant sources of bioactive compounds, hold immense potential for drug discovery. These compounds, residing in medicinal plants traditionally used for centuries to treat various health conditions, have demonstrated efficacy even in the absence of scientific evidence supporting their application (Montesino & Schmidt, 2018).

Previous research has shown that certain medicinal plants hold significant potential in combating infections. For example, quinine extracted from the Cinchona plant, artemisinin sourced from *Artemisia annua*, and emetine obtained from *Psychotria* (*Cephaelis*) have been identified for their promising anti-infective properties (Tagboto & Townson, 2001). Quinine alkaloid **1** (**Figure 2.1**), derived from the cinchona plant, is employed as an ingredient in antimalarial treatments, while ceftriaxone alkaloid **2** (**Figure 2.1**) is used in the treatment of gonorrhea and penicillin **3** (**Figure 2.1**) has been utilized to cure various bacterial infections (Siqueira-Batista et al., 2023).

However, due to continued pathogen mutations, these bioactive compounds are continuously losing activity and are unable to treat diseases anymore hence the need to develop effectively or modify existing drugs to improve their activity. Earlier research has shown that the genus *Vepris* (*Rutacea*) have been traditionally explored to treat pneumonia, eye troubles, malaria and rheumatism (Garcia *et al*., 2017), its species such as *Vepris nobilis* among others have been screened for antileishmanial, antimalarial and antitrypanosomal activities as aforementioned (Ombito et al., 2021).

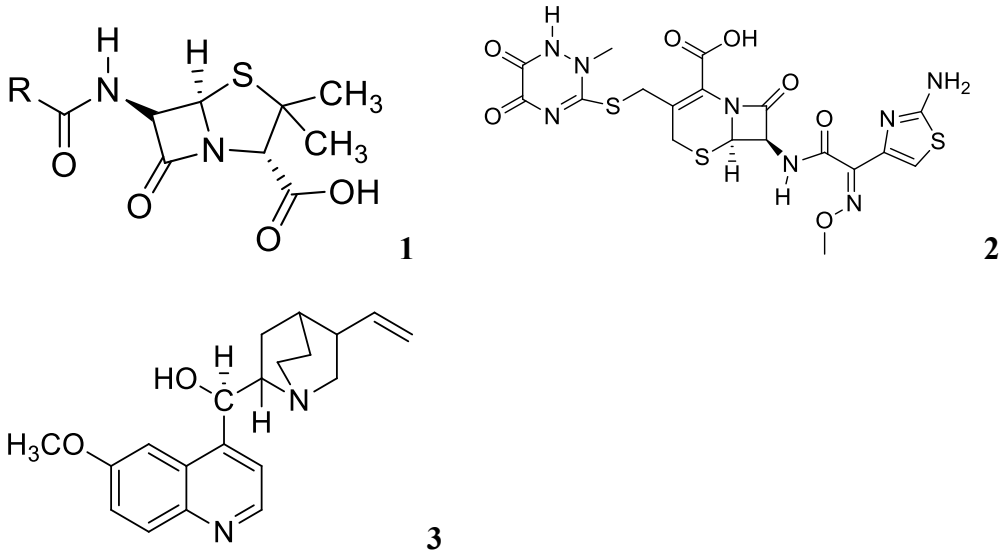

Figure 2.1: Structures of some potent phytochemicals since antiquity

2.4.1: Genus *Vepris*

The genus *Vepris* belongs to the *Rutaceae* family. The *Rutaceae* family comprises about 160 genera and 1730 species, typically categorized within the Sapindales order. They are found in evergreen, dry forests and across tropical regions globally (Wambua, 2020). Recent investigations into Rutaceae plants have unveiled a diverse array of bioactive compounds (Kubitzki et al., 2010). The *Vepris* genus comprises of various species that naturally occur in tropical regions globally (Imbenzi et al., 2014). These plants species were used in traditional pharmacopeia to treat several conditions, including protozoal infections and diabetes (Omujal et al., 2020).

2.4.2: Phytochemistry of the Genus *Vepris*

Genus *Vepris* has an excellent reputation in folklore medicine and has been documented to contain a diverse array of compounds with heightened biological activities (Ojuka et al., 2023; Ombito et al., 2021). These compounds include alkaloids, flavonoids, and limonoids.

2.4.2.1: Alkaloids from the Genus *Vepris*

These are nitrogen-containing compounds characterized as alkaline due to the presence of a nitrogen atom in a heterocyclic ring (Matsuura & Fett-Neto, 2015). Their biological features have garnered interest recently due to their potent anti-infective activities, including the suppression of several human diseases. **Table 2.1** and **Figure 2.2** list some of the alkaloids from the genus *Vepris* that have previously been reported.

Table 2.1: Alkaloids from the genus *Vepris* and their activities

Compounds	Species	Activity	References
Tecleine (**4**)	*V. heterophylla, V. verdoorniana*	Antimicrobial	(Ayafor *et al.*, 1982)
γ-fagarine (**5**)	*V. stolzii, V. renieri*	Antimitotic, antifungal, Antileishmanial	(Yang & Chen, 2008)(Ferreira et al., 2010) (Kouam et al., 2017)
Maculine (**6**)	*V. soyauxii, V. heterophylla, V. nobilis*	Antimicrobial, Antiplasmodial, Antileishmanial	(Kuete et al., 2008) (Wansi et al., 2010) (Wansi et al., 2010) (Lacroix *et al.*, 2012)
Kokusaginine (**7**)	*V. verdoorniana, V. suaveolens*	Antimicrobial, Antioxidant, Antiplasmodial	(Wansi et al., 2013) (Kuete et al., 2008) (Lacroix et al., 2012) (Happi et al., 2012)
Maculosidine (**8**)	*V. renieri, V. uguenensis*	Antiplasmodial	(Khalid & Waterman, 1981) (Cheplogoi et al., 2008)
Oriciacridone A (**9**)	*V. glaberrima*	Antimicrobial	(Wansi et al., 2006)
Xanthoxoline (**10**)	*V. dainellii*	Antiplasmodial,	(Tchinda et al., 2009) (Dagne et al., 1988)

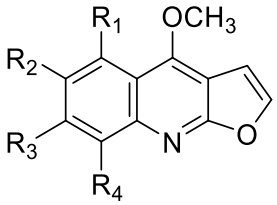

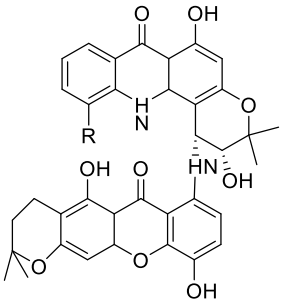

9 R=H

4 R_1 = H, R_2R_3 = OCH_2O, R_4 = OH

5 R_1 = R_2 = R_3 = H, R_4 = OCH_3

6 R_1 = R4 = H, R_2R_3 = OCH_2O

7 $R_1 = R_4 = H$, $R_2 = R_3 = OCH_3$

8 $R_1 = R_3 = H$, $R_2 = R_4 = OCH_3$

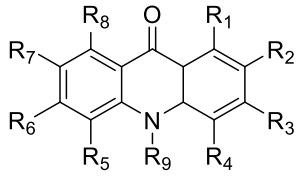

10 R_1=OH, R_2=R_3=OCH_3, R_5 =R_6 =R_7=R_8=R_9=H

Figure 2.2: Alkaloids from the genus *Vepris*

2.4.2.2: Limonoids from the Genus *Vepris*

Limonoids, mostly confined to the Meliaceae (mahogany) and Rutaceae (citrus) families, are highly oxygenated triterpenoid derivatives of limonin (Olatunji et al., 2021). They are produced via the terpenoids biosynthetic route and are stereochemically homogenous molecules with or derivatives from a 4,4,8-trimethyl-17 furanylsteroid backbone (Tan & Luo, 2011). **Table 2.2** and **Figure 2.3** list some limonoids isolated from this genus's species.

Table 2.2: Limonoids from the genus *Vepris* and their activities

Compounds	Species	Activity	References
Limonin (**11**)	*V. grandifolia, V. louisii, V. suaveolens, V. glomerata,*	Antimicrobial, antioxidant	(Ayafor et al., 1981) (Kiplimo *et al.*, 2012)
Oriciopsin (**12**)	*V. glaberrima*	antioxidant	(Ayafor & Okogun, 1982) (Wansi et al., 2006)
Methyl uguenenoate (**13**)	*V. uguenensis,*	Antioxidant, Antiplasmodial	(Cheplogoi et al., 2008)
Limonyl acetate (**14**)	*V. glomerata*	Antioxidant, Antimicrobial	(Kiplimo *et al.*, 2012)
Flindissol (**15**)	*V. tabouensis, V. soyauxii*	Antimicrobial	(Waterman et al., 1978) (Ngadjui et al., 1988) (Happi et al., 2012)

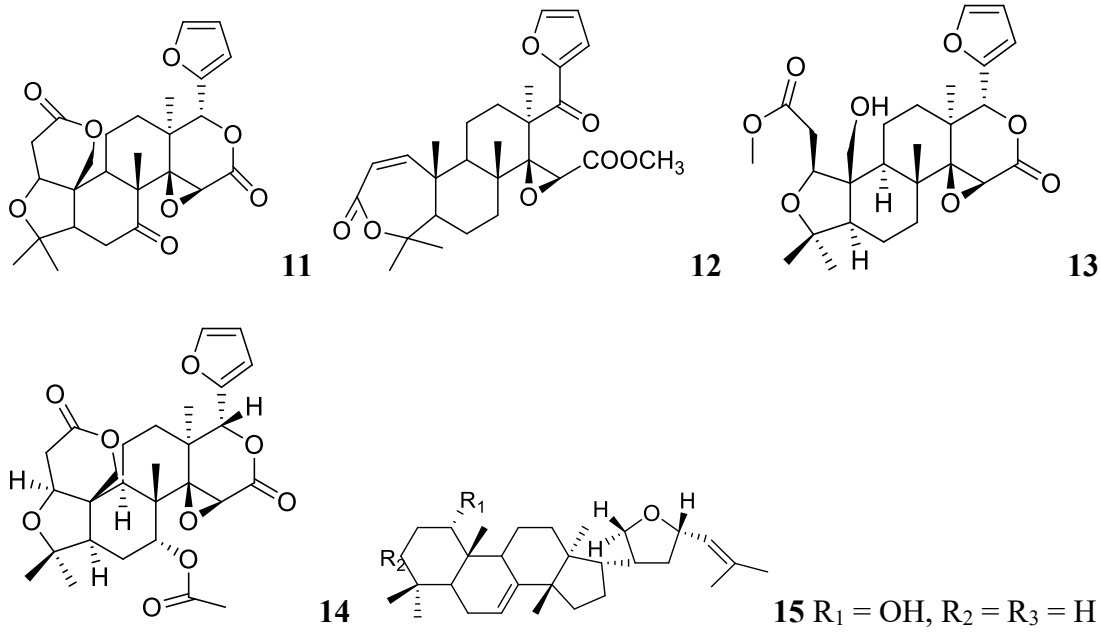

Figure 2.3: Limonoids from the genus *Vepris*

2.4.2.3: Flavonoids from the Genus *Vepris*

Flavonoids are compounds with a polyphenolic structure, known for their antioxidant properties (Rashid et al., 2019). Flavonoids have been studied for their potential health benefits, including anti-inflammatory, anti-cancer, and heart-protective effects (Ombito et al., 2021). **Table 2.3** and **Figure 2.4** below show some of the flavonoids that have previously been isolated from the genus *Vepris*.

Table 2.3: Flavonoids from genus *Vepris* and their activities

Compounds	**Species**	**Activity**	**References**
Veprisinol (**16**)	*V. glomerata*	Antioxidant	(Kiplimo *et al.*, 2011)
Hesperetin (**17**)	*V. glomerata*	Antimicrobial	(Kiplimo *et al.*, 2012)
Uguenenprenol (**18**)	*V. uguenensis*	Antioxidant	(Kiplimo *et al.*, 2012)
7-*O*-methylaromadenrin (**19**)	*V. uguenensis*	Antioxidant	(Kiplimo *et al.*, 2012)
Hesperidin (**20**)	*V. lecomteana, V. soyauxii*	Antimicrobial	(Kouam et al., 2019) (Noulala et al., 2020)

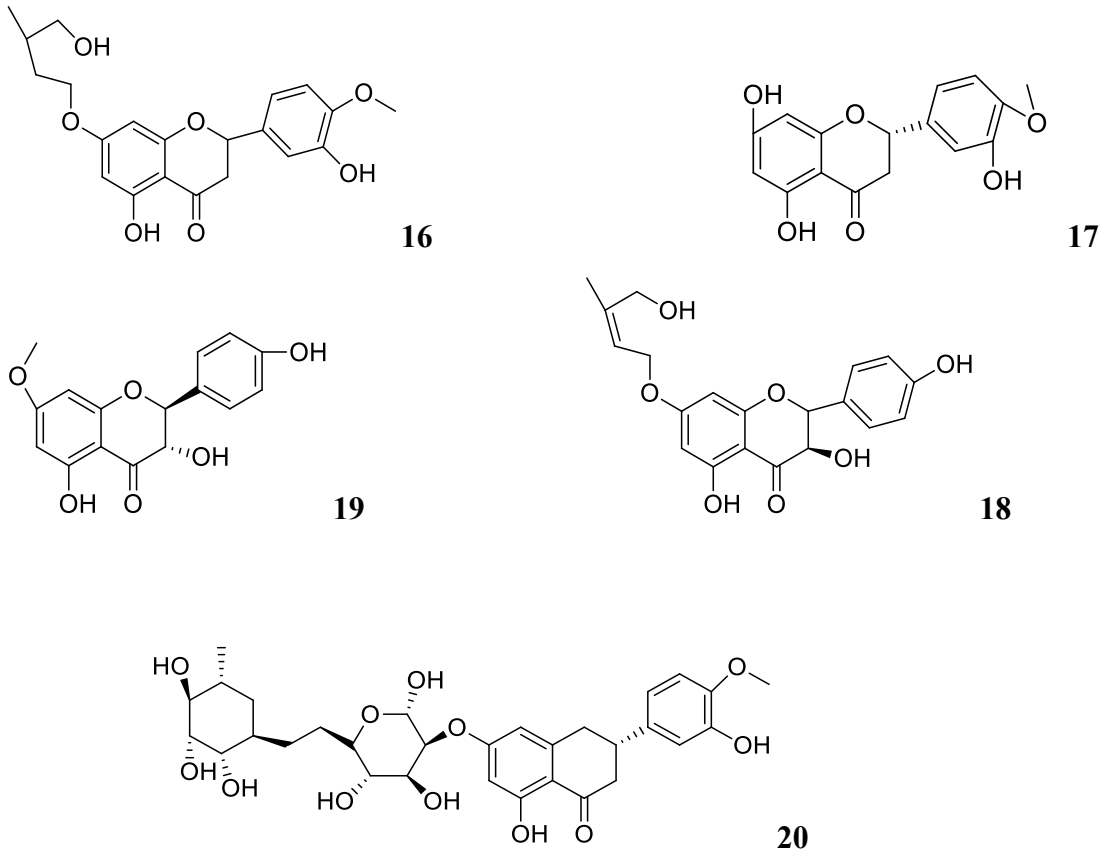

Figure 2.4: Flavonoids from the genus *Vepris*

2.4.2.4: Compounds from Genus *Vepris* with Antiprotozoal and Antidiabetic Properties

Numerous studies have reported anti-plasmodial, anti-kinetoplastid and antidiabetic activities of compounds from this genus (**Table 2.4**; **Figure 2.5**). This suggests that the genus possesses significant pharmacological potential for drug development. Additionally, Ombito et al. (2021) reported on the ethnomedicinal applications, phytochemical composition, and pharmacological properties of the genus *Vepris*, highlighting its richness in bioactive compounds. Furthermore, an *in-silico* assessment of ADMET parameters and drug-likeness of all compounds isolated from the *Vepris* genus from the earliest records up to August 2022, conducted by Ojuka et al. (2023), reveals that the molecules from genus *Vepris* are potential prospects for drug development.

Table 2.4: Antiprotozoal (anti-kinetoplastid and anti-plasmodial) and antidiabetic activities some of the compounds from the genus *Vepris*

Compounds	Species	Activity	References
Arborinine (**21**)	*V. natalensis, V. hiernii, V. suaveolens*	Antiplasmodial, Antitrypanosomal, Antileishmanial	(Muriithi et al., 2002; Ngadjui et al., 1982)
Skimmianine (**22**)	*V. tabouensis, V. soyauxii, V. hererophylla,*	Antiplasmodial Antitrypanosomal, Antileishmanial	(Kiplimo et al., 2011; Kuete et al., 2008; Lacroix et al., 2012; Muriithi et al., 2002; Mwangi et al., 2010)
Melicopicine (**23**)	*V. sclerophylla, V. trichocarpa,*	Antiplasmodial, Antitrypanosomal, Antileishmanial	(Lwande et al., 1983; Muriithi et al., 2002)
Normelicopicine (**24**)	*V. trichocarpa*	Antiplasmodial, Antitrypanosomal, Antileishmanial	(Muriithi et al., 2002)
Tecleoxine (**25**)	*V. nobilis*	Antidiabetic	(Ahmed et al., 2003)
Isotecleoxine (**26**)	*V. nobilis*	Antidiabetic	(Ahmed et al., 2003)
Methylnkolbisine (**27**)	*V. nobilis*	Antidiabetic	(Ahmed et al., 2003)
Atalaphyllidine (**28**)	*V. glaberrima*	Antidiabetic	(Wansi et al., 2006)

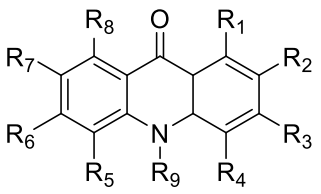

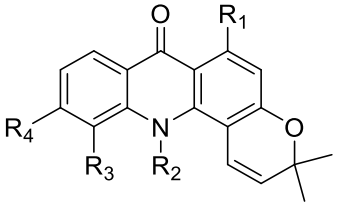

24 $R_1 = R_3 = OH$, $R_2 = R_4 = H$

21 R_1 = OH, R_2 = R_3 = OCH_3, R_4 = R_5 = R_6 = R_7 = R_8 = H, R_9 = CH_3

22 R_1 = R_2 = R_3 = R_4 = OCH_3, R_5 = R_6 = R_7 = R_8 = H, R_9 = CH_3

23 R_1 = OH, R_2 = R_3 = R_4 = OCH_3, R_5 = R_6 = R_7 = R_8 = H, R_9 = CH_3

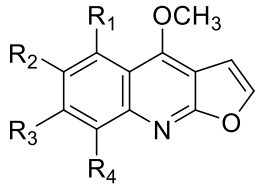

25 R_1 = R_2 = H, R_3 = R_4 = OCH_3

26 R_1 = R_4 = H, R_2 = 2,3-epoxy-3-methylbutyloxy, R_3 = OCH_3

27 R_1 = R_4 = H, R_2 = OCH_3, R_3 = 2,3-epoxy-3-methylbutyloxy

28 R_1 = R_4 = H, R_2 = 2-hydroxy-3-methoxy-3-methylbutyloxy, R_3 = OCH_3

Figure 2.5: Antiprotozoal and antidiabetic compounds from genus *Vepris*

2.4.3: *Vepris glandulosa*

Vepris glandulosa (**Figure 2.6)** belongs to the genus *Vepris* in the Rutacea family (Ngumburu, 2001). It is an endangered plant species that is threatened by habitat loss due to prolonged anthropogenic activities as a source of timber and it is endemic to Central Kenya hence called "Munderendu-itu" in kikuyu language (Division & Division, 1986; Faso et al., 1996). The tree has a very limited distribution, with fewer than 200 mature individuals recorded in 1995, along with a slightly higher number of saplings and coppices (Faso et al., 1996). It is listed as 'Endangered' on the International Union for Conservation of Nature (IUCN) Red List of Threatened Species. It is an unarmed evergreen shrub that grows from 4 to 7 m tall with a smooth grey bark and opposite trifoliate leaves. It thrives well in dry sub-humid as well as semi arid zones with a mean annual rainfall of 970 mm as well as 16^0 C mean monthly temperature (Kokwaro, 1978). Notwithstanding the ubiquitous existence of *V. glandulosa* universally, a little (if any) documentation and scientific research has been done with its antiprotozoal and antidiabetic activities disregarded. Thus, owing to its successful traditional use, it is believed to contain immense antiprotozoal and antidiabetic activities. Even so, such empirical knowledge needs to be backed up by scientific validation. However, there is limited information that explains *V. glandulosa*

secondary metabolites as an antiprotozoal and antidiabetic agent. Therefore, there is a necessity to screen its secondary metabolites for their potential antiprotozoal and antidiabetic activities, which served as the prerequisite for conducting this study.

(Photo taken by J. O. Kokwaro) (Kokwaro, 1978)

Figure 2.6: A photo of *Vepris glandulosa*

2.4.3.1: Ethnomedicinal uses of *Vepris glandulosa*

The leaves, stem and root bark of *V. glandulosa* has been used in traditional pharmacopeia as a potential medicine in management of various conditions. In Central Kenya, this plant species is used in alleviating symptoms like fever, headache, and stomach ailments (Division & Division, 1986). Additionally, it serves as both an antiseptic and a diuretic. Historical records indicate its application in treating various skin conditions, wounds, and ulcers among the Kikuyu community in Kenya (Kokwaro, 1978). Despite the reliance on *V. glandulosa* in folklore medicine, this plant has surprisingly not been a subject of scientific inquiry, probably due to its limited distribution.

2.5: *In -Silico* Prediction

Traditional drug discovery strategies have been effective in developing new medications, however, the process from identifying a lead compound to completing clinical trials typically spans over 12 years and incurs costs averaging $1.8 billion (Shaker et al., 2021). Recently, *in silico* techniques have garnered significant attention due to their ability to speed up the drug discovery process, reducing both time and labor costs. Numerous new drugs have been successfully developed using these

computational techniques (Shaker et al., 2021; Silva et al., 2021). Usually, the potency and safety (toxicity) of compounds, are investigated using *in vivo* and *in vitro* techniques. In cases where neither of these options is available, *in silico* prediction methods can be utilized to predict the activity of a drug candidate compound, and to evaluate various physicochemical properties, pharmacokinetics, medicinal chemistry, drug-likeness and lead-likeness of the compounds (Shaker et al., 2021).

2.5.1: Molecular Docking Simulation

Molecular docking serves as a tool to predict how small molecule drug candidates bind to their protein targets, aiding in the prediction of affinity and activity. In this investigation, the molecular interactions between the two alkaloids and protein targets of *P. falciparum* (*Plasmodium falciparum* lactate dehydrogenase), *L. donovani* (dihydroorotate dehydrogenase), *T. cruzi* (trypanothione reductase), *T. brucei* (L-threonine-3-dehydrogenase) and DM (α-amylase and α-glucosidase) (**Figure 2.7**) was carried out. Docking methods rely on an energy-based scoring function to identify the most energetically favorable conformation of the ligand when bound to the target protein. The fundamental hypothesis is that lower energy scores signify stronger protein-ligand bindings than higher energy values. Thus, molecular docking can be framed as an optimization problem, where the objective is to discover the ligand-binding mode with the lowest energy (Ribeiro et al., 2015).

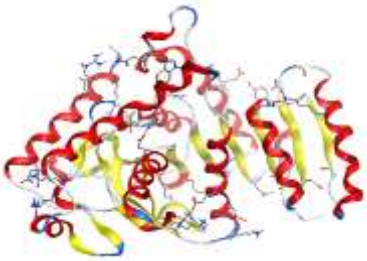

Pf lactate dehydrogenase

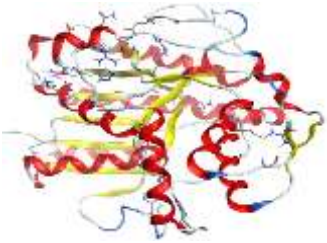

L-threonine-3-dehydrogenase

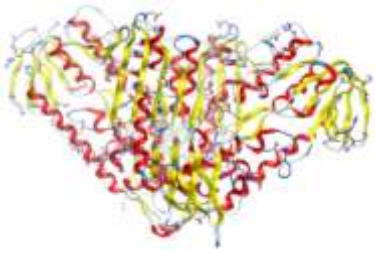

Trypanothione reductase

Dihydroorotate dehydrogenase

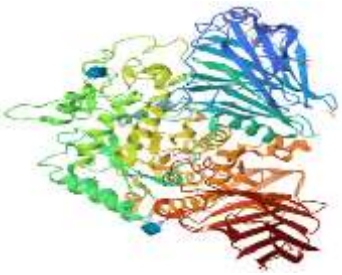

α-glucosidase

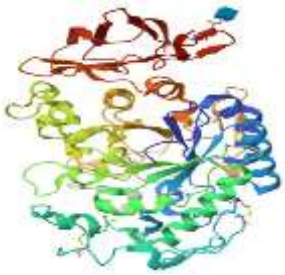

α-amylase

Figure 2.7: 3D Structure of Target Proteins

The *Plasmodium falciparum* Lactate Dehydrogenase protein (**Figure 2.7**) stands as a pivotal target in molecular pharmacology. Operating as a catalyst, it facilitates the reversible conversion of pyruvate to lactate, utilizing NAD+ as a co-factor within the glycolytic pathway (Shadrack et al., 2016). Devoid of this enzyme, *P. falciparum* cannot generate the essential energy needed for its growth, metabolism, and other developmental processes (Shadrack et al., 2016). Consequently, inhibiting this enzyme results in the parasite's death (Chaniad et al., 2021). Thus, researchers have directed efforts towards designing potential antimalarial drugs that specifically target the PfLDH enzyme (Chaniad et al., 2021; Shadrack et al., 2016).

The studies conducted by Adjogatse et al. (2018) contributed to unveiling the structure of the L-threonine-3-dehydrogenase protein (**Figure 2.7**) found in the protozoa *T.*

brucei. This protein plays a critical role in threonine synthesis, occurring within the gut of the tsetse fly, an essential vector for *T. brucei* transmission. Inhibiting L-threonine-3-dehydrogenase leads to parasite depletion by disrupting the synthesis of the fatty acid pathway, impeding energy production, and destabilizing physiological processes (Dhorajiwala et al., 2019).

Trypanothione reductase (**Figure 2.7**) and dihydroorotate dehydrogenase (**Figure 2.7**) serve vital functions in the biological processes of *T. cruzi* and *Leishmania spp* parasites respectively. Trypanothione reductase is instrumental in the regulation of the parasites' antioxidant defense system, facilitating the reduction of trypanothione, a specialized thiol compound crucial for maintaining cellular redox equilibrium and shielding against oxidative stress. Inhibiting trypanothione reductase disrupts this balance, resulting in the accumulation of reactive oxygen species (ROS) within the parasites (Ribeiro et al., 2015). Consequently, oxidative damage to essential cellular components occurs, ultimately leading to the demise of the parasites. On the other hand, dihydroorotate dehydrogenase plays a pivotal role in the *de novo* pyrimidine biosynthesis pathway. This enzyme catalyzes the conversion of dihydroorotate to orotate, a critical step in the synthesis of pyrimidine nucleotides essential for DNA and RNA production in the parasites. Inhibition of dihydroorotate dehydrogenase impedes this biosynthetic pathway, compromising the parasites' ability to synthesize DNA and RNA. As a result, their growth and replication are severely impaired (Ribeiro et al., 2015).

Alpha-amylase and glucosidase (**Figure 2.7**) are equally crucial enzymes in carbohydrate digestion, converting starches into glucose for absorption. Inhibiting these enzymes slows glucose release into the bloodstream, which helps manage diabetes. This inhibition reduces postprandial blood glucose spikes, improves overall glycemic control, and decreases insulin demand (Kimani et al., 2023). Consequently, alpha-amylase and glucosidase inhibitors are valuable for maintaining stable blood sugar levels and reducing diabetes-related complications. Targeting these proteins would essentially paralyze their functions and disrupting vital activities. Therefore, an ideal drug candidate should aim to inhibit these activities, which has been a key focus for researchers.

CHAPTER THREE

MATERIALS AND METHODS

3.1: General

The extraction and separation utilized distilled general-purpose methanol, n-hexane, and EtOAc. The distillation procedures involved several apparatuses, including the UMS-UK 1000ml heating mantle, borosil 4380 round bottom flask, pyrex quickfit UK C1/13SC 24/29 condenser, pyrex quickfit England RA1/13 24/29 receiver adapter, pyrex quickfit 13/23 adapter, Checktemp HI985001 thermometer, G.G-17 250ml conical flask, boro 3.3 500ml beaker, EX 20°C MC 100ml ± 1 measuring cylinder, tripod stands, water pipes, and tap water. Filtration was conducted using the Value VE125N vacuum pump, polypropylene buchner funnel 110mm-1 piece, and Whatman™ filter paper. Liquid-liquid partitioning procedures involved a 1G 500ml separating funnel, G.G 17 250 ml conical flask, EX 20°C MC 100ml ± 1 measuring cylinder, distilled water, and ISOLAB German 1000ml boro 3.3 duran glass bottles. While the concentration of the crude extract used a rotary evaporator (R-100 Büchi, Switzerland). Column chromatography (Column; ISOLAB Germany NS 29/32) utilized Scharlau Silica gel 60, 0,06 - 0,2 mm, for column chromatography 60 - 230 mesh ASTM and finer silica gel (Merk Silica gel100-200 mesh) as stationary phases. The elution process utilized a gradient of distilled n-hexane and EtOAc as the mobile phase. Thin layer chromatography was executed on pre-coated silica gel 60 plates (TLC aluminum sheets, silica gel layer, ALUGRAM Xtra SIL G/UV254, 20x20 cm) and STAEDLER 2B pencil. Visualization of compounds on TLC was achieved under UV light at 254 nm.

1D and 2D NMR spectra were recorded on a 600 MHz Agilent DD2 NMR spectrometer (Agilent Technologies, Santa Clara, CA, USA) at 298 K in $CDCl_3$. The solvent signals (^1H: 7.260 ppm and ^{13}C: 77.000 ppm) were used to reference the spectra. MestReNOVA v. 11 (Mestrelab Research, Chemistry Software Solutions, Santiago de Compostela, Spain) software was employed to process and analyze the spectra. HRESI-MS experiments were performed on a UHPLC/+ESIQTOFMS/MS instrument with a Bruker Daltonics micrOTOF-QII quadrupole/time-of-flight mass spectrometer (Bruker Daltonics, Bremen, Germany) with an Apollo electrospray ion source operated in positive ionization mode.

3.2: Plant Collection and Preparation

Fresh leaves of *V. glandulosa* were collected from their natural habitat located in Muguga Forest, Limuru, within Kiambu County (1° 11' 3" S · 36° 37' 31" E) on 9th November, 2021. The plant was identified and authenticated by Mr. Patrick Mutiso, a taxonomist at the Faculty of Science and Technology, University of Nairobi and a sample specimen was preserved under voucher number OP UON 2021/001. Gathered leaves material were washed using tap water and then dried under the shade. The dried leaves were then ground into soft powder by a grinder and then kept in a sample envelope.

3.3: Extraction and Isolation of Compounds from *V. glandulaosa*

Dry powdered plant materials (2kg) were extracted via maceration into methanol by cold percolation at room temperature (overnight extraction). The extracts were then filtered using Whatman™ filter paper 1 under vacuum filtration, vacuum pump (value VE125N) and a polypropylene Buchner 110mm funnel were used to get methanol extracts of the plant. The filtrates were concentrated using a rotary evaporator (R-100 pro Büchi, Switzerland) at 40°C and at 120 RPM while residue extracts were then subjected to a further exhaustive extraction (Ogbole et al., 2018). The sample yielded a dark green crude extract (310.45g) which represents 15.52% of the powdered material.

3.3.1: Liquid-liquid Extraction

Liquid-liquid partitioning was carried out to separate compounds contained in the crude extracts based on their polarities. Ethyl acetate extracted moderately polar compounds, and hexane extracted the least polar ones. 310.45 grams of dark green crude extract were suspended in 1 liter of water and sequentially partitioned with hexane and ethyl acetate respectively (Ogbole et al., 2018). This step produced three fractions; aqueous methanolic extract, ethyl acetate extract, and hexanoic extract.

3.3.2: TLC Analysis and Column Chromatography

The ethyl acetate extract (120.34 g) was adsorbed into equal amount of silica gel. The separation process employed column chromatography with silica gel (Scharlau Silica gel 60, 0,06 - 0,2 mm, for column chromatography 60 - 230 mesh ASTM) as the stationary matrix and initially utilized a mobile phase comprising 5% EtOAc in n-

hexane. Elution proceeded in a stepwise manner, gradually increasing the polarity of the solvent system. Specifically, polarity was increased by gradually increasing the proportion of the polar solvent, starting from 5% EtOAc and progressing through successive increments of 5% (e.g., 10%, 15%, 20%, 25%, 30%, 35%, and so on) until reaching neat EtOAc. This yielded 435 fractions of 10 mL each, which were pooled according to their TLC profiles to afford 5 fractions (Fr. A-E). Fractions A and B from the main column provided a dark green oily solid, which was subsequently combined with the hexanoic extract previously obtained through partitioning. Fractions D and E were merged and then subjected to separation on a more refined silica gel (Merk Silica gel 230-400 mesh) column using an eluent consisting of 50% EtOAc in 50% n-hexane to afford compound **30** (36.7 mg) as a yellowish powder. Fraction C underwent further column chromatography on silica gel (Scharlau Silica gel 60, 0,06 - 0,2 mm, for column chromatography 60 - 230 mesh ASTM) as the stationary phase, with elution gradients of 45% n-hexane and 55% EtOAc, yielding a semi-pure fraction. This fraction was subsequently purified through column chromatography using finer silica gel (Merk Silica gel 230-400 mesh) and an elution of 40% n-hexane and 60% EtOAc, resulting in the isolation of compound **29** (40.6 mg) as white amorphous solid. The extraction and isolation were carried out as illustrated in the **Figure 3.1**.

3.4: Characterization of the Isolated Compounds from *V. glandulosa*

The chemical structures were ascertained based on spectrometric and spectroscopic techniques. HRESI-MS was used to determine the molecular weight of purified compounds. NMR was used to determine the number of carbons and protons as well as their connectivity, 1D (^{1}H, ^{13}C), and 2D-NMR; HSQC, COSY, HMBC, NOESY and by comparison of published data for the compounds.

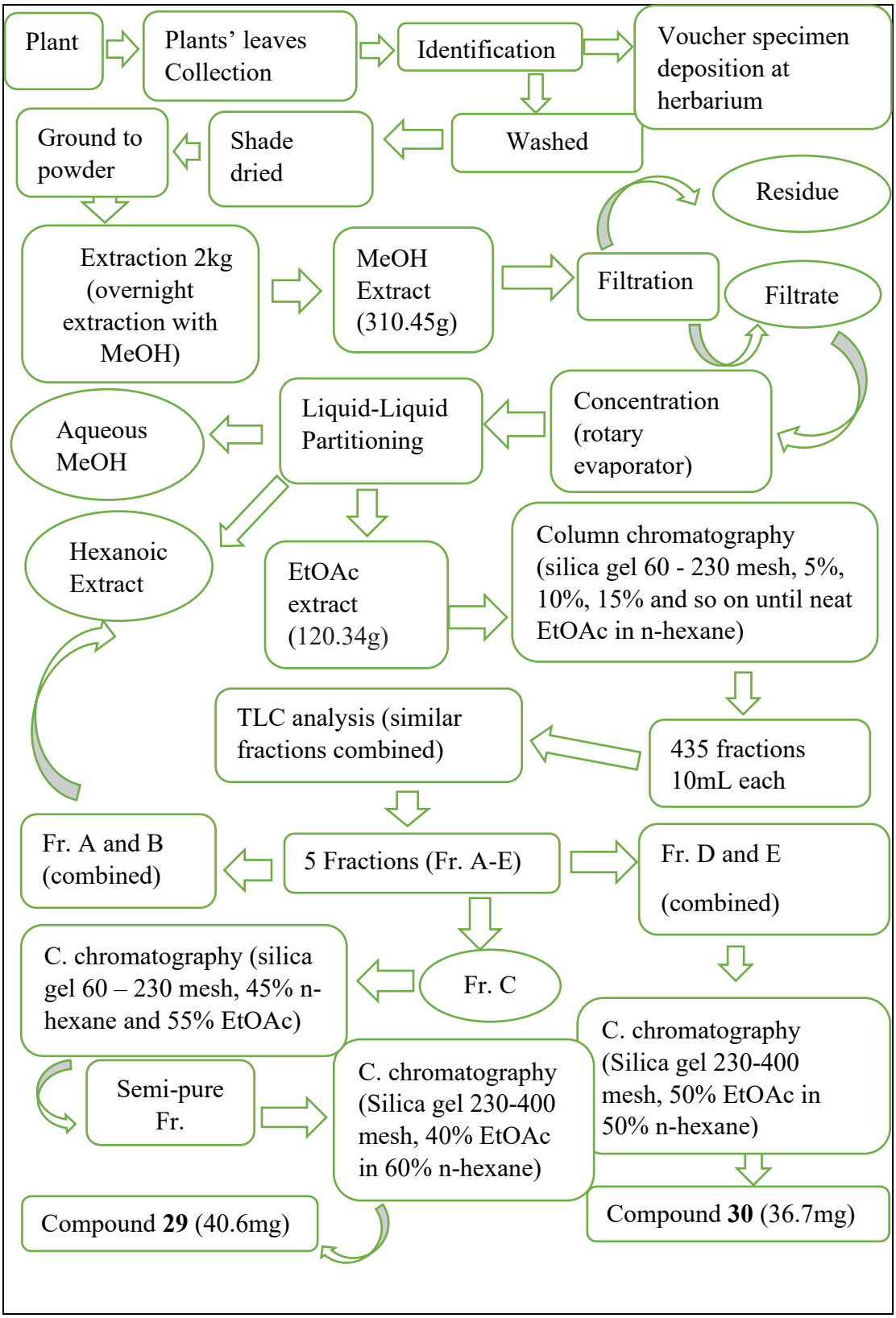

Figure 3.1: Flow chart illustrating the extraction and isolation of compounds 29 and 30

3.5: Antidiabetic Activity (α - Amylase Inhibition Assay)

A modified assay, outlined by Kwon et al. (2006), was used to test the pure isolated compounds' anti-hyperglycemic bioactivity against human salivary α-amylase. A 500 µL of 0.02M sodium phosphate buffer (pH 6.9 with 0.006 M NaCl) containing 0.5 mg/mL of α -amylase was pre-incubated for ten minutes at 25 ºC. Following the pre-incubation, 500 µL of a 1% starch solution in 0.02M sodium phosphate buffer (pH 6.9 with 0.006M NaCl) was gradually added at predetermined intervals to each tube holding pure isolates (0.625, 1.25, 2.5, and 5 mM). Afterwards, 1.0 mL of dinitrosalicylic (DNS) acid color reagent was used to stop the reaction.

After five minutes of incubation in a boiling water bath, the test tubes were allowed to cool to room temperature. To dilute it, 5 to 15 milliliters of distilled water were added to the reaction mixture. A SpectraMax GeminiXS Spectrofluorometer (Molecular Devices, Sunnyvale, CA) with 540 nm excitation and emission wavelengths was used to measure the fluorescence. The absorbance measurements were compared with the buffer-containing controls, which did not contain sample extract. The below formula was employed to determine the percentage of α-amylase inhibitory activity:

$$\%\ inhibition = \frac{\text{Absorbance (control)} - \text{Absorbance (compound)}}{\text{Absorbance (control)}} \times 100$$

Each sample's 50% inhibitory concentration (IC_{50}) was determined by regressing the expressed percentage inhibitions as probit units against the sample concentrations. The mechanism of molecule inhibition against porcine pancreas α-amylase was investigated at increasing concentrations of the substrate, pNPG, ranging from 0.25, 0.5, 1, 2, and 5 µg/ml. This was observed in the presence of acarbose at 0.625, 1.25, 2.5, and 5 mM and in the absence of these compounds. The inhibition constants (K_i) were subsequently identified via secondary plots (Dixon plots) based on the documented mechanism of inhibition, which was determined using Lineweaver–Burk plots.

$$\mathrm{V} = Vmax \times \frac{S}{Km(1 + [I]/ki} + S(1 + \frac{[\mathrm{I}]}{\alpha Ki})$$

Where;

v- initial velocity

V_{max} - maximum velocity

I- inhibitor concentration

K_m -Michaelis-Menten constant

S -substrate concentration

K_i-competitive inhibition constant

αK_i- uncompetitive inhibition constant

3.6: Molecular Docking Analysis of Compounds from *V. glandulosa*

The *in-silico* docking was conducted using the MOE software version 2015.10 from the Chemical Computing Group, Montreal, QC, Canada, along with the integrated Merck Molecular Force Field (MMFF94x).

3.6.1: Preparation of Ligands

The structures of compound **29** and **30** were drawn using ChemDraw and then converted into SMILES format for further processing in MOE. Additionally, standard drugs such as Chloroquine for *P. falciparum*, benznidazole for *T. cruzi*, melarsoprol for *T. brucei,* miltefosine for *L. donovani*, and acarbose for α-amylase and glucosidase acting as positive controls, were retrieved from PubChem (https://pubchem.ncbi.nlm.nih.gov/), accessed on 7th April 2024. Subsequently, all molecules were imported into MOE, where three-dimensional (3D) molecular models were generated (Kimani et al., 2023). The MMFF94x force field was utilized to optimize the geometries, followed by a low-mode molecular dynamics conformational search (LowModeMD) to identify the most appropriate conformers for each ligand. An energy threshold of 5 kcal/mol above the lowest energy conformation was applied, with a conformation limit set to 10 for each ligand. The resulting conformers with the lowest force field energy underwent minimization using the AM1 Hamiltonian (MOPAC module of MOE), and the minimized geometries were then stored in MOE database for further processing.

3.6.2: Preparation of Target Proteins

The three-dimensional structural (3D) conformers of the six target proteins were extracted from the RCSB protein databank (http://rcsb.org.) as PDB files (accessed on 7th April 2024). These targets include *Plasmodium falciparum* lactate dehydrogenase (PDB ID: 1LDG, Resolution: 1.74 Å, Ligands: 1,4-dihydronicotinamide adenine dinucleotide and oxamic acid), trypanothione reductase (PDB ID: 1GXF, Resolution: 2.70 Å, Ligands; flavin-adenine dinucleotide, quinacrine mustard, and maleic acid), dihydroorotate dehydrogenase (PDB ID: 4EF8, Resolution: 1.56 Å, Ligands: flavin mononucleotide, N-phenylthioformamide, sulfate ion and glycerol), L-threonine-3-dehydrogenase (PDB ID: 5K4Y, Resolution: 1.77 Å, Ligands: nicotinamide-adenine-dinucleotide, glycerol, acetate ion, chloride ion, and sodium ion), α-amylase (PDB ID:

3BAJ, Resolution: 2.10 Å, Ligands: acarbose derived pentasaccharide, 2-acetamido-2-deoxy-beta-d-glucopyranose, nitrate ion and calcium ion) and α-glucosidase (PDB ID: 2QMJ, Resolution: 1.90 Å, Ligands: 2-acetamido-2-deoxy-beta-D-glucopyranose, sulfate ion and glycerol). The initial step in preparing the protein models involved removing all water molecules (MOE: SEQ) and rectifying any incomplete or omitted residual amino acids identified from X-ray crystallographic data using MOE software (Quickprep). Subsequently, at 27 °C and pH 7.0, the models underwent virtual titration to adjust the ionization states of acidic and basic side chains of amino acids, followed by protonation using the MOE software (Kimani et al., 2023). The energy of the enzyme models was then decreased to minimize the protein structure while adhering to the allocated force field. This reduction was conducted gradually, with heavy atom sites set and a steady increase allowed within a radius of 0.5 to 1.5 Å using MOE software through the steps Compute, Energy Minimize, and Tether Atoms, ensuring minimal deviation from the experimentally determined protein structure. Finally, unconstrained energy minimization was done to yield fully relaxed protein structures suitable for further examination.

3.6.3: Docking Simulation

Each ligand underwent simulation to ascertain its optimal orientation within the binding site of each protein target using MOE software (Compute, Dock). Before docking, the binding interactions of amino acid residues with ligands and standard drugs were explored. Dummy atoms were then positioned within the active sites for each protein to facilitate docking. To investigate the binding modes of the two compounds with target proteins, ten conformations of each ligand were docked into the chosen binding pocket of the respective protein using the MOE-Dock module, employing conditions such as placement: triangle matcher, rescoring: London dG, refinement: forcefield, and retaining: 10. The RMSD (root mean square deviation) values and docking scores of the top-ranked conformers of ligands were analyzed to understand their binding mechanisms (Kimani et al., 2023). The Gibbs energy (MOE: London DG) determined from the resultant enzyme-ligand complexes (docking poses) served as the scoring parameters, with each complex's S-score indicative of its virtual free energy in kcal/mol. As a larger negative result indicates a stronger binding affinity, all docking scores were arranged in increasing S-score order, and the best score was selected based on the interaction.

3.7: Physicochemical and ADME Properties

The SwissADME (http://www.swissadme.ch/), accessed on April 11th, 2024, a freely available web tool, was employed to assess the physicochemical parameters of the compounds and predict their pharmacokinetic, lipophilicity, water solubility, and drug-likeness properties. Singly, the SMILES representations of the compounds were inserted into the designated field on the SwissADME website (Kibet et al., 2024). The analysis was initiated by clicking the "Run!" button, and upon completion, the results were exported into Excel in CSV format

3.8: Synthetic Accessibility, PAINS, Brenk, and Lead-likeness

The SwissADME tool, available online at http://www.swissadme.ch/ (accessed on April 11th, 2024), was utilized to evaluate the Synthetic Accessibility, PAINS, Brenk, and Lead-likeness. The compounds' SMILES were entered singly into the designated field on the SwissADME website, and the analysis was initiated by clicking the "Run!" icon (Kibet et al., 2024). Subsequently, the obtained data were exported to Excel in CSV format.

3.9: Toxicity

This study utilized PkCSM pharmacokinetics (http://structure.bioc.cam.ac.uk/pkcsm accessed on April 7th, 2024)) to predict the toxicity of compounds. In pKCSM, SMILES for each compound were submitted for toxicity assessment (Ojuka et al., 2023).

3.10: Statistical Analysis and Data Presentation

The MS-Excel-2019 version of a nonlinear regression program was utilized to assess the kinetic data. The inhibition constants were ascertained by doing Lineweaver-Burk plots on mono-replicate tests, followed by Dixon secondary plots. R^2 was used to determine the coefficient of determination, and the least significant difference was set at $p < 0.05$. It was calculated by taking the mean of the regression curves from Dixon plots of individual experiments. GraphPad Prism 10 version 10.2.2 (397) statistical software was used to plot the graphs.

CHAPTER FOUR

RESULTS AND DISCUSSION

4.1: Secondary Metabolites Isolated from *V. glandulosa*

The investigation of the leaves of *V. glandulosa* led to the isolation of two known furoquinoline alkaloids: Choisyine acetate **29** and Choisyine **30**. The comprehensive spectroscopic and spectrometric analysis of these compounds are as discussed below.

4.1.1: Choisyine Acetate (29)

Compound **29** was isolated as white amorphous solids. Analysis using positive mode HRESI-MS (**Appendix A1**) displayed a molecular adduct ion $[2M+Na]^+$ at m/z; 765.2623, $[M+Na]^+$ at m/z; 394.1258 and $[M+H]^+$ at m/z; 372.1443 aligning with the molecular formula $C_{20}H_{22}NO_6$ (calcd. 372.1447 for $C_{20}H_{22}NO_6$). The compound possesses a distinctive moiety, specifically observed at a carbon position with a chemical shift of 170.5 ppm in the ^{13}C NMR spectrum. This moiety corresponds to an acetate group, and its presence is indicated by the fragmentation at 312.1226, which corresponds to the loss of the ester group as acetic acid (60 daltons) as shown in the mass spectrum (**Appendix A1**). The ^{13}C NMR data (**Table 4.1** and **Appendix A2**) revealed signals at δc 151.3 (C-4), δc 148.6 (C-6), and δc 143.7 (C-2), aligning with the characteristic pattern of a furoquinoline alkaloid skeleton, as noted in a study by Lacroix et al. in 2012. Moreover, analysis of the ^1H NMR spectrum (**Appendix A3**) indicated the presence of a pair of coupled doublets at δH 7.66 (d, J=2 Hz, H-2) and δH 7.17 (d,J=2.5 Hz, H-3), resonating with the corresponding carbon atoms at δC 143.7 (C-2) and δc 105.9 (C-3), typically associated with a furan ring commonly found in furoquinoline alkaloids, as highlighted in research by Dagne et al. (1988).

Additionally, the NMR spectrum showcased methoxy signals appearing at higher chemical shift values (downfield) at δH 4.54 and δH 4.09, coupled with the corresponding carbon signals at δC 60.3 and δC 56.9, respectively, consistent with the characteristic signatures observed in furoquinoline alkaloids, as outlined in the work of Ayafor and Okogun in 1982. From the ^{13}C NMR spectrum (**Appendix A2**), a total of twenty (20) carbons were identified (**Table 4.1**). Of these carbons, four were Methine (- CH), one Methylene (CH_2), two methoxy (OCH_3), three methyls (CH_3), nine quaternary carbons (C), and one overlapping carbon (8a), according to ^{13}C NMR spectrum. The four methine carbons displayed distinct chemical shifts (δC: 143.7,

105.9, 88.7, and 101.7) assigned respectively to C-2, C-3, C-2', and C-8. Using HSQC (**Appendix A4**), the following carbon atoms; C-2 (δC 143.7), C-3 (δC 105.9), C- 2' (δC 88.7), MeO-4 (δC 60.3), MeO-C-7 (δC 56.9), C-1' (δC 33.6), C-7' (δC 22.6), C-4' (δC 22.2), C-5' (δC 21.3), and C-8 (δC 101.7), were found to be protonated. This was further confirmed by the correlations observed from ^{1}H-^{1}H COSY (**Appendix A5**), which confirmed that H-2, δH 7.66 (d, J=2.0 Hz, H-2) and H-3, δH 7.17 (d, J=3.0 H-3), were coupling partners. Also found to be coupling partners were; H-2' (t, J=10.2, Hz, H-2') and H-1', (s, H-1'; dd, J=17.0, 8.7 Hz, H-1'). Using HMBC (**Appendix A6**), H-2 (δH 7.66) correlated with C-3 (δC 105.9), C-3a (δC 103.4), and C-7 (δC 158.0), H-3 (δH 7.17) correlated with C-2 (δC 143.7), C-3a (δC 103.4), and C-4' (δC 22.2). H-MeO-4 (δH 45.4) correlated with C-9a (δC 161.4), H-MeO-7 (δH 4.09) correlated with C-4 (δC 151.3), while H-1' (δH 3.80, 3.64), correlated with C-3' (δC 82.3), C-4a (δC 119.5), C-2' (δC 88.7), C-6 (δC 148.6). Other observed correlations were H-4' (δH 1.63), with C-2' (δC 88.7), C-3' (δC 82.3), C- 5' (δC 21.3), while H-5' δH 1.59 with C-2' (δC 88.7), C-3' (δC 82.3), and C-4' (δC 22.2), and finally H-7' δH 1.99 with C-6' (δC 170.5).

From the ^{13}C NMR analysis, nine quaternary carbons were identified at δC 170.5, 161.4, 158.0, 151.3, 148.6, 119.5, 110.7, 103.4, and 82.3, corresponding to C-6', C-9a, C-7, C-4, C-6, C-4a, C-5, C-3a, and C-3', respectively. The δC 170.5 peak was associated with the acetate group at C-6'. Methoxy groups appeared at δC 56.9 (MeO-4) and δC 60.3 (MeO-7), assigned to positions 4 and 7 of the aromatic rings, respectively.

The NMR assignments were deduced through analysis of NOESY correlations (**Appendix A7**), providing insights into the spatial relationships and distances between protons within the molecule. This method elucidates the proximity of different protons, unravelling spatial interactions among them. Notably, NOESY correlations uncovered specific spatial relationships; for instance, H-3 (δH 7.19) exhibited correlations with H-MeO-4 (δH 4.54), and H-8 (δH 7.96) displayed correlations with H-MeO-7 (δH 4.09). Likewise, correlations were observed between H-2' (δH 5.17) and H-1' (δH 3.80), as well as between H-4' (δH 1.63) and H-5' (δH 1.59). Cross peaks indicating close proximity were evident among these protons.

Based on structural elucidation and comparison with existing literature, it was logically inferred that the alkaloid compound, depicted by the NMR data outlined in **Table 4.1** below, corresponded to Choisyine acetate (**29**). A similar compound was earlier reported from (Frolova & Kuzovkov, 1963).

Table 4.1: NMR (^{1}H 600MHz and ^{13}C 150 MHz, $CDCl_3$) data of compound 29

C-Position	δC	δH (*m*, *J* in *Hz*)	HMBC (^{2}J,^{3}J)
6'	170.5	-	
9a	161.4	-	
7	158.0	-	
4	151.3	-	
6	148.6	-	
2	143.7	7.66 *d* (2.0)	C-3a,3,9a
4a	119.5	-	
5	110.7	-	
3	105.9	7.17 *d* (2.5)	C-3a,2,9a
3a	103.4	-	
8	101.7	7.96 *s*	
2'	88.7	5.17 *t* (10.2)	
3'	82.3	-	
MeO-4	60.3	4.54 *s*	C-4
MeO-7	56.9	4.09 *s*	C-7
1'	33.6	3.80, 3.64 *s*; *dd*, (17.0, 8.7)	C-3',4a,2',6
7'	22.6	1.99 *s*	C-6'
4'	22.2	1.63 *s*	C-5',3',2'
5'	21.3	1.59 *s*	C-4',3',2'

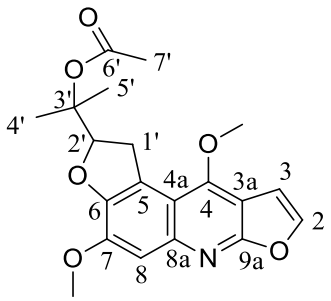

Compound **29**

4.1.2: Choisyine (30)

Compound **30** was isolated as a yellowish powder. Analysis using positive mode HRESI mass spectrum (**Appendix B1**) displayed a molecular adduct ion $[M+Na]^+$ at m/z; 352.1150 and $[M+H]^+$ at m/z; 330.1337 aligning with the molecular formula $C_{18}H_{20}NO_5$ (calcd. 330.1341 for $C_{18}H_{20}NO_5$). The compound also demonstrated traits of a furoquinoline alkaloid, evident from the carbon signals (**Table 4.2**) appearing at δc 143.8 (C-2), δc165.8 (C-9a), and δc148.7 (C-6), aligning with observations in the study by Lacroix et al. in 2012. Further analysis of the ^1H NMR spectrum (**Appendix B3**) highlighted the existence of coupled doublets akin to those observed in compound **29**, resonating at δH 7.68 (H-2) and 7.18 (d, J=3 Hz, H-3). These resonances corresponded to carbon atoms resonating at δC 143.8 and 106.0, respectively, which are characteristic signatures indicative of a furan ring typically found in furoquinoline alkaloids. The NMR spectrum, in addition, showed a downfield methoxy signal resonating at δH 4.56 and δH 4.11, alongside the corresponding carbon signals at δC 60.4 and δC 57.1, respectively.

As revealed by the ^{13}C NMR spectrum (**Appendix B2**), eighteen (18) carbons were identified (**Table 4.2**). Of these carbons, four were Methine (- CH), one Methylene (CH_2), two methoxy (OCH_3), two methyls (CH_3), seven quaternary carbons (C), one overlapping carbon (8a), and one C-OH, according to ^{13}C NMR spectrum. The four methyne carbons displayed distinct chemical shifts (δC: 143.8, 106.0, 91.1, and 100.6) assigned respectively to C-2, C-3, C-8, and C-2'. Using HSQC (**Appendix B4**) the following carbon atoms; C-2 (1H, δH 7.68), C-3 (1H, δH 7.18), C- 8 (1H, δH 6.97), C-2' (1H, δH 4.85), C-3' (1H, δH 2.04), MeO-4 (1H, δH 4.56), MeO-7 (1H, δH 4.11), C-1' (2H, δH 3.77), C-4' (3H, δH 1.44) and C-5' (3H, δH 1.31) were found to be protonated. This was further confirmed by the correlations observed from ^1H-^1H COSY (**Appendix B5**), which confirmed that H-2, δH 7.68 (d, J=2.5 Hz, H-2) and H-3, δH 7.18 (d, J=3.0 H-3), were coupling partners. Also found to be coupling partners were H-2' δH 4.85 (d, J=4.85 Hz, H-2') and H-1' δH 3.77, (s, H-1'), H-4' δH 1.44 (s, H-4') and H-5' δH 1.31 (s, H-5'). Using HMBC (**Appendix B6**), H-2 correlated with C-3 (δC 106.0), C-3a (δC 103.4), and C-9a (δC 165.8), H-3 correlated with C-2 (δC 143.8), C-3a (δC 103.4) and C-9a (δC 165.8). H-MeO-7 (δH 4.11) correlated with C-7 (δC 157.8), H-MeO-4 (δH 4.56), correlated with C-4 (δC 151.7), while H-1' (δH 3.77), correlated with C-2' (δC 91.1), C-3' (δC 71.9), C-6 (δC 148.7), C-4a (δC 120.9)

and C-5(δC110.6). Other observed correlations were H-4' (δH 1.44), with C-2' (δC 91.1), C-3' (δC 71.9), C- 5' (δC 24.7), and finally H-5' (δH 1.31), with C-4' (δC 26.3), C-2' (δC 91.1), and C-3' (δC 71.9).

The ^{13}C NMR analysis (**Appendix B2**) revealed the presence of seven quaternary carbons appearing at δC values (165.8, 157.8, 151.7, 148.7, 120.9, 110.6, and 103.4), assigned respectively to C-9a, C-7, C-4, C-6, C-4a, C-5, and C-3a. The δC 71.9 was associated with the OH group and attributed to C-3', while the methoxy groups, MeO-4 (δC 60.4) and MeO-7 (δC 57.1), were positioned at 4 and 7 within distinct aromatic rings. The NMR assignments were equally reasoned from NOESY (**Appendix B7**) correlations, which offer insights into the spatial relationships and distances between protons within a molecule. It details the proximity of various protons in the molecule, revealing spatial interactions among them. For instance, NOESY correlations revealed spatial interactions among these protons: H-3 (δH 7.18) with H-MeO-4 (δH 4.56), H-8 (δH 6.97) with H-MeO-7 (δH 4.11). Similarly, H-2' (δH 4.85) with H-1' (δH 3.77), H-4' (δH 1.44) and H-5' (δH 1.31). Cross peaks were observed on close protons.

Based on structural elucidation and comparison with literature, the alkaloid compound observed in the NMR data (illustrated in **Table 4.2**) was identified as Choisyine **(30)**, previously isolated from the *Choisya ternata* (Boyd et al., 2007; Leitão et al., 2017).

Table 4.2: NMR ((^{1}H 600MHz and ^{13}C 150 MHz, $CDCl_3$) data of compound 30

C-Position	δC	δH (*m*, *J* in *Hz*)	HMBC (^{2}J,^{3}J)	Reference: δC (Leitão et al., 2017)	Reference: δH (*m*, *J* in *Hz*) (Leitão et al., 2017)
9a	165.8	-		164.2	
7	157.8	-		156.5	
4	151.7	-		148.3	
6	148.7	-		144.5	
2	143.8	7.68 *d* (2.5)	C-3,3a,9a	142.5	7.51 *d* (2.4)
4a	120.9	-		118.7	
5	110.6	-		106.4	
3	106.0	7.18 *d* (2.48)	C-3a,2,9a	104.6	7.18 *s*
3a	103.4	-		102.7	
8	100.6	6.97 *d* (2.4)		93.08	6.97 *d* (2.4)
2'	91.1	4.85 *t* (9.6)		90.5	4.78 *t* (9.5)
3'	71.9	2.04 *s*		71.9	2.02 *s*
MeO-4	60.4	4.56 *s*	C-7	58.8	4.33 *s*
MeO-7	57.1	4.11 *s*	C-4	55.7	3.95 *s*
1'	33.5	3.77 *s*	C-2',3',6,4a	33.7	3.72 *s*
4'	26.3	1.44 *s*	C-5',2',3'	26.1	1.41 *s*
5'	24.7	1.31 *s*	C-4',2',3'	24.1	1.28 *s*

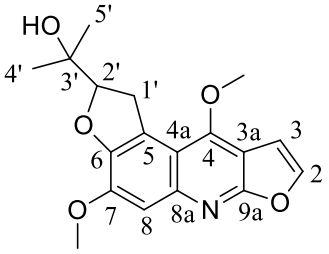

Compound **30**

4.2: Biological Activity

This study led to isolation, purification, and characterization of two known alkaloids, choisyine acetate (**29**) and choisyine (**30**). It is the first scientific research to explore the phytochemical properties of *V. glandulosa* and the first instance of these compounds being identified within the genus *Vepris*. Choisyine acetate (**29**) and Choisyine (**30**) have been identified in Choisya ternata (Donald et al., 2021; Frolova & Kuzovkov, 1963). Limited reports exist regarding the activity of choisyine, for instance, previous research highlighted its potent antinociceptive and anti-inflammatory activity (Leitão et al., 2017; Szewczyk & Pęczek, 2023). However, the activity of choisyine acetate remains largely unexplored. In the current study, anti-plasmodial, anti-kinetoplastid and antidiabetic activities of the two compounds were investigated *in silico* and *in vitro* and the results revealed their potent activities, as detailed in the subsequent sections.

4.2.1: α-Amylase Inhibition Assay

The IC_{50} and *Ki* values (**Table 4.3**) of the isolated compounds were used to evaluate how well they inhibited the activity of α-amylase. The concentration needed to inhibit 50% of the α-amylase activity for compound **29** was noted to be lower compared to the standard drug acarbose and to that of compound **30** ($P<0.05$), implying compound **29** was a strong inhibitor for the amylase activities. The noted significant difference in activities for compound **29**, could be postulated as due from the acetylation of hydroxyl unit (acetate moeity).

Table 4.3: α-amylase inhibitory action of compounds 29 and 30 relative to acarbose

Compound	**IC_{50} (mM)**	***K_i* (mM) Dixon plot**	**Inhibition mode (Lineweaver-Burk plot)**
Compound **29**	4.74±0.17	4.75 (y=0.1344+0.0175; R^2 =0.9681)	Noncompetitive
Compound **30**	11.29±0.44[a]	12.37 (y=0.0865x+0.075; R^2=0.9019)	Noncompetitive
Acarbose	11.99±0.02[a]	12.676 (y=0.4519x+0.0203; R^2=0.892)	Competitive

Key: Values IC_{50} column are mean ± SEM (n = 3). Common superscript ([a]) signifies statistically nonsignificant ($P<0.05$) based on one way ANOVA followed by Turkey's multiple comparison post hoc test.

The mode of inhibition of compounds against porcine pancreas α-amylase was determined using Lineweaver-Burk and Dixon plots. Lineweaver-Burk Plot is a double reciprocal plot (1/V vs. 1/[S]) which helps determine the type of inhibition (competitive, noncompetitive, or uncompetitive) by analyzing changes in the enzyme's kinetics in the presence of inhibitors (Freitas et al., 2023; Khyade et al., 2019). In competitive inhibition, the inhibitor competes with the substrate for the active site of the enzyme and the plot shows lines intersecting on the y-axis, indicating that V_{max} remains unchanged while K_m increases. Additionally, in noncompetitive inhibition, the inhibitor binds to an enzyme at a site other than the active site, altering the enzyme's function. The plot shows lines intersecting on the x-axis, indicating that V_{max} decreases while K_m remains unchanged. Furthermore, in uncompetitive inhibition, the inhibitor binds only to the enzyme-substrate complex. The plot shows parallel lines, indicating both V_{max} and K_m decrease proportionally (Copeland & Anderson, 2002).

In the case of compounds **29** and **30**, the Lineweaver-Burk plot showed that these compounds exhibit noncompetitive inhibition (**Figure 4.1**). This means they bind to a site other than the enzyme's active site (allosteric site). When these compounds are bound to this allosteric site, they alter the enzyme's structure and function, reducing its ability to catalyze the reaction, regardless of the substrate concentration. This results in a decrease in the maximum reaction rate (V_{max}) while the affinity of the enzyme for the substrate (K_m) remains unchanged. For the standard drug acarbose, it inhibits α-amylase by competing with the substrate for the enzyme's active site. This reduces the enzyme's ability to bind with the substrate at lower substrate concentrations. While the V_{max} remains unchanged, the presence of acarbose increases the K_m value, indicating a higher substrate concentration is needed to reach half of V_{max}.

Dixon Plot is a secondary plot used to determine the inhibition constants (K_i) based on the mode of inhibition established from the Lineweaver-Burk plots. This plot is a secondary analysis where 1/V is plotted against the inhibitor concentration ([I]) for different substrate concentrations (Thompson & Bachelard, 1976). The intersection points on this plot provide the K_i values, representing the inhibitor concentration needed to halve the enzyme activity (Butterworth, 1972). The K_i value, or inhibition constant, is a measure of how effectively an inhibitor can bind to an enzyme. Lower K_i values indicate stronger binding affinities, meaning the inhibitor is more effective

at lower concentrations. For compound **29**, the K_i value of 4.75 mM, the lowest among the three, suggesting that this compound binds strongly to the enzyme. This means that compound **29** is more effective in inhibiting the enzyme at lower concentrations compared to compound **30** and acarbose. The Dixon plot also provides a linear relationship between the inhibitor concentration and the inverse of the reaction rate (**Figure 4.1**). The equation y = 0.1344 + 0.0175 indicates the slope and intercept of this line, with the high R^2 value (0.9681) suggesting a good fit for the data.

Compound **30** has a K_i value of 12.37 mM, which indicates a weaker binding affinity compared to compound **29**. This higher K_i value means that a greater concentration of compound **30** is needed to achieve the same level of inhibition. The Dixon plot equation y = 0.0865x + 0.075 shows the relationship between inhibitor concentration and enzyme activity, with an R^2 value of 0.9019 indicating a reasonably good fit. Acarbose, the standard dug used as a positive control had a K_i value of 12.676 mM, indicating the weak binding affinity to the enzyme. The Dixon plot equation y = 0.4519x + 0.0203 describes its linear relationship, and the R^2 value of 0.892 (**Figure 4.1**), though lower than those of compounds **29** and **30**, still indicates a reasonably good fit to the linear model. Therefore, these alkaloids show potential as promising candidates for the development of inhibitors targeting α-amylase, thereby aiding in the treatment of diabetes. To broaden the understanding of the inhibitory mechanisms of compounds **29** and **30** against the α-amylase enzyme, an in-depth *in silico* analysis was conducted using molecular docking techniques, as detailed *vide infra* in section 4.3.

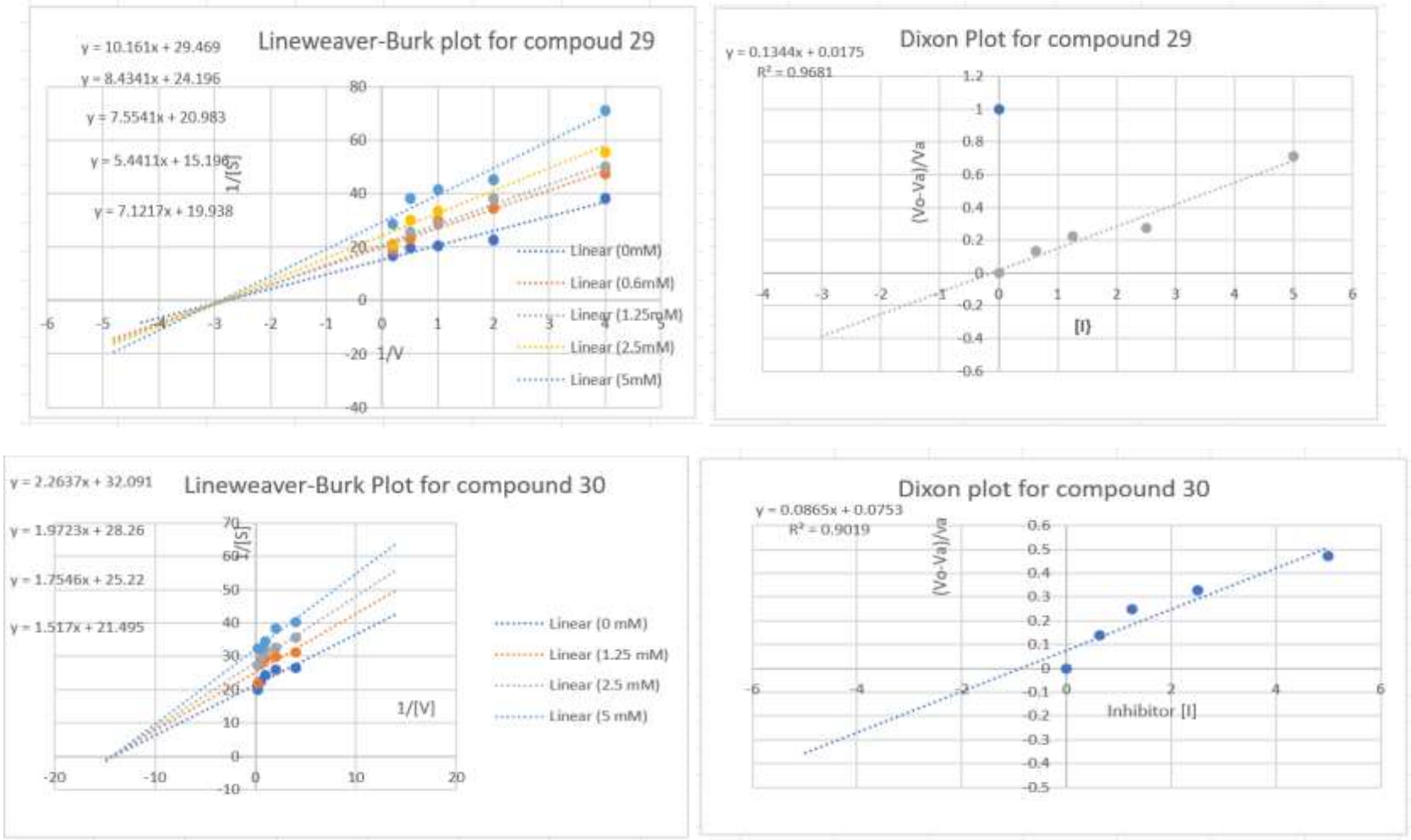

Figure 4.1: Dixon plots and Lineweaver-Burk plot for inhibition of α-amylase by compounds 29 and 30

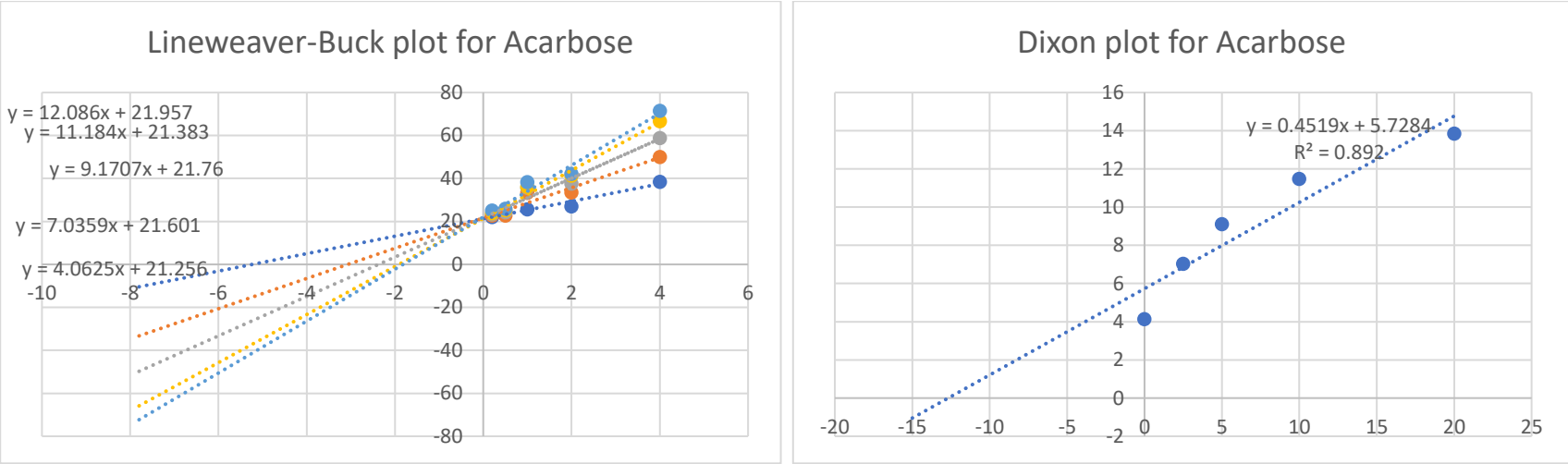

Figure 4.2: Dixon plots and Lineweaver-Burk plot for inhibition of α-amylase by Acarbose (standard drug)

4.3: *In -Silico* Prediction

In this study, the evaluation of the isolated compounds followed a different approach by incorporating an *in-silico* prediction.

4.3.1: Molecular Docking Analysis of the Compounds

Before conducting molecular docking investigations on the protein targets, the docking protocol used in this study was validated using α-amylase and α-glucosidase. This validation was done by re-docking the co-crystallized ligand (acarbose) into the enzymes' binding sites (self-docking). The docking simulation involved docking the lowest energy conformer of the ligand into the active sites of the two proteins in various conformations, treating the proteins as rigid structures (MOE: Rigid Receptor). The top ten results from this simulation were then analyzed further. The postures obtained from self-docking were compared with the experimental conformation (crystallographic pose), resulting in the binding modes and orientations illustrated in **Figure 4.3**. Additionally, the RMSD values for the co-crystallized ligands were 1.6451 Å for α-amylase and 1.5903 Å for α-glucosidase. These values, being below the recommended threshold of 2 Å (Kimani et al., 2023; Silva et al., 2021), confirm that the docking method was properly validated.

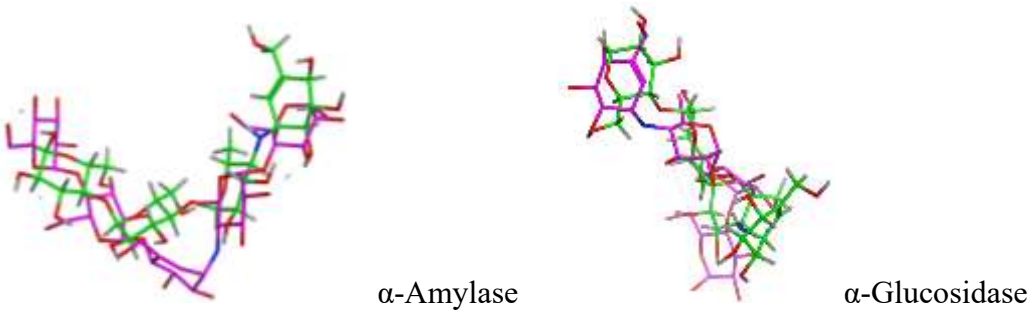

Figure 4.3: Superposed structures of acarbose after validation: The crystallographic pose (purple), and the highest-ranked docking pose (green).

4.3.2: Docking Results

The obtained energies (in kcal/mol) and RMSD values from the interaction of the ligands with the enzymes *Pf* lactate dehydrogenase, trypanothione reductase, dihydroorotate dehydrogenase, L-threonine-3-dehydrogenase, α-amylase and α-glucosidase alongside the standard drugs are presented in **Tables 4.4** to **4.6**.

Table 4.4: Binding affinity of compounds 29, 30 and standard drugs with *Pf* lactate dehydrogenase (chloroquine) and trypanothione reductase (benznidazole)

Compound	*Pf* lactate dehydrogenase				Trypanothione reductase			
	S(kcal/mol)	**RMSD (Å)**	**Binding Residues**	**Interaction**	**S(kcal/mol)**	**RMSD** (Å)	**Binding Residues**	**Interaction**
29	-7.0997	1.7276	PRO 246	H- donor	-8.1911	1.0785	LYS 61	H-acceptor
			THR 97	π-H			THR 335	H- acceptor
30	-7.1973	2.0608	ARG 109	H- acceptor	-7.8106	0.3801	ASP 327	H- donor
			ASN 140	H- acceptor			THR 335	H- acceptor
							LYS 61	H- acceptor
Standard Drug	-6.8829	1.2766	GLY 29	π-H	-6.2445	1.1998	SER 163	H- acceptor
			MET 30	π-H			ARG 288	H- acceptor
							SER 15	H- acceptor
							CYS 53	H- acceptor
							GLY 16	H- acceptor

Table 4.5: Binding affinity of compounds 29, 30 and standard drugs with dihydroorotate dehydrogenase (miltefosine) and L-threonine-3-dehydrogenase (melarsoprol)

Compound	Dihydroorotate dehydrogenase				L-threonine-3-dehydrogenase			
	S (kcal/mol)	RMSD (Å)	Binding Residues	Interaction	S(kcal/mol)	RMSD (Å)	Binding Residues	Interaction
29	-7.1938	1.6238	PRO 1117	π-H	-6.3125	1.3462	THR 273	H- acceptor
30	-7.0889	2.0669	LEU 1077	H- donor	-6.9697	0.9903		
Standard Drug	-8.0114	1.9451	ALA 1079	H- donor	-7.3286	1.4203	LYS 215	H- acceptor
			PRO 1172	H- donor			ASN 199	H- acceptor
			ILE 1014	H- acceptor			PHE 172	H- acceptor
			LEU 1171	π-H			LYS 215	Ionic

Table 4.6: Binding affinity of compounds 29, 30 and standard drug (acarbose) with α-amylase and α-glucosidase

Compound	α- amylase				α- glucosidase			
	S (kcal/mol)	**RMSD (Å)**	**Binding Residues**	**Interaction**	**S(kcal/mol)**	**RMSD (Å)**	**Binding Residues**	**Interaction**
29	-6.4201	0.7825	TYR 62	π-H	-6.1743	0.9462	THR 204	π-H
30	-6.0655	1.6412	ASP 197	H- donor	-5.3775	1.4918	ASP 327	H- donor
			LEU 162	π-H				
Standard Drug	-8.0334	1.6451	GLU 240	H- donor	-8.4888	1.5903	ASP 203	H- donor
			HIS 305	H- donor			ASP 327	H- donor
							ASP 542	H- donor
							THR 205	H- acceptor
							ARG 202	H- acceptor
							HIS 600	H- acceptor
							ARG 526	H- acceptor
							LYS 480	H- acceptor

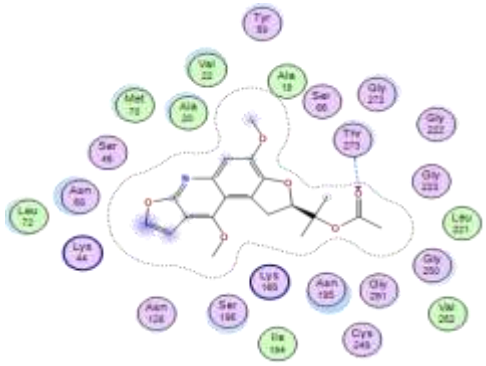

Cpd **29** with dihydroorotate dehydrogenase

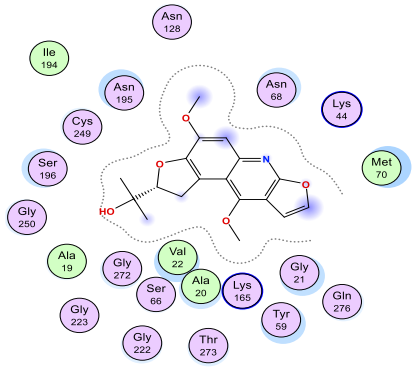

Cpd **30** with dihydroorotate dehydrogenase

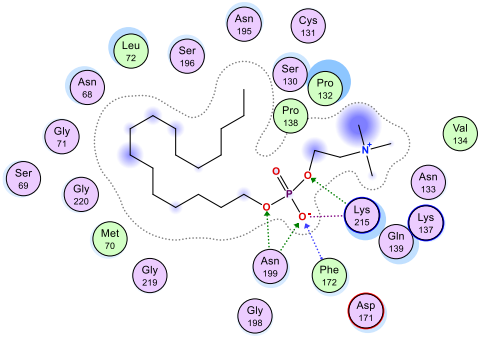

Miltefosine with dihydroorotate dehydrogenase

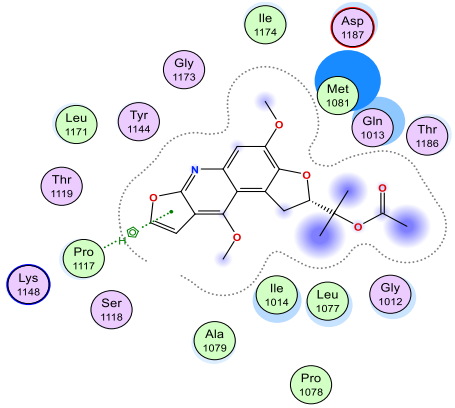

Cpd **29** with L-threonine-3-dehydrogenase

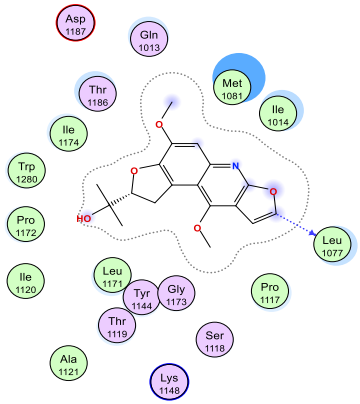

Cpd **30** L-threonine-3-dehydrogenase

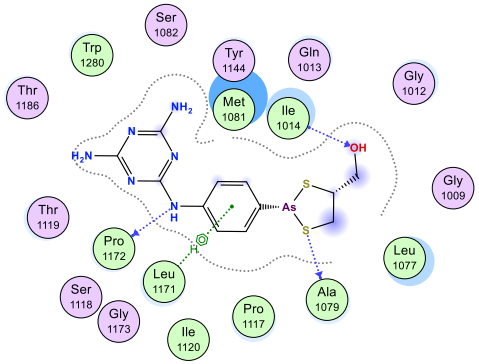

Melarsoprol with L-threonine-3-dehydrogenase

Figure 4.5: 2D interaction of compound 29, 30 and standard drugs with dihydroorotate dehydrogenase and L-threonine-3-dehydrogenase

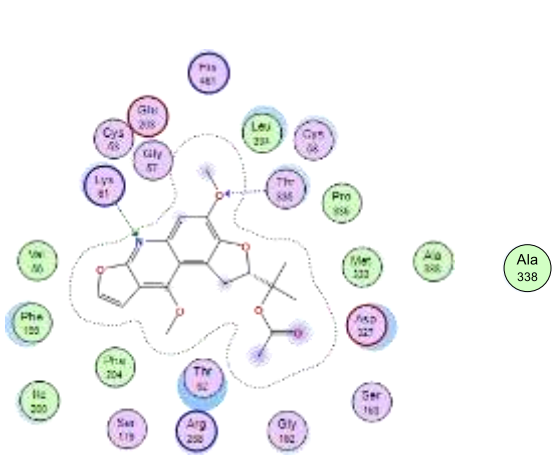

Cpd **29** with trypanothione reductase

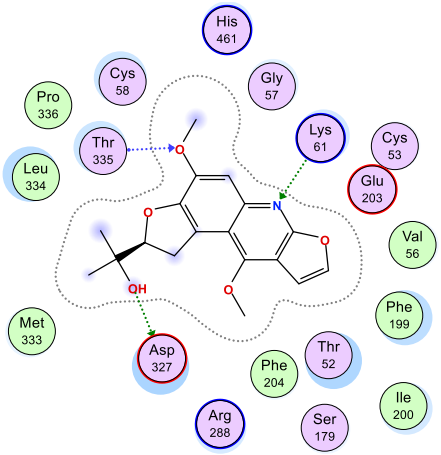

Cpd **30** with trypanothione reductase

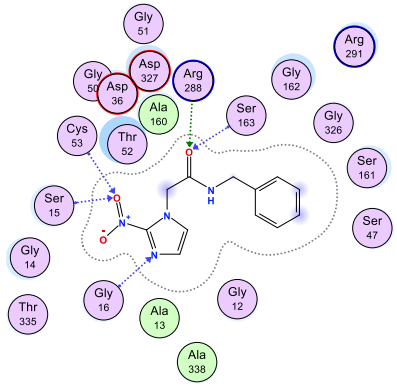

Benznidazole with trypanothione reductase

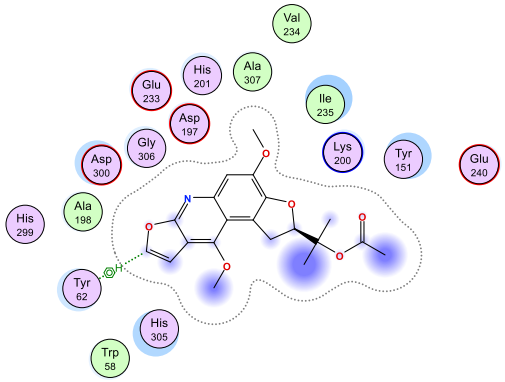

Cpd **29** with α-glucosidase

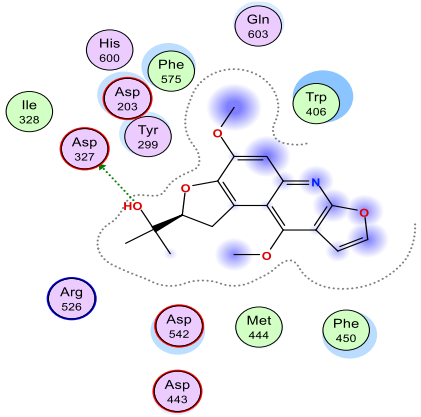

Cpd **30** with α-glucosidase

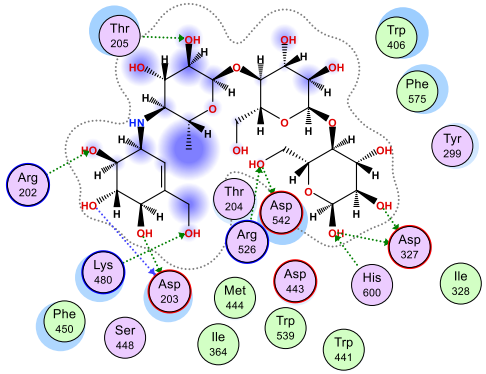

Acarbose with α-glucosidase

Figure 4.6: 2D interaction of compound 29, 30 and standard drugs with trypanothione reductase and α-glucosidase

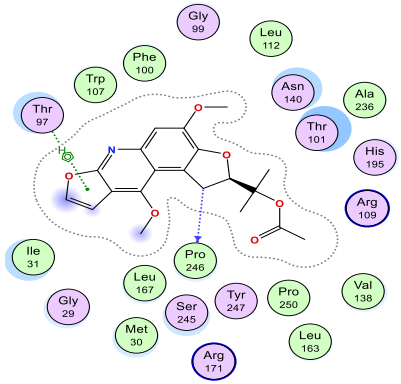

Cpd **29** with *Pf*LDH

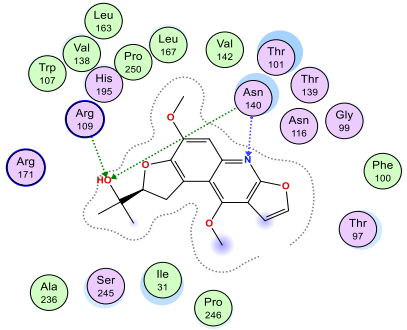

Cpd **30** with *Pf*LDH

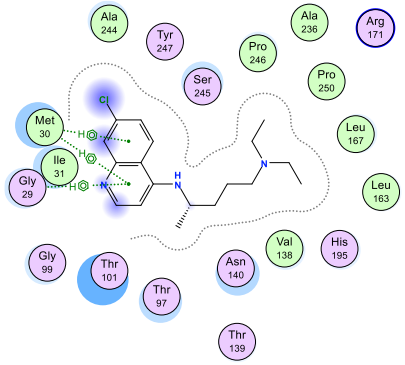

Chloroquine with *Pf*LDH

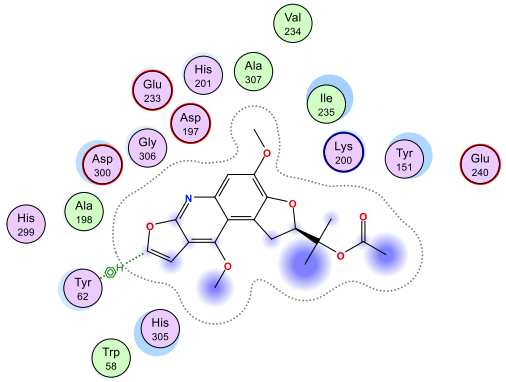

Cpd **29** with α- amylase

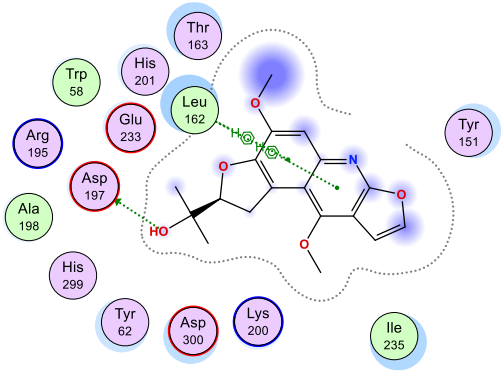

Cpd **30** with α- amylase

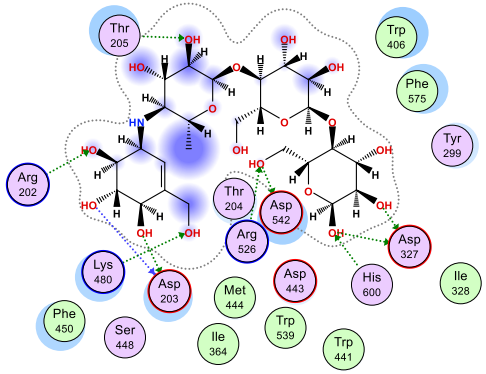

Acarbose with α-amylase

Figure 4.7: 2D interaction of compound 29,30 and the standard drugs with *Pf*LDH and α- amylase

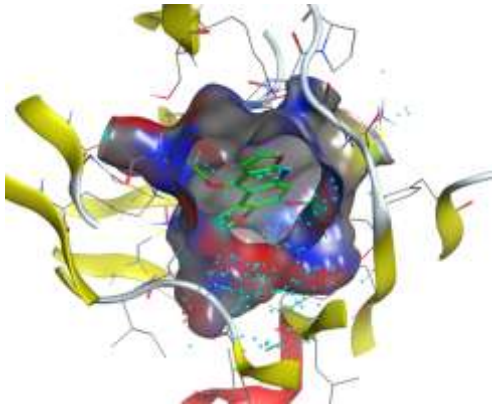

Cpd **29** with dihydroorotate dehydrogenase

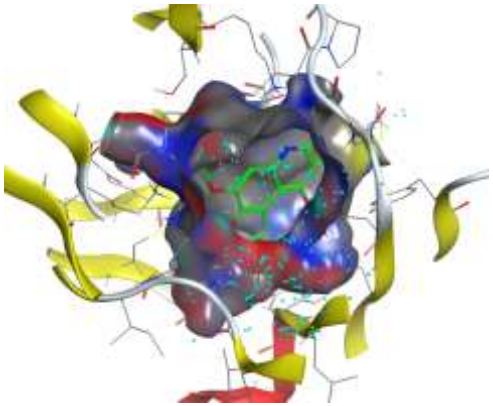

Cpd **30** with dihydroorotate dehydrogenase

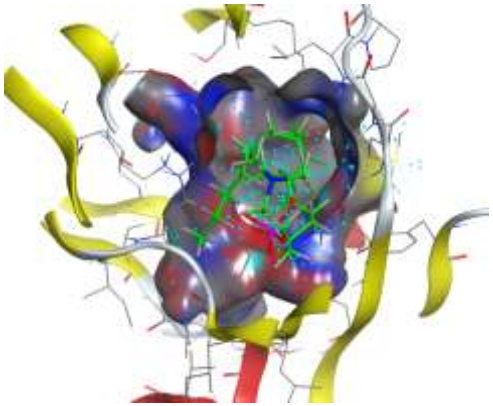

Miltefosine with dihydroorotate dehydrogenase

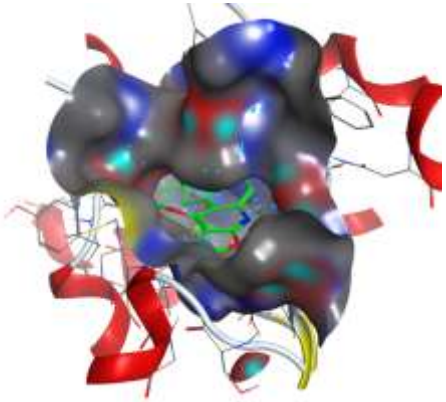

29 with *Pf* LDH

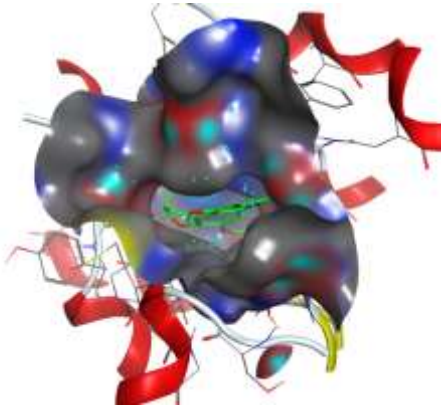

30 with *Pf* LDH

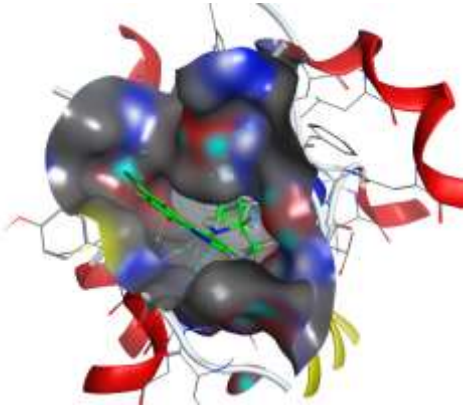

Chloroquine with *Pf* LDH

Figure 4.8: 3D interaction of compound 29, 30 and the standard drugs with dihydroorotate dehydrogenase and *Pf* LDH

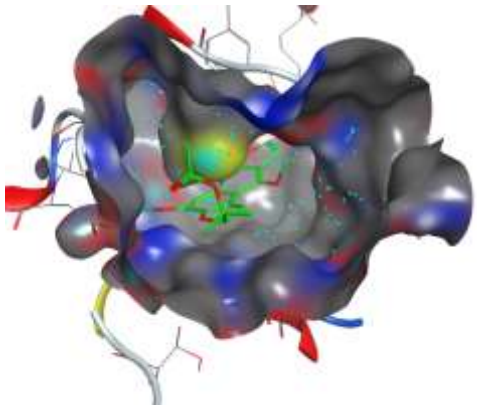

Cpd **29** L-threonine-3-dehydrogenase

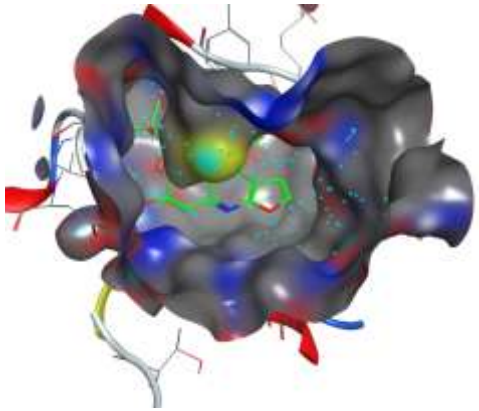

Cpd **30** L-threonine-3-dehydrogenase

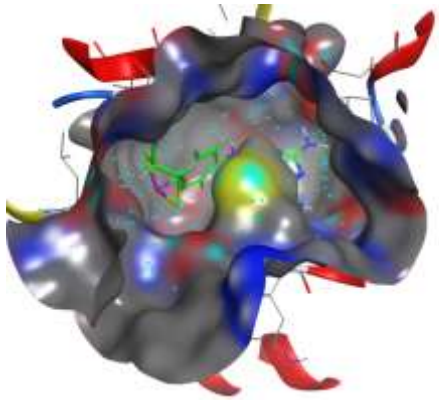

Melarsoprol with L-threonine-3-dehydrogenase

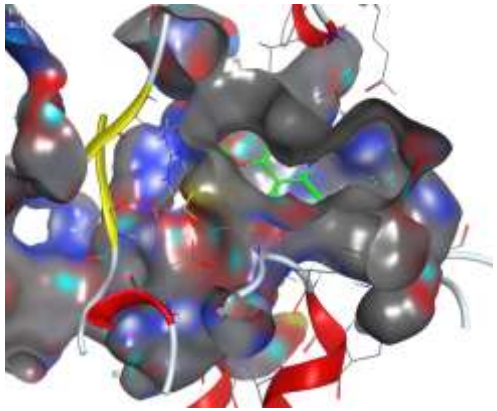

Cpd **29** with trypanothione reductase

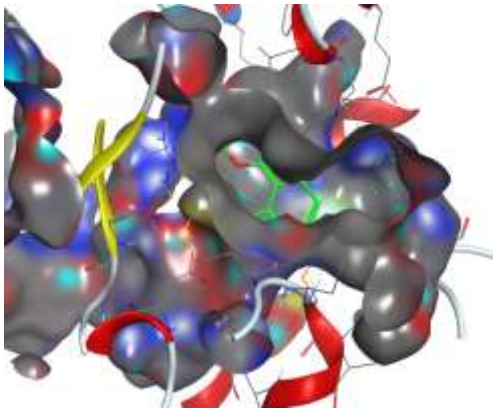

Cpd **30** with trypanothione reductase

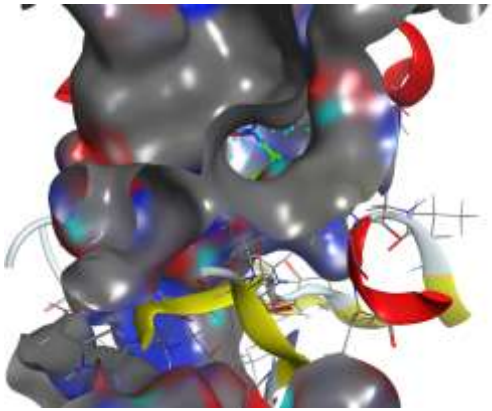

Benznidazole with trypanothione reductase

Figure 4.9: 3D interaction of compounds 29, 30 and the standard drugs with L-threonine-3-dehydrogenase and trypanothione reductase

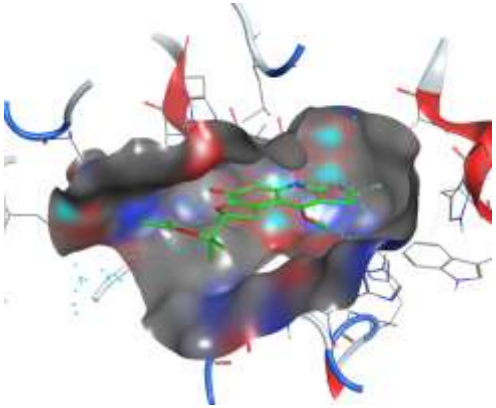

Cpd **29** with α- amylase

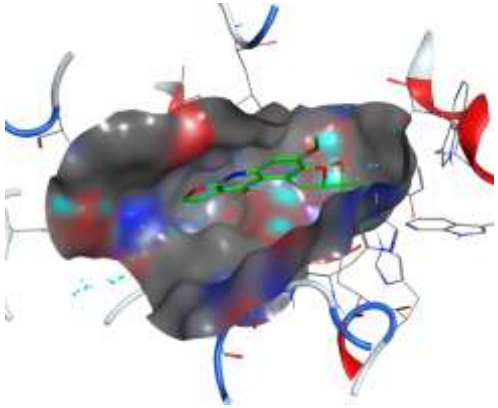

Cpd **30** with α- amylase

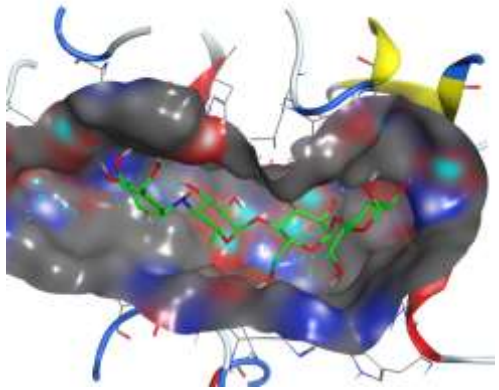

Acarbose with α- amylase

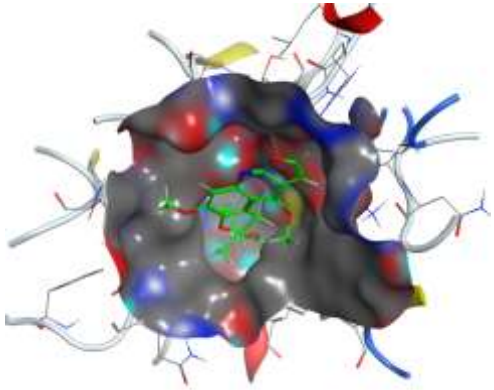

Cpd **29** with α-glucosidase

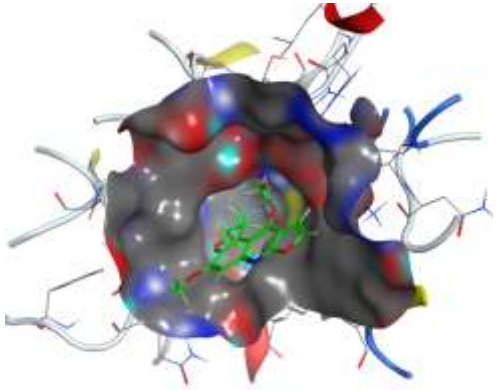

Cpd **30** with α-glucosidase

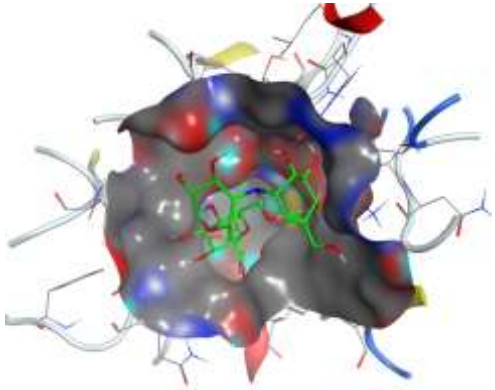

Acarbose with α-glucosidase

Figure 4.10: 3D interaction of compounds 29, 30 and the standard drugs with α- amylase α-glucosidase

Docking compound **29** into the binding pocket of *Plasmodium falciparum* lactate dehydrogenase revealed hydrogen bond interactions with interface residues PRO 246, along with hydrophobic π-H-type interactions with THR 97 residues, resulting in a binding affinity of -7.0997 kcal/mol. It also formed hydrogen bond interactions with THR 273 residues of dihydroorotate dehydrogenase, achieving a docking score of -7.1938 kcal/mol. Additionally, conventional hydrogen interactions were observed with trypanothione reductase interface residues LYS 61 and THR 335, leading to a binding affinity of -8.1911 kcal/mol. Upon analysis of its interaction with L-threonine-3-dehydrogenase, compound **29** exhibited π-H hydrophobic interactions with the PRO 1117 residue and a binding affinity of -6.3125 kcal/mol.

For compound **30**, binding scores of −7.1973 and –7.0889 kcal/mol with *Plasmodium falciparum* lactate dehydrogenase and dihydroorotate dehydrogenase were noted, respectively. Interaction with *Plasmodium falciparum* lactate dehydrogenase involved hydrogen bonds with ASN 140 and ARG 109 residues. Hydrogen bond interaction was also observed with trypanothione reductase, involving ASP 327, THR 335, and LYS 61 residues, with a binding affinity of -7.8106 kcal/mol. The molecule formed hydrogen bonds with the LEU 1077 residue of L-threonine-3-dehydrogenase, with a binding affinity of −6.9697 kcal/mol.

Additionally, compound **29** displayed a docking score of -6.4201 kcal/mol with α-amylase and involved π-H hydrophobic interactions with TYR 62 residue. It exhibited π-H interaction with THR 204 residue of α-glucosidase, with a binding score of -6.1743 kcal/mol. On the other hand, compound **30** exhibited π-H hydrophobic and hydrogen bond interactions with ASP 197 and LEU 162 respectively, with α-amylase, achieving a binding score of -6.0655 kcal/mol. The interaction of compound **30** with α-glucosidase displayed hydrogen interaction with ASP 327, with a binding score of 5.3775 kcal/mol.

Chloroquine, used as the control, exhibited a binding score of −6.8829 kcal/mol with *Pf* lactate dehydrogenase and formed hydrophobic π-H-type interactions with residues GLY 29 and MET 30. Benznidazole displayed a binding affinity of −6.2445 kcal/mol with trypanothione reductase, forming hydrogen bond interactions with SER 163, ARG 288, SER 15, CYS 53, and GLY 16 residues. Melarsoprol showed a binding affinity of -7.3286 kcal/mol with L-threonine-3-dehydrogenase and formed hydrogen

bonds with ALA 1079, PRO 1172, ILE 1014 residues, along with hydrophobic π-H-type interactions with LEU 1171. Miltefosine formed hydrogen bonds with dihydroorotate dehydrogenase LYS 215, ASN 199, and PHE 172 residues, along with an ionic bond with LEU 215, achieving a binding score of -8.0114 kcal/mol. Acarbose, displayed a binding affinity of -8.4888 kcal/mol with α-amylase, forming hydrogen bond interactions with ASP 203, ASP 327, ASP 542, THR 205, ARG 202, ARG 526, and LYS 480 residues. Docking compound acarbose into the binding pocket of α-glucosidase, it exhibited a binding affinity of -8.0334 kcal/mol and showcased hydrogen interaction with GLU 240 and HIS 305.

In comparison with standard drugs, both compounds **29** and **30** exhibited higher docking scores, than chloroquine and benznidazole (**Table 4.4**) indicating potentially stronger binding affinities with PfLDH and trypanothione reductase. Both compounds **29** and **30** displayed comparable docking scores with dihydroorotate dehydrogenase and L-threonine-3-dehydrogenase, although slightly lower than the standard drug (melarsoprol and miltefosine). This validates their use as first-line treatments for kinetoplastid diseases (Alunda, 2023). Furthermore, the two compounds demonstrated a lower binding affinity with both α-glucosidase and α-amylase compared to the standard drug, acarbose (Table 4.6). These docking results are consistent with the α-amylase inhibition experimental outcomes, supporting the conclusions made *vide supra*. The binding score and ligand interactions of the compounds and the control drugs are illustrated in **Figures 4.5** to **4.11** and detailed in **Tables 4.4** to **4.6**.

The two compounds, along with the control drugs, formed various bonds with main amino acid residues, potentially interfering with the normal physiological functions of the enzymes. This suggests that the compounds are good inhibitors, effectively targeting various proteins with comparable potency. These compounds demonstrated remarkable inhibition potential comparable to, and even greater than some currently available drugs, highlighting their potential as viable alternatives in the fight against these diseases. The scores for these compounds, which surpassed those of some currently available drugs, were intriguing. While traditional medicinal use of the plant hinted at its therapeutic potential, the extent of the activity observed in the isolated compounds exceeded expectations. The docking studies indicate that the ligands bind to the active sites of the receptors with good binding energy and RMSD values. These

findings contribute to the understanding of the mechanism(s) of action of these natural products in managing protozoal diseases and diabetes. However, further *in vivo* and *in vitro* antiprotozoal activity are recommended to validate the findings from the docking simulations.

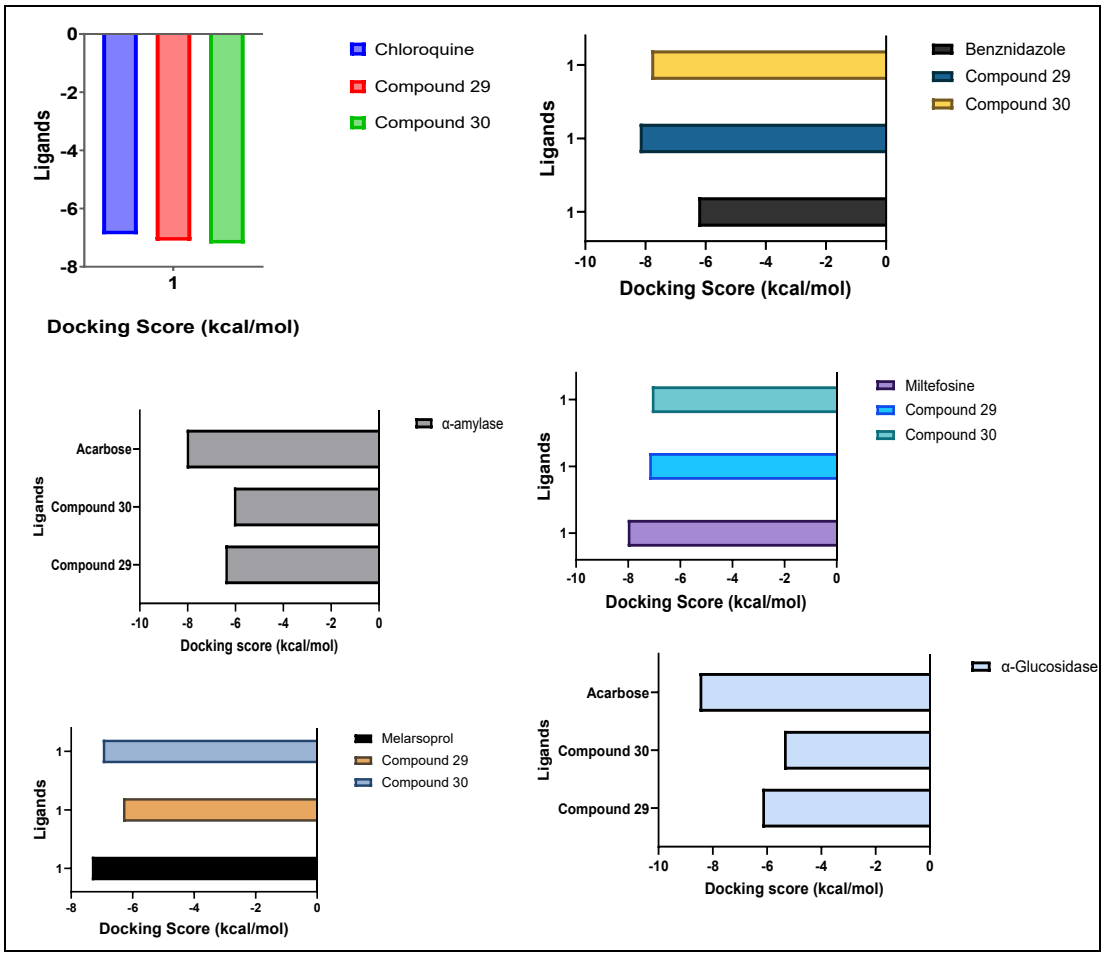

Figure 4.11: Graphical representation of docking Scores for Compounds 29 and 30 Compared to Standard Drugs

4.3.3: Physicochemical and ADME Properties

Physicochemical properties are crucial for determining a compound's solubility, stability, and bioavailability, which directly affect its effectiveness as a drug (Kibet et al., 2024). ADME (Absorption, Distribution, Metabolism, and Excretion) properties are essential for understanding how a drug is absorbed, distributed within the body, metabolized, and excreted, influencing its overall therapeutic potential and safety.

Molecular weight is a crucial physicochemical descriptor that is taken into consideration while developing new drugs since it directly impacts how molecules

diffuse across cell membranes (Ojuka et al., 2023). A fundamental theory in drug design is the Lipinski principle, which states that a compound's optimal molecular weight for efficient absorption and distribution should be less than 500 g/mol (Lipinski et al., 1997). With molecular weights below 500 g/mol (compound **29** = 371.38 g/mol and compound **30** = 329.35 g/mol), the two isolated compounds met this criterion making them potential lead compounds.

The number of rotatable bonds in a compound significantly influences a molecule's physicochemical and biological properties. Rotatable bonds more than nine impede diffusion across cell membranes, reducing oral bioavailability (Kibet et al., 2024). Thus, the therapeutic potency is compromised, frequently resulting in decreased binding affinity with the intended target. According to Bryant et al. (2019), molecules with extreme flexibility may not comply with the prerequisites for drug-likeness. Compound **29** and **30** demonstrated rotatable bonds that fell below the threshold of nine (Compound **29** = 5 and **30** = 3), indicating that they can easily permeate the cell membrane and reach the desired target.

One crucial physicochemical factor in predicting a drug candidate's oral bioavailability is the quantification of hydrogen bond donors and acceptors (Wekesa et al., 2023). These properties significantly impact the adsorption and distribution of pharmacological drugs since they affect the passive diffusion mechanisms across cell membranes. The rules of Lipinski and Veber state that an optimal number of hydrogen bond donors is ≤ 5, and acceptors ≤ 10 and that violating this threshold could suggest potential challenges with bioavailability (Lipinski et al., 2012; Veber et al., 2002). Both compounds (compound **29**; hydrogen bond donors = 0 and acceptors = 7; Compound **30**; hydrogen bond donors = 1 and acceptors = 6) adhere to these criteria, signaling their potential as lead candidates.

Topological polar surface area (TPSA) determines drug-likeness by influencing drug transport properties such as GI absorption and blood brain barrier (BBB) permeation (Kimani et al., 2023). This parameter is beneficial as it does not necessitate the creation of three-dimensional structures. Additionally, it is highly associated with passive molecule transport across membranes (Ertl et al., 2000). Therapeutic molecule penetration of the blood-brain barrier and intestinal absorption have been studied using this parameter, which quantifies a drug-like molecule's capacity to cross cell

membranes (Prasanna & Doerksen, 2009). The TPSA of an appropriate medicine should be less than 140 $Å^2$, as stated by Verber et al. (2002). The two compounds exhibited a recommended TPSA values (compound **29**; TPSA = 80.02 $Å^2$, compound **30**; TPSA =73.95 $Å^2$), implying that these compounds are bioavailable.

The number of aromatic heavy atoms is a crucial descriptor in drug design, influencing drug permeation and contributing to compound drug-likeness (Ojuka et al., 2023). Both compounds adhere to the prescribed rules for the number of heavy atoms, with 13 heavy atoms in each compound.

Fsp3 is a fraction of hybridized sp3 carbon atoms, crucial in evaluating a compound's drug potential. Molecules with high Fsp3 values possess better characteristics, like higher solubility and lower protein binding (Kibet et al., 2024). Empirical evidence demonstrates that higher saturation, measured by the fraction of carbon atoms with sp3 hybridization (Csp3), is associated with a higher likelihood of positive clinical results for pharmacological treatments. This is because, molecules with high saturation are more likely to be metabolized and excreted from the body (Wei et al., 2020). This parameter has been employed as a solubility predictor (Yan & Gasteiger, 2003), potentially associated with elevated solubility attributes. The two compounds (Compound **29**; Fraction Csp3=0.40, Compound **30**; Fraction Csp3 = 0.39) each exhibited superior solubility and, as a result, superior drug-like properties, evidently indicating their potential as drugs in light of the specified threshold criterion (fraction Csp3 of ≥ 0.42).

4.3.4: Lipophilicity and Water Solubilities

Lipophilicity and water solubility influence a drug candidate's bioavailability (Ononamadu & Ibrahim, 2021). A compound's ability to dissolve in fats or lipids is measured by its lipophilicity, also known as the n-octanol/water partition coefficient ($\log P_{o/w}$) (Ojuka et al., 2023). Predicting the biological efficacy of possible drugs is based on this property, which substantially influences molecule penetration across membranes and impacts binding to target receptors and plasma proteins. The generally held notion is that drug molecules must be lipophilic to exhibit efficient absorption (Zupančič & Bernkop-Schnürch, 2017).

Nevertheless, the ideal lipophilicity of a drug-like molecule is contingent upon the target protein and the intended application (Young et al., 2022). Too lipophilic compounds can have poor solubility and bioavailability, whereas too hydrophilic compounds can have poor membrane permeability (Wardecki et al., 2023). A lipophilicity greater than five is frequently associated with undesirable pharmacological properties such as reduced water solubility, tissue accumulation, elevated metabolic turnover, and potent binding to plasma proteins (Kibet et al., 2024; Tsaioun et al., 2016). Furthermore, research suggests that molecules with moderate lipophilicity, varying around two, often exhibit the best capabilities to bind to molecules (Tsaioun et al., 2016). Compound **29** and **30** had consensus lipophilicities (Log $P_{o/w}$) of 3.21 and 2.77, respectively, indicating that these compounds exhibit promising potential candidates for drug design and study.

SwissADME employs two topological approaches, the ESOL model and the Ali model, along with a fragmental approach developed by SILICOS-IT, to predict water solubility (Daina et al., 2017). The Ali model exhibits a stronger positive correlation for predicted water solubility with experimental values (R^2= 0.81) compared to SILICOS-IT (R^2 = 0.75) and the ESOL model (R^2= 0.69) (Daina et al., 2017). Based on the solubility classification criteria provided by Daina et al., 2017, (insoluble < −10 < poorly < −6 < moderately < −4 < soluble < −2 < very < 0 < highly), compound **29** was moderately soluble according to the Ali, SILICOS-IT, and ESOL approaches. However, compound **30** was highly soluble based on the ESOL approach and moderately soluble based on SILICOS-IT and Ali approaches. Empirical evidence suggests that the target log S range of −1 to −5 for most drugs reflects a desired compromise to achieve aqueous solubility and hydrophobicity necessary for crossing a membrane. Arguably, both compounds fell within this range, suggesting their potential to traverse cell membranes and be absorbed. Compound **30**'s presence in both the yellow and white regions of the BOILED-Egg (**Figure 4.12**) suggests it has higher lipophilicity and lower polarity, optimizing its ability to cross both the GI tract and the BBB (Daina et al., 2017). In contrast, Compound **29** has higher polarity, contributing to its inability to penetrate the BBB while still maintaining adequate lipophilicity for GI absorption.

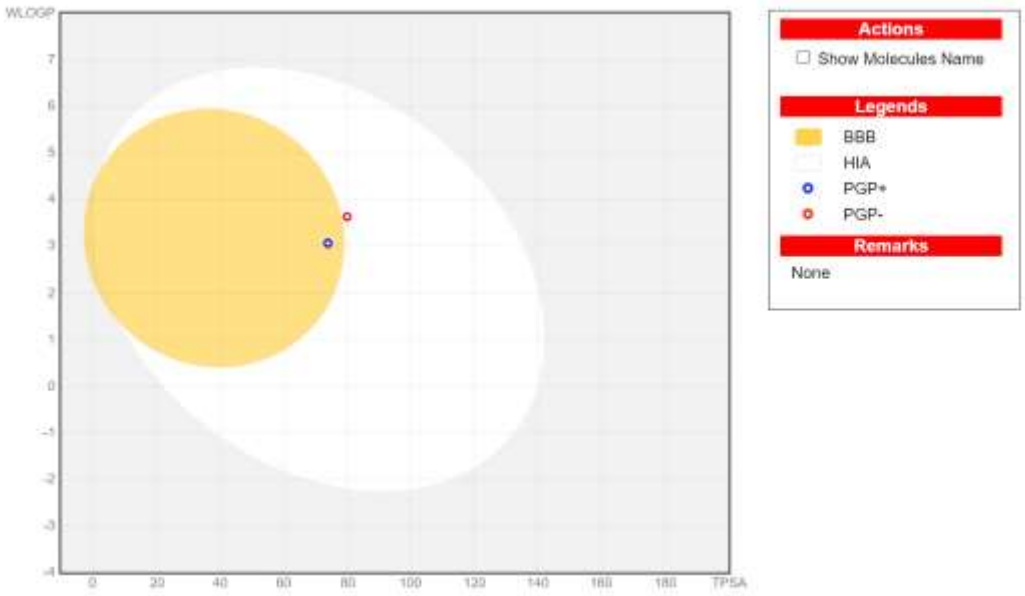

Figure 4.12: BOILED-Egg Plot for compound 29 and 30

4.3.5: Pharmacokinetic Properties

Pharmacokinetic characteristics such as GI absorption, BBB permeability, P-gp substrates, and the inhibition of the main cytochromes also impact bioavailability (Jia et al., 2020). The proportion of a dose that reaches the portal vein is used to measure the amount of GI absorption in humans. The amount of drug that enters the bloodstream depends on how much of it is absorbed by the intestinal villi and microvilli (Kibet et al., 2024). It is a complex metric that depends on several variables, such as the substance's physicochemical state, GI physiology, formulation, and additional biopharmaceutical parameters (Sjögren et al., 2016).

The two compounds exhibited a high gastrointestinal absorption, as indicated by their positions in the white region of the BOILED-Egg plot (**Figure 4.12**). This region signifies compounds that possess favorable properties for oral bioavailability. Effective GI absorption generally requires a balance of lipophilicity and solubility to ensure that the compound can dissolve in the aqueous environment of the GI tract and subsequently cross the lipid-rich cellular membranes (Daina & Zoete, 2016).

The BBB acts as a protective barrier, regulating the penetration of substances between the bloodstream and the central nervous system (CNS). It regulates CNS homeostasis as a barrier to entering undesirable substances into the brain (Kibet et al., 2024). Nonetheless, it also prevents drugs from reaching the brain and having their desired

effect. BBB permeability prediction assists in ascertaining the potential of drugs to enter the CNS (Ojuka et al., 2023). The BBB descriptor predicted the permeable compounds using yes/no in a binary format by SwissADME (Daina et al., 2017). Compound **30**, which is located in the yellow region of the BOILED-Egg plot (**Figure 4.12**), was predicted to have BBB permeability, indicating high bioavailability to the brain. This indicates that compound **30** has the necessary physicochemical properties, such as higher lipophilicity and lower polarity, which allow it to navigate the hydrophobic environment of the BBB. Compound **29** does not penetrate the BBB, as it falls outside the yellow region of the BOILED-Egg plot (**Figure 4.12**).

This suggests that compound **29** has higher polarity or insufficient lipophilicity, preventing it from effectively crossing into the brain. However, this might not present a major obstacle as numerous strategies have been developed to facilitate the transport of drugs that do not naturally pass through the BBB into the brain. Some of these approaches include the use of nanotechnology to package drugs in nanoparticles that can pass through the BBB such as; increasing BBB permeability using ultrasound and microbubbles and using blockers of efflux transporters or directly injecting the drugs into the brain. As illustrated in **Figure 4.12** and **4.13** compound **29**, despite not penetrating the BBB, shows good GI tract absorption, making it viable candidate for oral medications targeting non-CNS conditions. Compound **30**, which also demonstrates good GI absorption, is versatile, as it can be effectively delivered orally and reach the CNS.

P-glycoprotein (P-gp) is a transmembrane protein that mediates drug efflux and transport in the GI, BBB, and other organs (Ojuka et al., 2023). This protein in enterocytes binds drug substrates and transports them into the GI lumen, thus reducing their bioavailability and leading to lower drug efficacy. There is evidence that multidrug resistance of tumor cells is associated with increased expression of the MDR1 gene (multidrug resistance 1 gene) encoding this protein (Newman & Cragg, 2016). Since this protein is specific to the substrate, it is important to determine how potential drug-like compounds might bind, predicting an appropriate dosage for administration (Ononamadu & Ibrahim, 2021). P-gp was determined as a substrate of compound **30**. This suggests that P-gp can recognize and eject this compound from its substrates. Conversely, compound **29** did not interact with P-gp (**Figure 4.13**). In order

to guarantee the drug substrate's practical therapeutic consequences, these findings highlight the significance of comprehending the substrate–P–gp interactions and potential strategies for avoiding the binding or releasing of the drug substrate from this protein.

Knowledge of the interactions between compounds and cytochrome P450 (CYP) is essential in drug development and metabolism (Kibet et al., 2024; Ojuka et al., 2023; Wekesa et al., 2023). The inhibition of these isoforms primarily influences pharmacokinetic interactions between co-administered medications. Inhibiting the activity of these enzymes by one drug may cause the other drugs' metabolisms to change, which may cause the other drugs to accumulate or produce other potentially hazardous compounds (Kirchmair et al., 2015). The binary (yes/no) prediction of primary cytochrome inhibition was determined using SwissADME. Compound **30** inhibited a subset of the major CYP enzymes studied, indicating differences in their metabolic profiles and potential for medication interactions. Compound **29** inhibited all major CYP enzymes tested as illustrated in **Figure 4.13**.

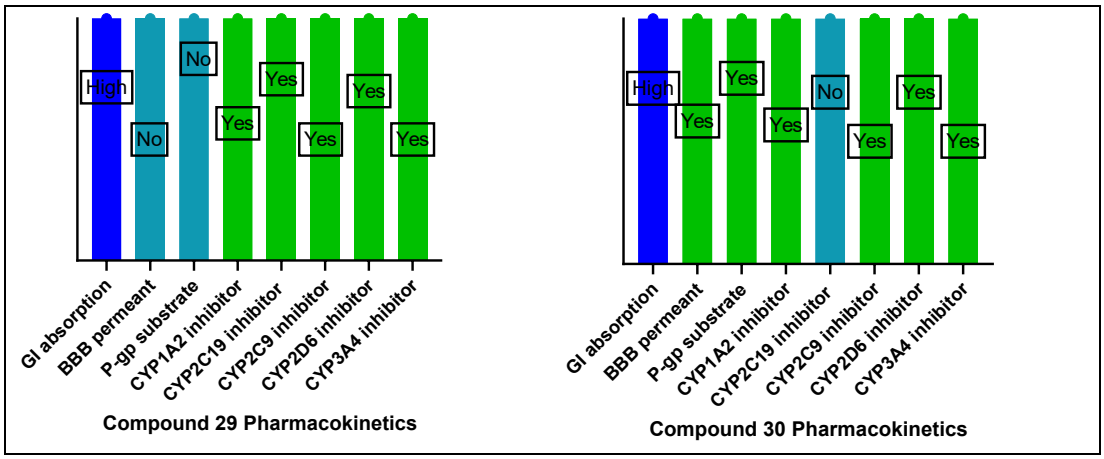

Figure 4.13: Graphs showing pharmacokinetic properties of Compound 29 and 30

4.3.6: Medicinal Chemistry: Synthetic Accessibility, PAINS, Brenk, and Lead-likeness

Synthetic accessibility refers to the simplicity of a molecule's synthesis, an essential consideration in compound profiling for drug discovery, as potential synthesis may occur in later stages (Kibet et al., 2024). SA is typically rated on a scale from 1 to 10, where a lower score indicates easier synthesis and a higher score implies greater

difficulty (Daina et al., 2017). These two compounds fell within the category of being relatively easy to synthesize (SA: **29** = 3.88; **30** = 3.67), likely due to their simple structural features facilitating synthesis.

Pan Assay Interference Compounds (PAINS), are molecules containing substructures that elicit strong responses in assays, irrespective of the protein target. They serve to flag potentially problematic fragments that could yield false positive results in *in silico* assays (Ononamadu & Ibrahim, 2021). Since neither compound was flagged as a PAINS compound, it suggests a reduced likelihood of generating misleading positive responses when interacting with various protein targets in *in silico* assays. The absence of PAINS classification for these compounds underscores their favorable suitability for assays, minimizing concerns regarding false-positive outcomes.

Brenk alerts identify compound fragments that may exhibit toxicity, chemical reactivity, or metabolic instability, aiding in the identification of compounds with undesirable properties (Kibet et al., 2024). The absence of brenk alerts for these compounds suggests that they lack fragments associated with toxic, reactive, or metabolically unstable properties.

Lead-likeness focuses on identifying compounds suitable for optimization in drug discovery based on their physicochemical properties (Polinsky, 2008). Compound **29** deviates from one lead-likeness rule, with its molecular weight exceeding the recommended threshold of 350 Da, potentially impacting its suitability for drug optimization. Conversely, compound **30** fully complies with lead-likeness rules, indicating its favorable characteristics for optimization in drug discovery.

4.3.7: Toxicity

Toxicity is the extent to which a molecule can affect an organism's organs, cells, and tissues. Majority of drugs fail at the clinical trial phase or are withdrawn from the market due toxicity (Ojuka et al., 2023). Hence, early detection of toxicity would be highly advantageous. In this study, several toxicity endpoints were employed to evaluate the potential toxicity of the compounds. hERG potassium ion channel inhibition, which is essential for the regulation of the heart's electrical activity, was assessed. Blockers of this channel could cause arrhythmia or other cardiac toxicity,

thus highlighting the importance of early cardiac toxicity prediction in drug discovery (Sato et al., 2018).

The AMES test was also used to determine the carcinogenicity potential; the test is based on the principle that mutant bacterial cells can grow and revert mutations in the presence of mutagenic substances (Tayebi & Moharamzadeh, 2017). Hepatotoxicity, stemming from liver damage disrupting metabolic processes, and skin sensitization, a concern for externally applied substances causing allergic dermatitis (Durán-Iturbide et al., 2020), were also examined. The findings indicate a lower toxicity profile for these compounds. Compound **29** and **30** both exhibited similar toxicity predictions for most endpoints. Both compounds were not predicted to be AMES toxic, hERG I or II inhibitors, or skin sensitizers. However, both compounds were flagged as hepatotoxic. Although additional experimentation would be imperative to validate whether these compounds exhibit hepatotoxic effects.

CHAPTER FIVE

CONCLUSION AND RECOMMENDATIONS

5.1: Conclusion

In this study, investigation of methanol leaves extracts of *Vepris glandulosa* was conducted. Two known furoquinoline compounds; choisyine acetate and choisyine were isolated and characterized.

The antiprotozoal activity prediction through molecular docking simulation targeting various proteins revealed significant interactions with the target proteins and potential to inhibit protozoa-associated biomarkers.

Additionally, α-amylase inhibition assay and molecular docking demonstrate that these compounds are effective inhibitors of α-amylase and glucosidase enzyme making them suitable for diabetes drug development.

The physicochemical and ADMET properties further justify their potential as lead candidates in drug research. Synthetic accessibility, PAINS, Brenk alerts and toxicity revealed their ease of synthesis, lack of undesirable features and low toxicity profile.

The findings from this study also revealed that *V. glandulosa* contains alkaloids with the potential to inhibit diabetes and protozoa-associated biomarkers, thereby providing a scientific rationale for using the plant in Kenyan folk medicine as treatment for various health issues.

5.2: Recommendations for Further Studies

1. Further exploration of *V. glandulosa* leaves using advanced separation methods like HPLC to thoroughly isolate most of the minor phyto-constituents

2. Investigation into the antiprotozoal activity and toxicity of the isolated compounds through both *in vivo* and *in vitro* experiments is recommended. This is to validate the findings obtained from the molecular docking analysis.

3. A thorough investigation of root and stem barks of *V. glandulosa* is recommended for a more comprehensive understanding of its chemical composition.

REFERENCES

Agents, A., Lee, S., Kim, M., Hayat, F., & Shin, D. (2019). *Recent Advances in the Discovery of Novel*.

Ahmed, B., Al-Rehaily, A. J., Al-Howiriny, T. A., El-Sayed, K. A., & Ahmad, M. S. (2003). Scropolioside-D2 and harpagoside-B: two new iridoid glycosides from Scrophularia deserti and their antidiabetic and antiinflammatory activity. *Biological and Pharmaceutical Bulletin*, *26*(4), 462–467.

Aksoy, S., Buscher, P., Lehane, M., Solano, P., & Van Den Abbeele, J. (2017). Human African trypanosomiasis control: achievements and challenges. *PLoS Neglected Tropical Diseases*, *11*(4), e0005454.

Al-Musayeib, N. M., Mothana, R. A., Al-Massarani, S., Matheeussen, A., Cos, P., & Maes, L. (2012). Study of the in vitro antiplasmodial, antileishmanial and antitrypanosomal activities of medicinal plants from Saudi Arabia. *Molecules*, *17*(10), 11379–11390. https://doi.org/10.3390/molecules171011379

Al, H. (2008). Natural products in drug discovery Drug Discov. *Today*, *13*, 894–901.

Alam, U., Asghar, O., Azmi, S., & Malik, R. A. (2014). General aspects of diabetes mellitus. *Handbook of Clinical Neurology*, *126*, 211–222.

Alemayehu, B., & Alemayehu, M. (2017). Leishmaniasis: a review on parasite, vector and reservoir host. *Health Science Journal*, *11*(4), 1.

Alsan, M. (2015). The effect of the tsetse fly on African development. *American Economic Review*, *105*(1), 382–410.

Alunda, J. M. (2023). *Antileishmanial and Antitrypanosomes Drugs for the Current Century. Microorganisms 2024, 12, 43*.

Andrews, K. T., Fisher, G., & Skinner-Adams, T. S. (2014). Drug repurposing and human parasitic protozoan diseases. *International Journal for Parasitology: Drugs and Drug Resistance*, *4*(2), 95–111. https://doi.org/10.1016/j.ijpddr.2014.02.002

Antonovics, J., Wilson, A. J., Forbes, M. R., Hauffe, H. C., Kallio, E. R., Leggett, H. C., Longdon, B., Okamura, B., Sait, S. M., & Webster, J. P. (2017). The evolution of transmission mode. *Philosophical Transactions of the Royal Society B: Biological Sciences*, *372*(1719), 20160083.

Artasensi, A., Pedretti, A., Vistoli, G., & Fumagalli, L. (2020). Type 2 diabetes mellitus: a review of multi-target drugs. *Molecules*, *25*(8), 1987.

Ashley, E. A., & Phyo, A. P. (2018). Drugs in Development for Malaria. *Drugs*, *78*(9), 861–879. https://doi.org/10.1007/s40265-018-0911-9

Ayafor, J. F., & Okogun, J. I. (1982). Isolation and identification of three new phenolic furoquinoline alkaloids from Teclea verdoorniana Exell & Mendonça (Rutaceae). *Journal of the Chemical Society, Perkin Transactions 1*, 909–915.

Ayafor, J. F., Sondengam, B. L., Connolly, J. D., Rycroft, D. S., & Okogun, J. I. (1981). Tetranortriterpenoids and related compounds. part 26. tecleanin, a possible precursor of limonin, and other new tetranortriterpenoids from Teclea grandifolia Engl.(Rutaceae). *Journal of the Chemical Society, Perkin Transactions 1*, 1750–1753.

Ayafor, J. F., Sondengam, B. L., & Ngadjui, B. T. (1982). Quinoline and indolopyridoquinazoline alkaloids from Vepris louisii. *Phytochemistry*, *21*(11), 2733–2736.

Bello, O. M., Zaki, A. A., Khan, S. I., Fasinu, P. S., Ali, Z., Khan, I. A., Usman, L. A., & Oguntoye, O. S. (2017). Assessment of selected medicinal plants indigenous to West Africa for antiprotozoal activity. *South African Journal of Botany*, *113*, 200–211. https://doi.org/10.1016/j.sajb.2017.08.002

Boyd, D. R., Sharma, N. D., Loke, P. L., Malone, J. F., McRoberts, W. C., & Hamilton, J. T. G. (2007). Synthesis, structure and stereochemistry of quinoline alkaloids from Choisya ternata. *Organic and Biomolecular Chemistry*, *5*(18), 2983–2991. https://doi.org/10.1039/b707576f

Bryant, M. J., Black, S. N., Blade, H., Docherty, R., Maloney, A. G. P., & Taylor, S. C. (2019). The CSD drug subset: The changing chemistry and crystallography of small molecule pharmaceuticals. *Journal of Pharmaceutical Sciences*, *108*(5), 1655–1662.

Butterworth, P. J. (1972). The use of Dixon plots to study enzyme inhibition. *Biochimica et Biophysica Acta (BBA)-Enzymology*, *289*(2), 251–253.

Capela, R., Moreira, R., & Lopes, F. (2019a). An overview of drug resistance in protozoal diseases. *International Journal of Molecular Sciences*, *20*(22), 5748.

Capela, R., Moreira, R., & Lopes, F. (2019b). An overview of drug resistance in protozoal diseases. *International Journal of Molecular Sciences*, *20*(22). https://doi.org/10.3390/ijms20225748

Chanda, K. (2021). An overview on the therapeutics of neglected infectious diseases—Leishmaniasis and Chagas diseases. *Frontiers in Chemistry*, *9*, 622286.

Chaniad, P., Mungthin, M., Payaka, A., Viriyavejakul, P., & Punsawad, C. (2021). Antimalarial properties and molecular docking analysis of compounds from Dioscorea bulbifera L. as new antimalarial agent candidates. *BMC Complementary Medicine and Therapies*, *21*(1), 1–10. https://doi.org/10.1186/s12906-021-03317-y

Cheplogoi, P. K., Mulholland, D. A., Coombes, P. H., & Randrianarivelojosia, M. (2008). An azole, an amide and a limonoid from Vepris uguenensis (Rutaceae). *Phytochemistry*, *69*(6), 1384–1388.

Committee, W. H. O. E. (2002). Control of Chagas disease. *World Health Organization Technical Report Series*, *905*, i.

Copeland, R. A., & Anderson, P. S. (2002). Enzymes and enzyme inhibitors. *Textbook of Drug Design and Discovery*, *3*, 328–363.

Coura, J. R., & Viñas, P. A. (2010). Chagas disease: a new worldwide challenge. *Nature*, *465*(7301), S6–S7.

Cowie, C. C., Casagrande, S. S., Menke, A., Cissell, M. A., Eberhardt, M. S., Meigs, J. B., Gregg, E. W., Knowler, W. C., Barrett-Connor, E., & Becker, D. J. (2018). *Diabetes in America*.

Dagne, E., Yenesew, A., Waterman, P. G., & Gray, A. I. (1988). The chemical systematics of the Rutaceae, subfamily Toddalioideae, in Africa. *Biochemical Systematics and Ecology*, *16*(2), 179–188.

Dahal, P., Singh-Phulgenda, S., Olliaro, P. L., & Guerin, P. J. (2021). Gender disparity in cases enrolled in clinical trials of visceral leishmaniasis: A systematic review and meta-analysis. *PLoS Neglected Tropical Diseases*, *15*(3), 1–15. https://doi.org/10.1371/journal.pntd.0009204

Daina, A., Michielin, O., & Zoete, V. (2017a). SwissADME: a free web tool to evaluate pharmacokinetics, drug-likeness and medicinal chemistry friendliness of small molecules. *Scientific Reports*, *7*(1), 1–13.

Daina, A., Michielin, O., & Zoete, V. (2017b). SwissADME: A free web tool to evaluate pharmacokinetics, drug-likeness and medicinal chemistry friendliness of small molecules. *Scientific Reports*, *7*(March), 1–13. https://doi.org/10.1038/srep42717

Daina, A., & Zoete, V. (2016). A boiled-egg to predict gastrointestinal absorption and brain penetration of small molecules. *ChemMedChem*, *11*(11), 1117–1121.

Division, F. A. O. F. D. F. R., & Division, A. O. of the U. N. F. R. (1986). *Databook on endangered tree and shrub species and provenances* (Vol. 77). Food & Agriculture Org.

Donald, G. R., de Carvalho, P. R., Fernandes, P. D., & Boylan, F. (2021). Antinociceptive activity of puberulin and choisyine from ethanol extract of Choisya ternata Kunth var. Sundance. *Biomedicine & Pharmacotherapy*, *141*, 111926.

Durán-Iturbide, N. A., Díaz-Eufracio, B. I., & Medina-Franco, J. L. (2020). In Silico ADME/Tox Profiling of Natural Products: A Focus on BIOFACQUIM. *ACS*

Omega, *5*(26), 16076–16084. https://doi.org/10.1021/acsomega.0c01581

Dysted, M. P., Esztergalyos, B., & Gautam, S. (2021). IDF Diabetes Atlas. EJ Boyko, DJ Magliano, S. Karuranga et al. Brussel, Belgium. *International Diabetes Federation*.

Ehrenberg, J. P., Zhou, X.-N., Fontes, G., Rocha, E. M. M., Tanner, M., & Utzinger, J. (2020). Strategies supporting the prevention and control of neglected tropical diseases during and beyond the COVID-19 pandemic. *Infectious Diseases of Poverty*, *9*(1), 1–7.

Engels, D., & Zhou, X.-N. (2020). Neglected tropical diseases: an effective global response to local poverty-related disease priorities. *Infectious Diseases of Poverty*, *9*(1), 1–9.

Ertl, P., Rohde, B., & Selzer, P. (2000). Fast calculation of molecular polar surface area as a sum of fragment-based contributions and its application to the prediction of drug transport properties. *Journal of Medicinal Chemistry*, *43*(20), 3714–3717.

Faso, B., Republic, C. A., Leone, S., Status, P., Status, C., Measures, C., & Workshop, A. R. (1996). *Afzelia africana Afzelia bipindensis Afzelia ; (Red) Doussié*. *4*(November 1995), 22–110.

Ferreira, M. E., de Arias, A. R., Yaluff, G., de Bilbao, N. V., Nakayama, H., Torres, S., Schinini, A., Guy, I., Heinzen, H., & Fournet, A. (2010). Antileishmanial activity of furoquinolines and coumarins from Helietta apiculata. *Phytomedicine*, *17*(5), 375–378.

Fletcher, S. M., Stark, D., Harkness, J., & Ellis, J. (2012). Enteric protozoa in the developed world: a public health perspective. *Clinical Microbiology Reviews*, *25*(3), 420–449.

Forbes, K., Basáñez, M.-G., Hollingsworth, T. D., & Anderson, R. M. (2023). Introduction to the special issue: challenges and opportunities in the fight against neglected tropical diseases: a decade from the London Declaration on NTDs. *Philosophical Transactions of the Royal Society B*, *378*(1887), 20220272.

Franco, J. R., Cecchi, G., Priotto, G., Paone, M., Diarra, A., Grout, L., Simarro, P. P., Zhao, W., & Argaw, D. (2020). Monitoring the elimination of human African trypanosomiasis at continental and country level: Update to 2018. *PLoS Neglected Tropical Diseases*, *14*(5), 1–18. https://doi.org/10.1371/journal.pntd.0008261

Freitas, M., Proença, C., Ribeiro, D., Quinaz-Garcia, M. B., Araújo, A. N., & Fernandes, E. (2023). Assessment of α-amylase activity in a microanalysis system: Experimental optimization and evaluation of type of inhibition. *Journal of Chemical Education*, *100*(3), 1237–1245.

Frolova, V. I., & Kuzovkov, A. D. (1963). Alkaloids of Choisya ternata: structure of choisyine. *Zl Obshchei Khimii*, *33*, 125.

Galicia-Garcia, U., Benito-Vicente, A., Jebari, S., Larrea-Sebal, A., Siddiqi, H., Uribe, K. B., Ostolaza, H., & Martín, C. (2020). Pathophysiology of type 2 diabetes mellitus. *International Journal of Molecular Sciences*, *21*(17), 6275.

Garcia, G., Charmillon, J. M., Roux, E., Sutour, S., Rakotozafy, J. B., Désiré, O., Paoli, M., Tomi, F., & Rabehaja, D. J. R. (2017). Chemical composition of leaf and bark essential oils of Vepris unifoliolata from Madagascar. *Journal of Essential Oil Research*, *29*(3), 214–220. https://doi.org/10.1080/10412905.2016.1251982

Gascon, J., Bern, C., & Pinazo, M.-J. (2010). Chagas disease in Spain, the United States and other non-endemic countries. *Acta Tropica*, *115*(1–2), 22–27.

Happi, E. N., Tcho, A. T., Sirri, J. C., Wansi, J. D., Neumann, B., Stammler, H.-G., Wandji, J., & Sewald, N. (2012). Tirucallane triterpenoids from the stem bark of Araliopsis synopsis. *Phytochemistry Letters*, *5*(3), 423–426.

Harvey, A. L., Edrada-Ebel, R., & Quinn, R. J. (2015). The re-emergence of natural products for drug discovery in the genomics era. *Nature Reviews Drug Discovery*, *14*(2), 111–129.

Hotez, P. J., Aksoy, S., Brindley, P. J., & Kamhawi, S. (2020). *What constitutes a neglected tropical disease?* Public Library of Science San Francisco, CA USA.

Imbenzi, P. S., Osoro, E. K., Aboud, N. S., & Omollo, J. (2014). *A review on chemistry of some species of genus Vepris (Rutaceae family)*. *3*(3), 357–362.

Jackson, Y., Alirol, E., Getaz, L., Wolff, H., Combescure, C., & Chappuis, F. (2010). Tolerance and safety of nifurtimox in patients with chronic chagas disease. *Clinical Infectious Diseases*, *51*(10), e69–e75.

Jia, C. Y., Li, J. Y., Hao, G. F., & Yang, G. F. (2020). A drug-likeness toolbox facilitates ADMET study in drug discovery. *Drug Discovery Today*, *25*(1), 248–258. https://doi.org/10.1016/j.drudis.2019.10.014

John, C. C., Kutamba, E., Mugarura, K., & Opoka, R. O. (2010). Adjunctive therapy for cerebral malaria and other severe forms of Plasmodium falciparum malaria. *Expert Review of Anti-Infective Therapy*, *8*(9), 997–1008.

Khalid, S. A., & Waterman, P. G. (1981). Alkaloids from stem barks of Oricia renieri and Oricia gabonensis. *Phytochemistry*, *20*(12), 2761–2763.

Khyade, V. B., Dongare, S. K., & Shinde, M. R. (2019). *The Indian Square for Enzyme Kinetics Through the Regular Form of Lineweaver-Burk Plot (Double Reciprocal Plot); It's Inverse Form and Other Additional Form of Plots (Equations)*.

Kibet, S., Kimani, N. M., Mwanza, S. S., Mudalungu, C. M., Santos, C. B. R., & Tanga, C. M. (2024). *Unveiling the Potential of Ent -Kaurane Diterpenoids : Multifaceted Natural Products for Drug Discovery*. 1–20.

Kimani, N. M., Ochieng, C. O., Ogutu, M. D., Yamo, K. O., Onyango, J. O., & Santos, C. B. R. (2023). Inhibition Kinetics and Theoretical Studies on Zanthoxylum chalybeum Engl. Dual Inhibitors of α-Glucosidase and α-Amylase. *Journal of Xenobiotics*, *13*(1), 102–120.

Kiplimo, J. J. (2012). *The phytochemistry and biological activity of secondary metabolites from Kenyan Vernonia and Vepris species.*

Kiplimo, J. J., Islam, M. S., & Koorbanally, N. A. (2011). A novel flavonoid and furoquinoline alkaloids from Vepris glomerata and their antioxidant activity. *Natural Product Communications*, *6*(12), 1934578X1100601215.

Kiplimo, J. J., Islam, M. S., & Koorbanally, N. A. (2012). Ring A-seco limonoids and flavonoids from the Kenyan Vepris uguenensis Engl. and their antioxidant activity. *Phytochemistry*, *83*, 136–143.

Kirchmair, J., Göller, A. H., Lang, D., Kunze, J., Testa, B., Wilson, I. D., Glen, R. C., & Schneider, G. (2015). Predicting drug metabolism: experiment and/or computation? *Nature Reviews Drug Discovery*, *14*(6), 387–404.

Kokwaro, J. O. (1978). New taxa and combinations in Rutaceae of E. and NE. Africa. *Kew Bulletin*, 785–798.

Kouam, A. D. K., Bissoue, A. N., Tcho, A. T., Happi, E. N., Waffo, A. F. K., Sewald, N., & Wansi, J. D. (2017). Antimicrobial Furoquinoline Alkaloids from Vepris lecomteana (Pierre) Cheek & T. Heller (Rutaceae). *Molecules*, *23*(1), 13.

Kouam, A. D. K., Kenmogne, S. B., Lobe, J. S., Happi, E. N., Stammler, H.-G., Waffo, A. F. K., Sewald, N., & Wansi, J. D. (2019). A rotameric tryptamide alkaloid from the roots of Vepris lecomteana (Pierre) Cheek & T. Heller (Rutaceae). *Fitoterapia*, *135*, 9–14.

Kubitzki, K., Kallunki, J. A., Duretto, M., & Wilson, P. G. (2010). Rutaceae. In *Flowering plants. Eudicots: Sapindales, Cucurbitales, Myrtaceae* (pp. 276–356). Springer.

Kuete, V., Wansi, J. D., Mbaveng, A. T., Sop, M. M. K., Tadjong, A. T., Beng, V. P., Etoa, F.-X., Wandji, J., Meyer, J. J. M., & Lall, N. (2008). Antimicrobial activity of the methanolic extract and compounds from Teclea afzelii (Rutaceae). *South African Journal of Botany*, *74*(4), 572–576.

Kumar, R., Saha, P., Kumar, Y., Sahana, S., Dubey, A., & Prakash, O. (2020). A Review on Diabetes Mellitus: Type1 & Type2. *World Journal of Pharmacy and Pharmaceutical Sciences*, *9*(10), 838–850.

Kwon, Y.-I. I., Vattem, D. A., & Shetty, K. (2006). Evaluation of clonal herbs of Lamiaceae species for management of diabetes and hypertension. *Asia Pacific Journal of Clinical Nutrition*, *15*(1), 107.

Lacroix, D., Prado, S., Kamoga, D., Kasenene, J., & Bodo, B. (2012a). Absolute configuration of 2′(R)-acetylmontrifoline and 2′(R)-montrifoline, furoquinolines from the fruits of Teclea nobilis. *Phytochemistry Letters*, *5*(1), 22–25. https://doi.org/10.1016/j.phytol.2011.08.012

Lacroix, D., Prado, S., Kamoga, D., Kasenene, J., & Bodo, B. (2012b). Absolute configuration of 2′(R)-acetylmontrifoline and 2′(R)-montrifoline, furoquinolines from the fruits of Teclea nobilis. *Phytochemistry Letters*, *5*(1), 22–25.

Leitão, G. G., Pereira, J. P. B., De Carvalho, P. R., Ropero, D. R., Fernandes, P. D., & Boylan, F. (2017). Isolation of quinoline alkaloids from three Choisya species by high-speed countercurrent chromatography and the determination of their antioxidant capacity. *Revista Brasileira de Farmacognosia*, *27*(3), 297–301. https://doi.org/10.1016/j.bjp.2017.01.003

Lenk, E. J., Redekop, W. K., Luyendijk, M., Fitzpatrick, C., Niessen, L., Stolk, W. A., Tediosi, F., Rijnsburger, A. J., Bakker, R., & Hontelez, J. A. C. (2018). Socioeconomic benefit to individuals of achieving 2020 targets for four neglected tropical diseases controlled/eliminated by innovative and intensified disease management: Human African trypanosomiasis, leprosy, visceral leishmaniasis, Chagas disease. *PLoS Neglected Tropical Diseases*, *12*(3), e0006250.

Lindoso, J. A., Cota, G. F., Da Cruz, A. M., Goto, H., Maia-Elkhoury, A. N. S., Romero, G. A. S., de Sousa-Gomes, M. L., Santos-Oliveira, J. R., & Rabello, A. (2014). Visceral leishmaniasis and HIV coinfection in Latin America. *PLoS Neglected Tropical Diseases*, *8*(9), e3136.

Lipinski, C. A., Lombardo, F., Dominy, B. W., & Feeney, P. J. (1997). In vitro models for selection of development candidatesexperimental and computational approaches to estimate solubility and permeability in drug discovery and development settings. *Adv Drug Deliv Rev*, *23*(1), 3–25.

Lipinski, C. A., Lombardo, F., Dominy, B. W., & Feeney, P. J. (2012). Experimental and computational approaches to estimate solubility and permeability in drug discovery and development settings. *Advanced Drug Delivery Reviews*, *64*, 4–17.

Lozano, R., Naghavi, M., Foreman, K., Lim, S., Shibuya, K., Aboyans, V., Abraham, J., Adair, T., Aggarwal, R., & Ahn, S. Y. (2012). Global and regional mortality from 235 causes of death for 20 age groups in 1990 and 2010: a systematic analysis for the Global Burden of Disease Study 2010. *The Lancet*, *380*(9859), 2095–2128.

Lwande, W., Gebreyesus, T., Chapya, A., Macfoy, C., Hassanali, A., & Okech, M. (1983). 9-Acridone insect antifeedant alkaloids from Teclea trichocarpa bark. *International Journal of Tropical Insect Science*, *4*(4), 393–395.

Matsuura, H. N., & Fett-Neto, A. G. (2015). Plant alkaloids: main features, toxicity, and mechanisms of action. *Plant Toxins*, *2*(7), 1–15.

Misra, A., Gopalan, H., Jayawardena, R., Hills, A. P., Soares, M., Reza-Albarrán, A. A., & Ramaiya, K. L. (2019). Diabetes in developing countries. *Journal of Diabetes*, *11*(7), 522–539.

Montesino, N. L., Kaiser, M., Brun, R., & Schmidt, T. J. (2015). Search for antiprotozoal activity in herbal medicinal preparations; new natural leads against neglected tropical diseases. *Molecules*, *20*(8), 14118–14138. https://doi.org/10.3390/molecules200814118

Montesino, N. L., & Schmidt, T. J. (2018). Salvia species as sources of natural products with antiprotozoal activity. *International Journal of Molecular Sciences*, *19*(1). https://doi.org/10.3390/ijms19010264

Monzote, L., & Siddiq, A. (2011). Drug development to protozoan diseases. *The Open Medicinal Chemistry Journal*, *5*, 1.

Mougabure-Cueto, G., & Picollo, M. I. (2015). Insecticide resistance in vector Chagas disease: evolution, mechanisms and management. *Acta Tropica*, *149*, 70–85.

Muñoz-Calderón, A., Díaz-Bello, Z., Valladares, B., Noya, O., López, M. C., De Noya, B. A., & Thomas, M. C. (2013). Oral transmission of Chagas disease: typing of Trypanosoma cruzi from five outbreaks occurred in Venezuela shows multiclonal and common infections in patients, vectors and reservoirs. *Infection, Genetics and Evolution*, *17*, 113–122.

Muriithi, M. W., Abraham, W.-R., Addae-Kyereme, J., Scowen, I., Croft, S. L., Gitu, P. M., Kendrick, H., Njagi, E. N. M., & Wright, C. W. (2002). Isolation and in Vitro Antiplasmodial Activities of Alkaloids from Teclea t richocarpa: In vivo Antimalarial Activity and X-ray Crystal Structure of Normelicopicine. *Journal of Natural Products*, *65*(7), 956–959.

Muthee, J. K., Gakuya, D. W., Mbaria, J. M., Kareru, P. G., Mulei, C. M., & Njonge, F. K. (2011). Ethnobotanical study of anthelmintic and other medicinal plants traditionally used in Loitoktok district of Kenya. *Journal of Ethnopharmacology*, *135*(1), 15–21.

Mwangi, E. S. K., Keriko, J. M., Machocho, A. K., Wanyonyi, A. W., Malebo, H. M., Chhabra, S. C., & Tarus, P. K. (2010). Antiprotozoal activity and cytotoxicity of metabolites from leaves of Teclea trichocarpa. *J Med Plants Res*, *4*(9), 726–731.

Nagle, A. S., Khare, S., Kumar, A. B., Supek, F., Buchynskyy, A., Mathison, C. J. N., Chennamaneni, N. K., Pendem, N., Buckner, F. S., Gelb, M. H., & Molteni, V. (2014). Recent developments in drug discovery for leishmaniasis and human african trypanosomiasis. *Chemical Reviews*, *114*(22), 11305–11347. https://doi.org/10.1021/cr500365f

Newman, D. J., & Cragg, G. M. (2016). Natural products as sources of new drugs from 1981 to 2014. *Journal of Natural Products*, *79*(3), 629–661.

Ngadjui, B. T., Ayafor, J. F., Sondengam, B. L., Koch, M., Tillequin, F., & Connolly, J. D. (1988). Araliopdimerines A, B, and C, dimeric quinolone alkaloids from the bark of Araliopsis tabouensis. *Phytochemistry*, *27*(9), 2979–2981.

Ngadjui, T. B., Ayafor, J. F., Sondengam, B. L., Connolly, J. D., Rycroft, D. S., Khalid, S. A., Waterman, P. G., Brown, N. M. D., Grundon, M. F., & Ramachandran, V. N. (1982). The structures of vepridimerines AD, four new dimeric prenylated quinolone alkaloids from Vepris lousii and Oricia renieri (Rutaceae). *Tetrahedron Letters*, *23*(19), 2041–2044.

Ngumburu, R. H. (2001). *Studies on the Conservation Status of Some Exploited Endangered Species in Ragati Forest, Mount Kenya*. Kenyatta University.

Noulala, C. G. T., Fotso, G. W., Rennert, R., Lenta, B. N., Sewald, N., Arnold, N., Happi, E. N., & Ngadjui, B. T. (2020). Mesomeric form of quaternary indoloquinazoline alkaloid and other constituents from the Cameroonian Rutaceae Araliopsis soyauxii Engl. *Biochemical Systematics and Ecology*, *91*, 104050.

Ogbole, O. O., Segun, P. A., & Fasinu, P. S. (2018). Antimicrobial and antiprotozoal activities of twenty-four Nigerian medicinal plant extracts. *South African Journal of Botany*, *117*, 240–246. https://doi.org/10.1016/j.sajb.2018.05.028

Ojuka, P., Kimani, N. M., Apollo, S., Nyariki, J., Ramos, R. S., & Santos, C. B. R. (2023). Phytochemistry of the Vepris genus plants: A review and in silico analysis of their ADMET properties. *South African Journal of Botany*, *157*, 106–114.

Olatunji, T. L., Odebunmi, C. A., & Adetunji, A. E. (2021). Biological activities of limonoids in the Genus Khaya (Meliaceae): A review. *Future Journal of Pharmaceutical Sciences*, *7*, 1–16.

Ombito, J. O., Chi, G. F., & Wansi, J. D. (2021). Ethnomedicinal uses, phytochemistry, and pharmacology of the genus Vepris (Rutaceae): A review. *Journal of Ethnopharmacology*, *267*, 113622. https://doi.org/10.1016/j.jep.2020.113622

Omujal, F., Tenda, K. I., Lutoti, S., Kirabo, I., Kasango, S. D., & Nambatya, K. G. (2020). Phytochemistry and anti-inflammatory activity of ethanolic root bark extract of Vepris nobilis Mziray (Rutaceae family). *Scientific African*, *9*, e00484. https://doi.org/10.1016/j.sciaf.2020.e00484

Ononamadu, C. J., & Ibrahim, A. (2021). Molecular docking and prediction of ADME/drug-likeness properties of potentially active antidiabetic compounds isolated from aqueous-methanol extracts of Gymnema sylvestre and Combretum micranthum. *BioTechnologia*, *102*(1), 85.

Pérez-Molina, J. A., & Molina, I. (2018). Chagas disease. *The Lancet*, *391*(10115), 82–94. https://doi.org/10.1016/S0140-6736(17)31612-4

Pinazo, M.-J., Espinosa, G., Cortes-Lletget, C., Posada, E. de J., Aldasoro, E., Oliveira, I., Munoz, J., Gallego, M., & Gascon, J. (2013). Immunosuppression and Chagas disease: a management challenge. *PLoS Neglected Tropical Diseases*, *7*(1), e1965.

Pinto, A. Y. das N., Valente, V. da C., Coura, J. R., Valente, S. A. da S., Junqueira, A. C. V., Santos, L. C., Ferreira Jr, A. G., & de Macedo, R. C. (2013). Clinical follow-up of responses to treatment with benznidazol in Amazon: a cohort study of acute Chagas disease. *PLoS One*, *8*(5), e64450.

Polinsky, A. (2008). Lead-likeness and drug-likeness. In *The practice of medicinal chemistry* (pp. 244–254). Elsevier.

Ponte-Sucre, A., Gamarro, F., Dujardin, J. C., Barrett, M. P., López-Vélez, R., García-Hernández, R., Pountain, A. W., Mwenechanya, R., & Papadopoulou, B. (2017). Drug resistance and treatment failure in leishmaniasis: A 21st century challenge. *PLoS Neglected Tropical Diseases*, *11*(12), 1–24. https://doi.org/10.1371/journal.pntd.0006052

Prasanna, S., & Doerksen, R. J. (2009). Topological polar surface area: a useful descriptor in 2D-QSAR. *Current Medicinal Chemistry*, *16*(1), 21–41.

Prata A. (2001). Clinical and epidemiological aspects of chagas disease.Lancet infection disease. *Clinical and Epidemiological Aspects of Chagas Disease*, *1*(September), 92–100.

Premji, Z. G. (2009). Coartem®: the journey to the clinic. *Malaria Journal*, *8*(1), 1–6.

Price, R. N., Von Seidlein, L., Valecha, N., Nosten, F., Baird, J. K., & White, N. J. (2014). Global extent of chloroquine-resistant Plasmodium vivax: a systematic review and meta-analysis. *The Lancet Infectious Diseases*, *14*(10), 982–991.

Rashid, M. I., Fareed, M. I., Rashid, H., Aziz, H., Ehsan, N., Khalid, S., Ghaffar, I., Ali, R., Gul, A., & Hakeem, K. R. (2019). Flavonoids and their biological secrets. *Plant and Human Health, Volume 2: Phytochemistry and Molecular Aspects*, 579–605.

Ribeiro, F. F., Junior, F. J. B. M., da Silva, M. S., Scotti, M. T., & Scotti, L. (2015). Computational and Investigative Study of Flavonoids Active against Trypanosoma cruzi and Leishmania spp. *Natural Product Communications*, *10*(6). https://doi.org/10.1177/1934578X1501000630

Sato, T., Yuki, H., Ogura, K., & Honma, T. (2018). Construction of an integrated database for hERG blocking small molecules. *PLoS One*, *13*(7), e0199348.

Shadrack, D. M., Nyandoro, S. S., Munissi, J. J. E., & Mubofu, E. B. (2016). In silico evaluation of anti-malarial agents from Hoslundia opposita as inhibitors of Plasmodium falciparum lactate dehydrogenase (PfLDH) enzyme. *Computational Molecular Bioscience*, *6*(2), 23–32.

Shaker, B., Ahmad, S., Lee, J., Jung, C., & Na, D. (2021). In silico methods and tools for drug discovery. *Computers in Biology and Medicine*, *137*(July), 104851. https://doi.org/10.1016/j.compbiomed.2021.104851

Siciliano, G., & Alano, P. (2015). Enlightening the malaria parasite life cycle: bioluminescent Plasmodium in fundamental and applied research. *Frontiers in Microbiology*, *6*, 134327.

Silva, R. C., Freitas, H. F., Campos, J. M., Kimani, N. M., Silva, C. H. T. P., Borges, R. S., Pita, S. S. R., & Santos, C. B. R. (2021). Natural products-based drug design against sars-cov-2 mpro 3clpro. *International Journal of Molecular Sciences*, *22*(21). https://doi.org/10.3390/ijms222111739

Singh, N., Mishra, B. B., Bajpai, S., Singh, R. K., & Tiwari, V. K. (2014). Natural product based leads to fight against leishmaniasis. *Bioorganic & Medicinal Chemistry*, *22*(1), 18–45.

Siqueira-Batista, R., Alves, M. M. R., Lara, M. A. G., & Patrícia, A. (2023). *Penicillins: update for clinical practice*.

Sjögren, E., Thorn, H., & Tannergren, C. (2016). In silico modeling of gastrointestinal drug absorption: predictive performance of three physiologically based absorption models. *Molecular Pharmaceutics*, *13*(6), 1763–1778.

Snow, R. W., Trape, J.-F., & Marsh, K. (2001). The past, present and future of childhood malaria mortality in Africa. *TRENDS in Parasitology*, *17*(12), 593–597.

Suryasa, I. W., Rodríguez-Gámez, M., & Koldoris, T. (2021). Health and treatment of diabetes mellitus. *International Journal of Health Sciences*, *5*(1), 1–5.

Szewczyk, A., & Pęczek, F. (2023). Furoquinoline alkaloids: Insights into chemistry, occurrence, and biological properties. *International Journal of Molecular Sciences*, *24*(16), 12811.

Tagboto, S., & Townson, S. (2001). *Antiparasitic properties of medicinal plants and other naturally occurring products*.

Tan, Q.-G., & Luo, X.-D. (2011). Meliaceous limonoids: chemistry and biological activities. *Chemical Reviews*, *111*(11), 7437–7522.

Tayebi, L., & Moharamzadeh, K. (2017). *Biomaterials for oral and dental tissue engineering*. Woodhead Publishing.

Tchinda, A. T., Fuendjiep, V., Sajjad, A., Matchawe, C., Wafo, P., Khan, S., Tane, P., & Choudhary, M. I. (2009). Bioactive compounds from the fruits of Zanthoxylum leprieurii. *Pharmacologyonline*, *1*, 406–415.

Tempone, A. G., Pieper, P., Borborema, S. E. T., Thevenard, F., Lago, J. H. G., Croft, S. L., & Anderson, E. A. (2021). Marine alkaloids as bioactive agents against protozoal neglected tropical diseases and malaria. *Natural Product Reports*. https://doi.org/10.1039/d0np00078g

Thompson, M. F., & Bachelard, H. S. (1976). Determination of true Ki values in enzyme dead-end inhibition kinetic studies. *Analytical Biochemistry*, *71*(2), 507–518.

Tiwari, N., Gedda, M. R., Tiwari, V. K., Singh, S. P., & Singh, R. K. (2018). Limitations of current therapeutic options, possible drug targets and scope of natural products in control of leishmaniasis. *Mini Reviews in Medicinal Chemistry*, *18*(1), 26–41.

Tomic, D., Shaw, J. E., & Magliano, D. J. (2022). The burden and risks of emerging complications of diabetes mellitus. *Nature Reviews Endocrinology*, *18*(9), 525–539.

Torres, F. A. E., Passalacqua, T. G., Velásquez, A. M. A., de Souza, R. A., Colepicolo, P., & Graminha, M. A. S. (2014). New drugs with antiprotozoal activity from marine Algae: A review. *Revista Brasileira de Farmacognosia*, *24*(3), 265–276. https://doi.org/10.1016/j.bjp.2014.07.001

Tsaioun, K., Blaauboer, B. J., & Hartung, T. (2016). Evidence-based absorption, distribution, metabolism, excretion (ADME) and its interplay with alternative toxicity methods. *ALTEX-Alternatives to Animal Experimentation*, *33*(4), 343–358.

Veber, D. F., Johnson, S. R., Cheng, H.-Y., Smith, B. R., Ward, K. W., & Kopple, K. D. (2002). Molecular properties that influence the oral bioavailability of drug candidates. *Journal of Medicinal Chemistry*, *45*(12), 2615–2623.

Venkatesan, P. (2024). The 2023 WHO World malaria report. *The Lancet Microbe*.

Verlinden, B. K., Louw, A., & Birkholtz, L.-M. (2016). Resisting resistance: is there a solution for malaria? *Expert Opinion on Drug Discovery*, *11*(4), 395–406.

Wambua, M. J. (2020). *Anti-Cancer and Anti-Inflammatory Secondary Metabolites of Fagaropsis Angolensis (Engl.) HM Gardner*. University of Embu.

Wang, W., Peng, D., Baptista, R. P., Li, Y., Kissinger, J. C., & Tarleton, R. L. (2021). Strain-specific genome evolution in Trypanosoma cruzi, the agent of Chagas

disease. *PLoS Pathogens*, *17*(1), e1009254.

Wansi, J. D., Devkota, K. P., Tshikalange, E., & Kuete, V. (2013). Alkaloids from the Medicinal Plants of Africa. In *Medicinal Plant Research in Africa: Pharmacology and Chemistry*. Elsevier Inc. https://doi.org/10.1016/B978-0-12-405927-6.00014-X

Wansi, J. D., Hussain, H., Tcho, A. T., Kouam, S. F., Specht, S., Sarite, S. R., Hoerauf, A., & Krohn, K. (2010). Antiplasmodial activities of furoquinoline alkaloids from Teclea afzelii. *Phytotherapy Research: An International Journal Devoted to Pharmacological and Toxicological Evaluation of Natural Product Derivatives*, *24*(5), 775–777.

Wansi, J. D., Wandji, J., Meva'a, L. M., Waffo, A. F. K., Ranjit, R., Khan, S. N., Asma, A., Iqbal, C. M., Lallemand, M.-C., & Tillequin, F. (2006). α-Glucosidase inhibitory and antioxidant acridone alkaloids from the stem bark of Oriciopsis glaberrima E NGL.(Rutaceae). *Chemical and Pharmaceutical Bulletin*, *54*(3), 292–296.

Wardecki, D., Dołowy, M., & Bober-Majnusz, K. (2023). Assessment of Lipophilicity Parameters of Antimicrobial and Immunosuppressive Compounds. *Molecules*, *28*(6), 2820.

Waterman, P. G., Meshal, I. A., Hall, J. B., & Swaine, M. D. (1978). Biochemical systematics and ecology of the Toddalioideae in the central part of the West African forest zone. *Biochemical Systematics and Ecology*, *6*(3), 239–245.

Wei, W., Cherukupalli, S., Jing, L., Liu, X., & Zhan, P. (2020). Fsp3: A new parameter for drug-likeness. *Drug Discovery Today*, *25*(10), 1839–1845.

Wekesa, E. N., Kimani, N. M., Kituyi, S. N., Omosa, L. K., & Santos, C. B. R. (2023). Therapeutic potential of the genus Zanthoxylum phytochemicals: A theoretical ADME/Tox analysis. *South African Journal of Botany*, *162*, 129–141.

WHO. (2010). First WHO report on neglected tropical diseases: working to overcome the global impact of neglected tropical diseases. *World Health Organization*, 1–184. https://doi.org/10.1177/1757913912449575

WHO (2013). *Sustaining the drive to overcome the global impact of neglected tropical diseases: second WHO report on neglected diseases* (Issue WHO/HTM/NTD/2013.1). World Health Organization.

WHO (2018). Malaria vaccine: WHO position paper, January 2016–recommendations. *Vaccine*, *36*(25), 3576–3577.

WHO (2023). *Global report on neglected tropical diseases 2023*. World Health Organization.

World malaria report 2019. (2019). World malaria report 2019. In *WHO Regional Office for Africa*. https://www.who.int/news-room/fact-sheets/detail/malaria

Yan, A., & Gasteiger, J. (2003). Prediction of aqueous solubility of organic compounds based on a 3D structure representation. *Journal of Chemical Information and Computer Sciences*, *43*(2), 429–434.

Yang, G., & Chen, D. (2008). Alkaloids from the roots of Zanthoxylum nitidum and their antiviral and antifungal effects. *Chemistry and Biodiversity*, *5*(9), 1718–1722. https://doi.org/10.1002/cbdv.200890160

Young, R. J., Flitsch, S. L., Grigalunas, M., Leeson, P. D., Quinn, R. J., Turner, N. J., & Waldmann, H. (2022). The time and place for nature in drug discovery. *Jacs Au*, *2*(11), 2400–2416.

Zupančič, O., & Bernkop-Schnürch, A. (2017). Lipophilic peptide character–What oral barriers fear the most. *Journal of Controlled Release*, *255*, 242–257.

APPENDICES

Appendix A1: Mass spectrum of compound 29

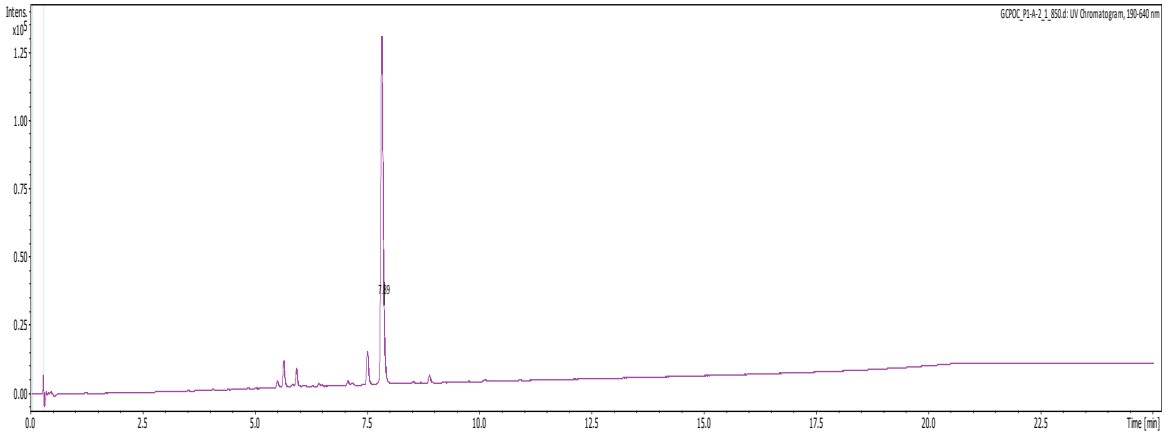

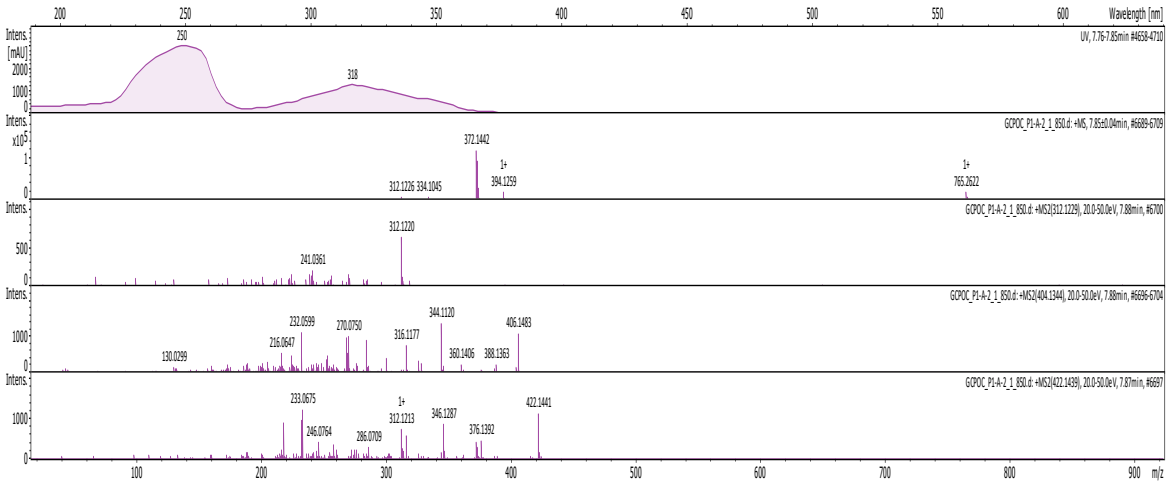

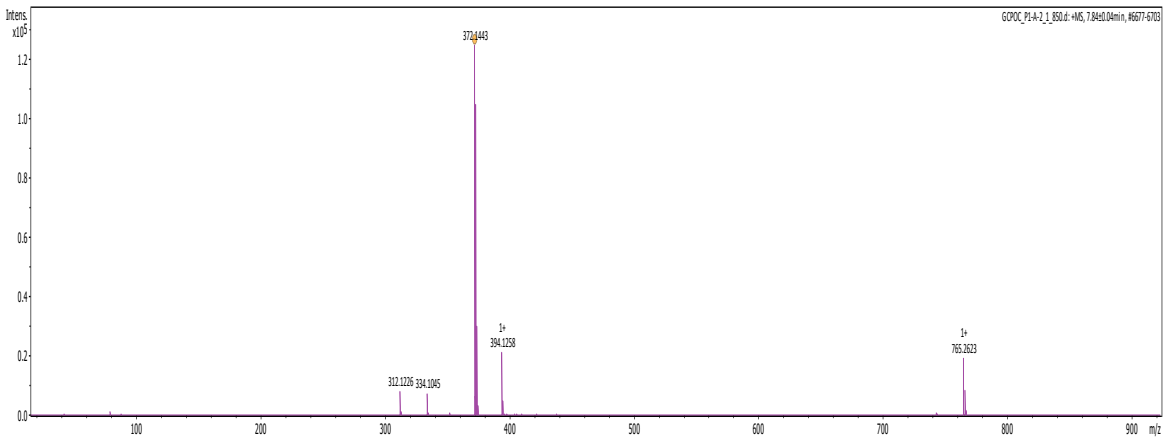

Appendix A2: ^{13}C NMR spectrum (150 MHz, $CDCl_3$) of compound 29

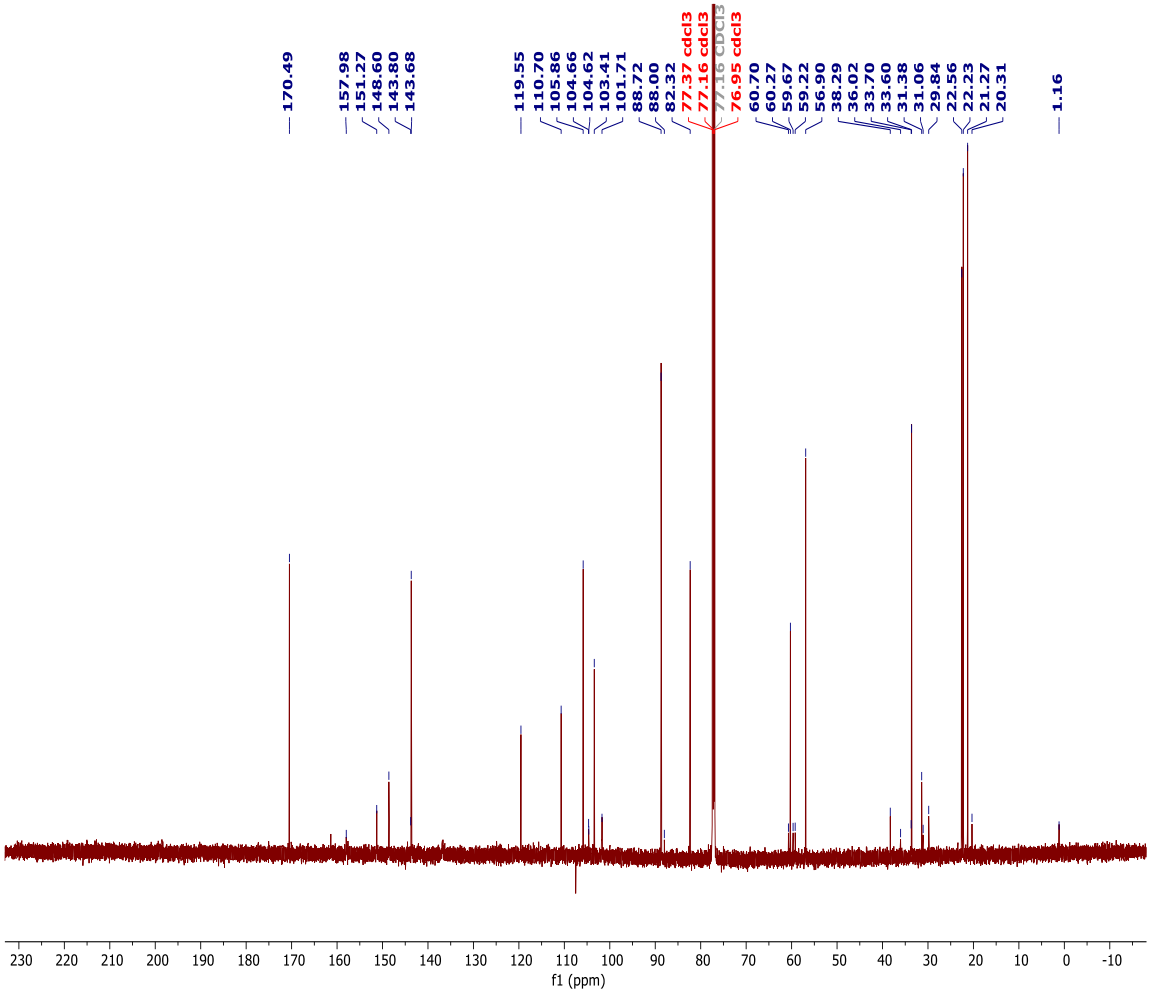

Appendix A3: ^{1}H NMR spectrum (600 MHz, $CDCl_3$) of compound 29

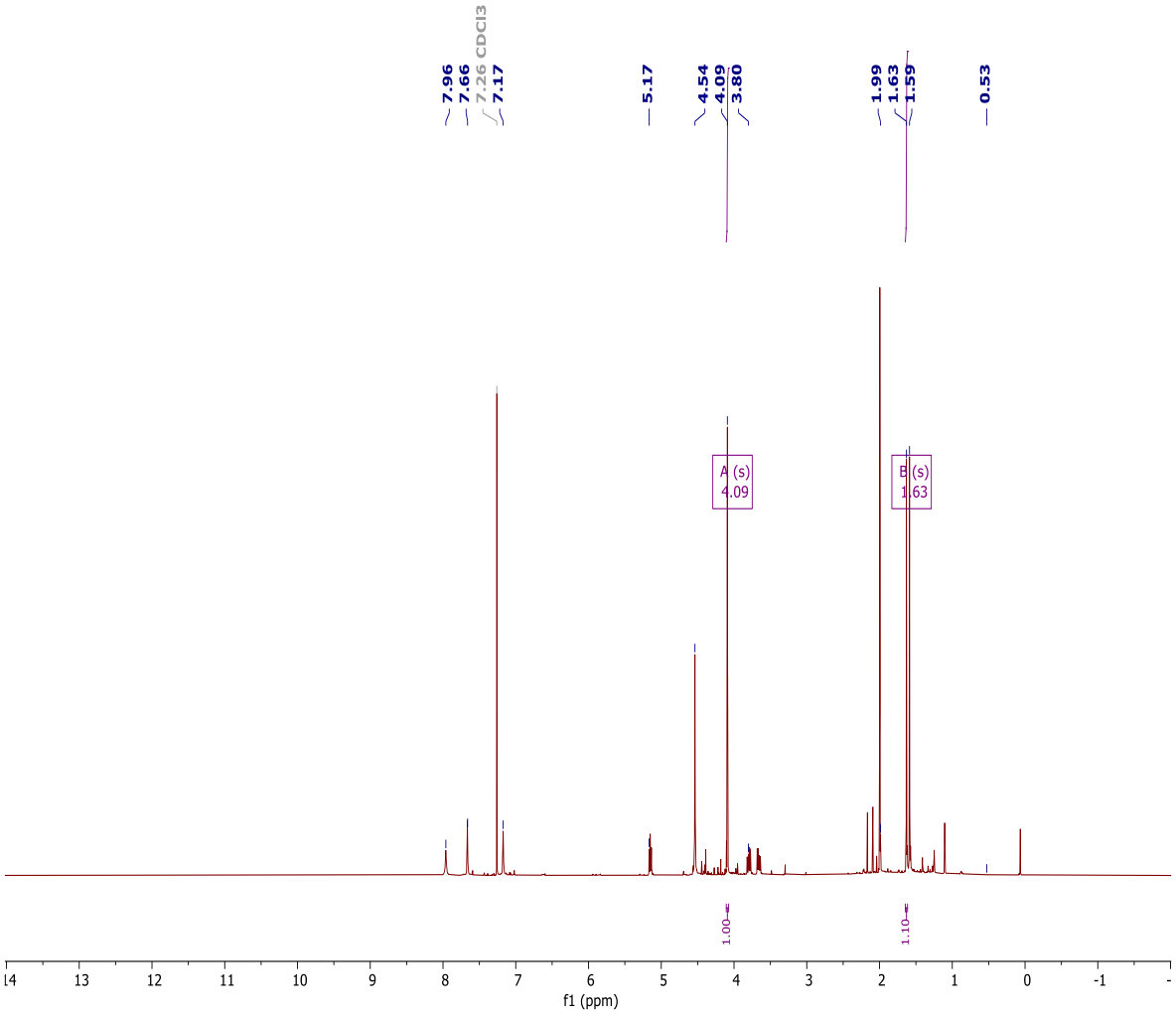

Appendix A4: HSQC spectrum ($CDCl_3$) of compound 29

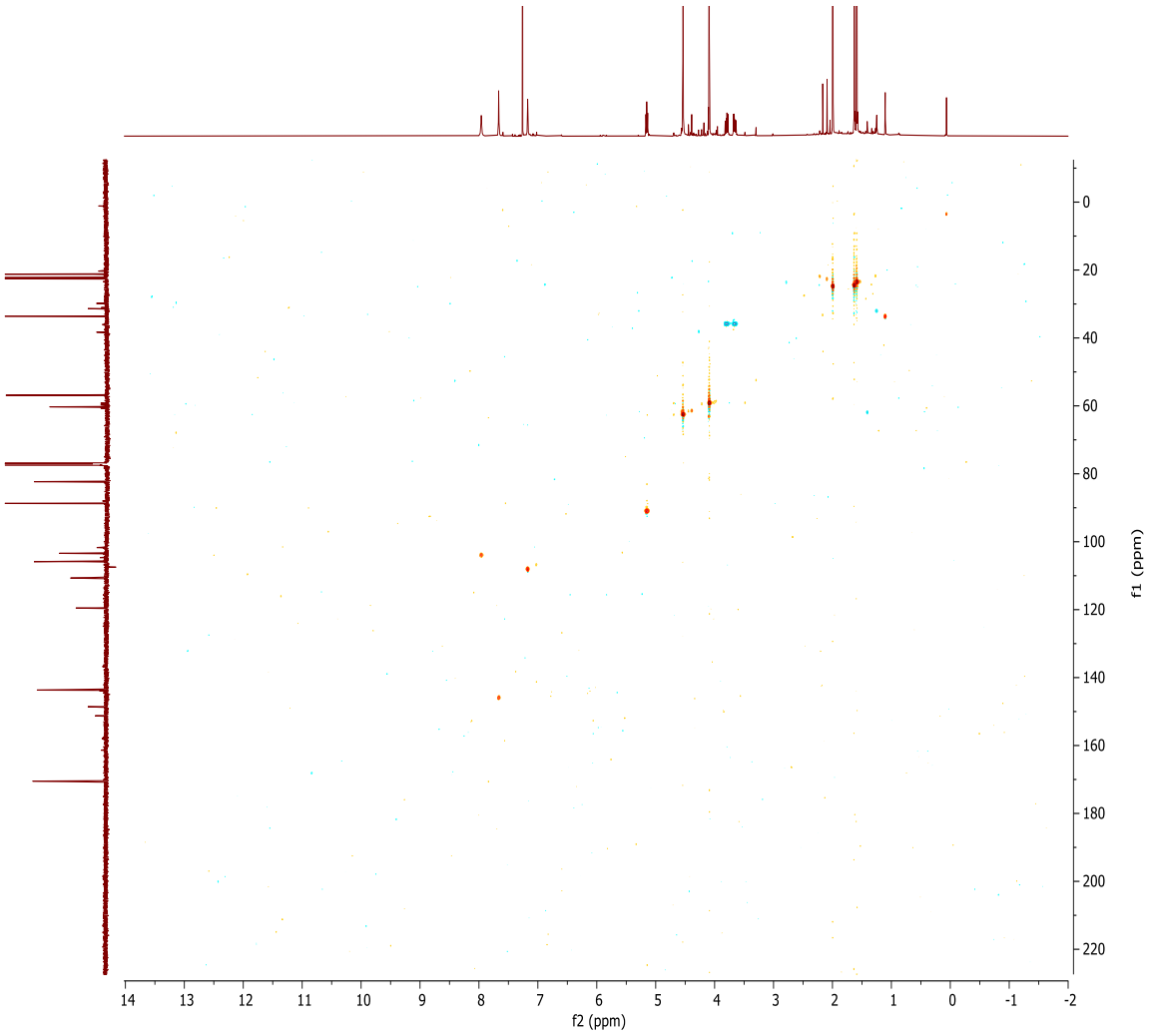

Appendix A5: ^{1}H-^{1}H COSY spectrum ($CDCl_3$) of compound 29

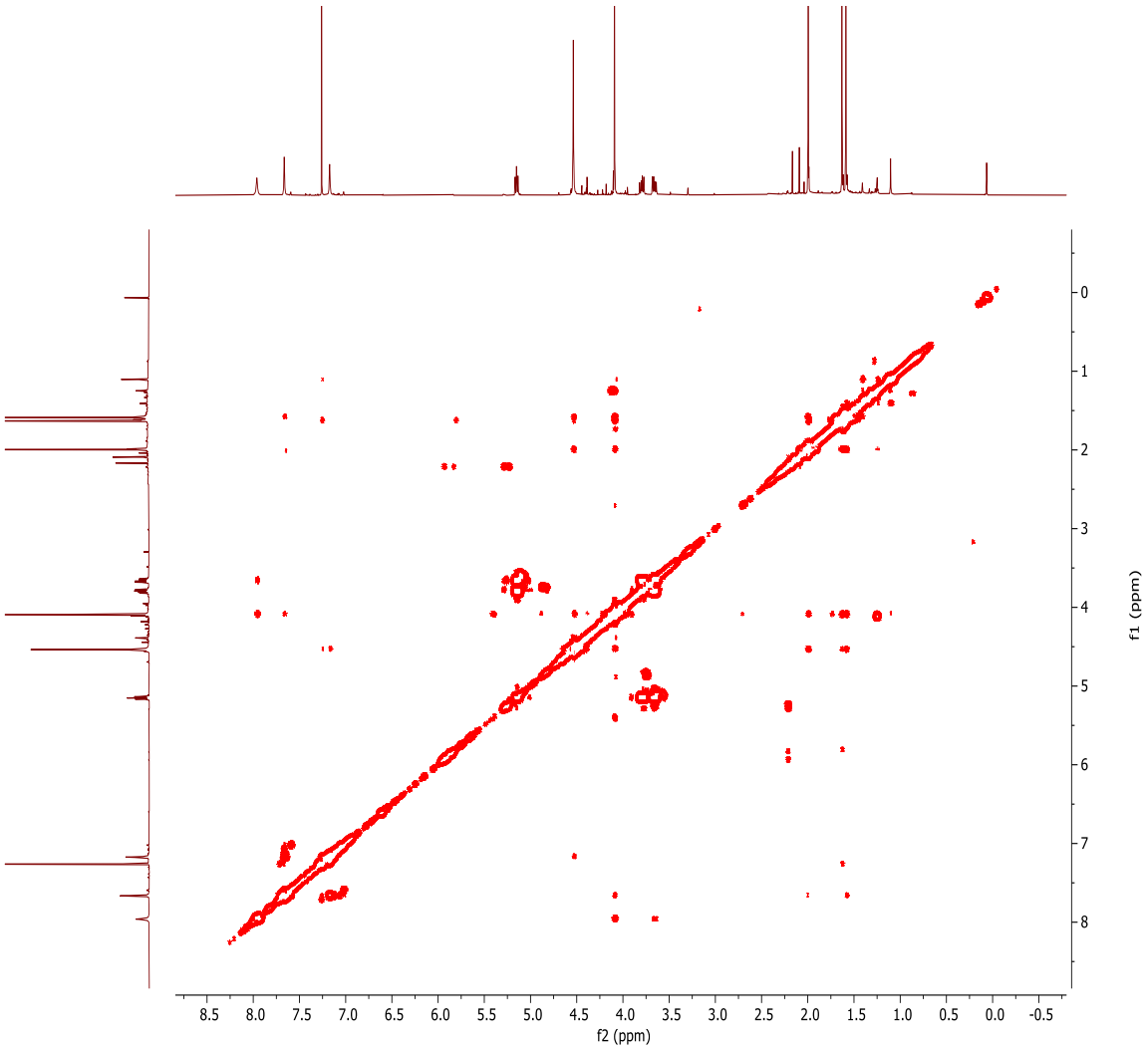

Appendix A6: HMBC spectrum ($CDCl_3$) of compound 29

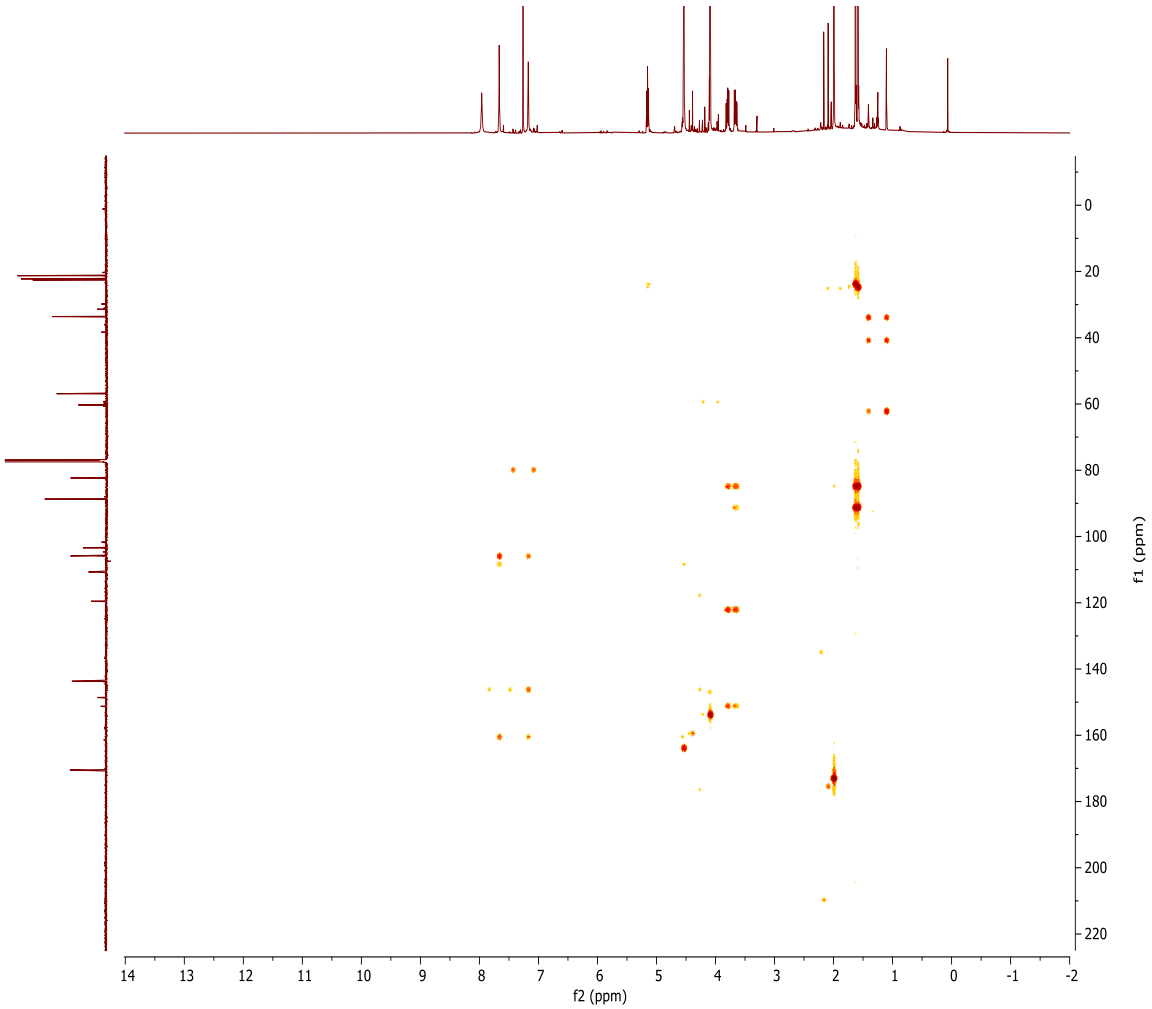

Appendix A7: NOESY spectrum ($CDCl_3$) of compound 29

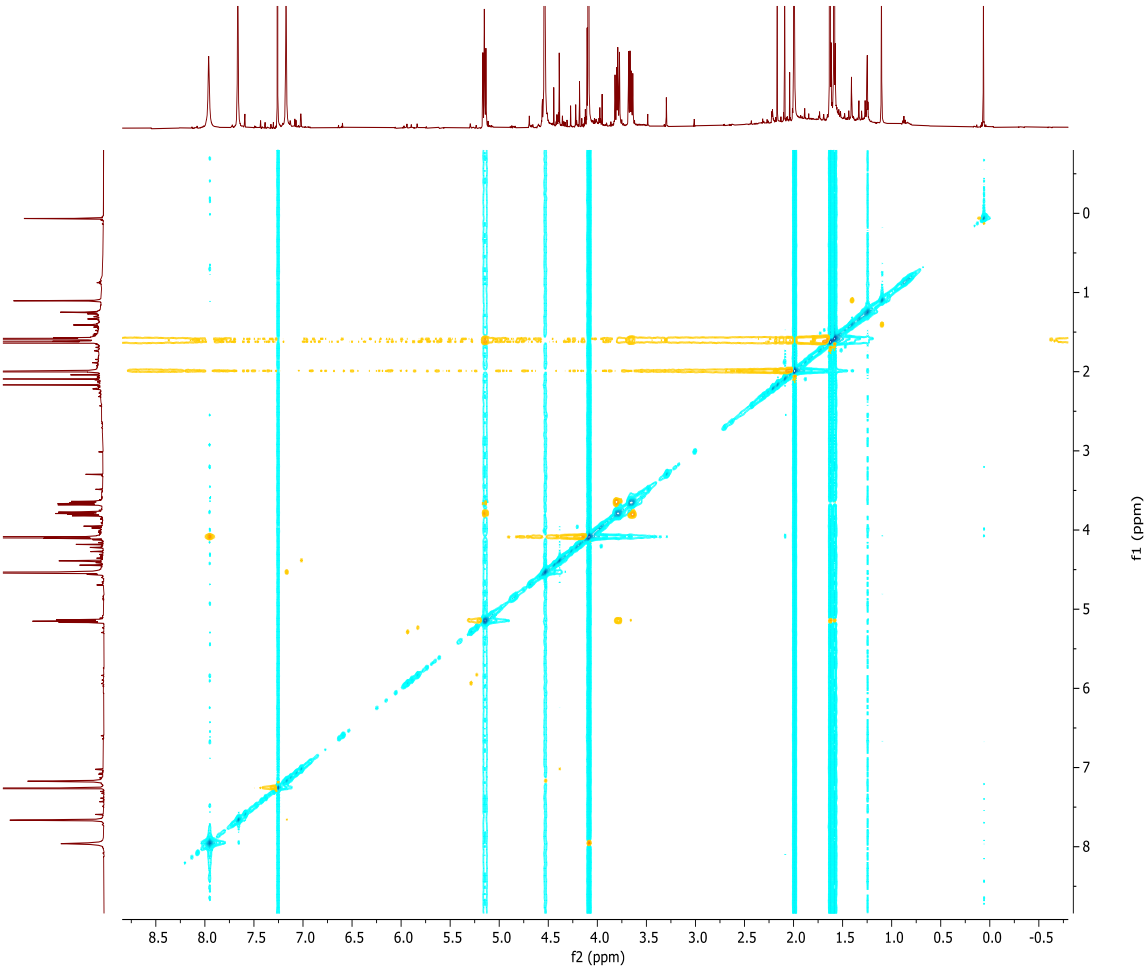

Appendix B1: Mass spectrum of compound 30

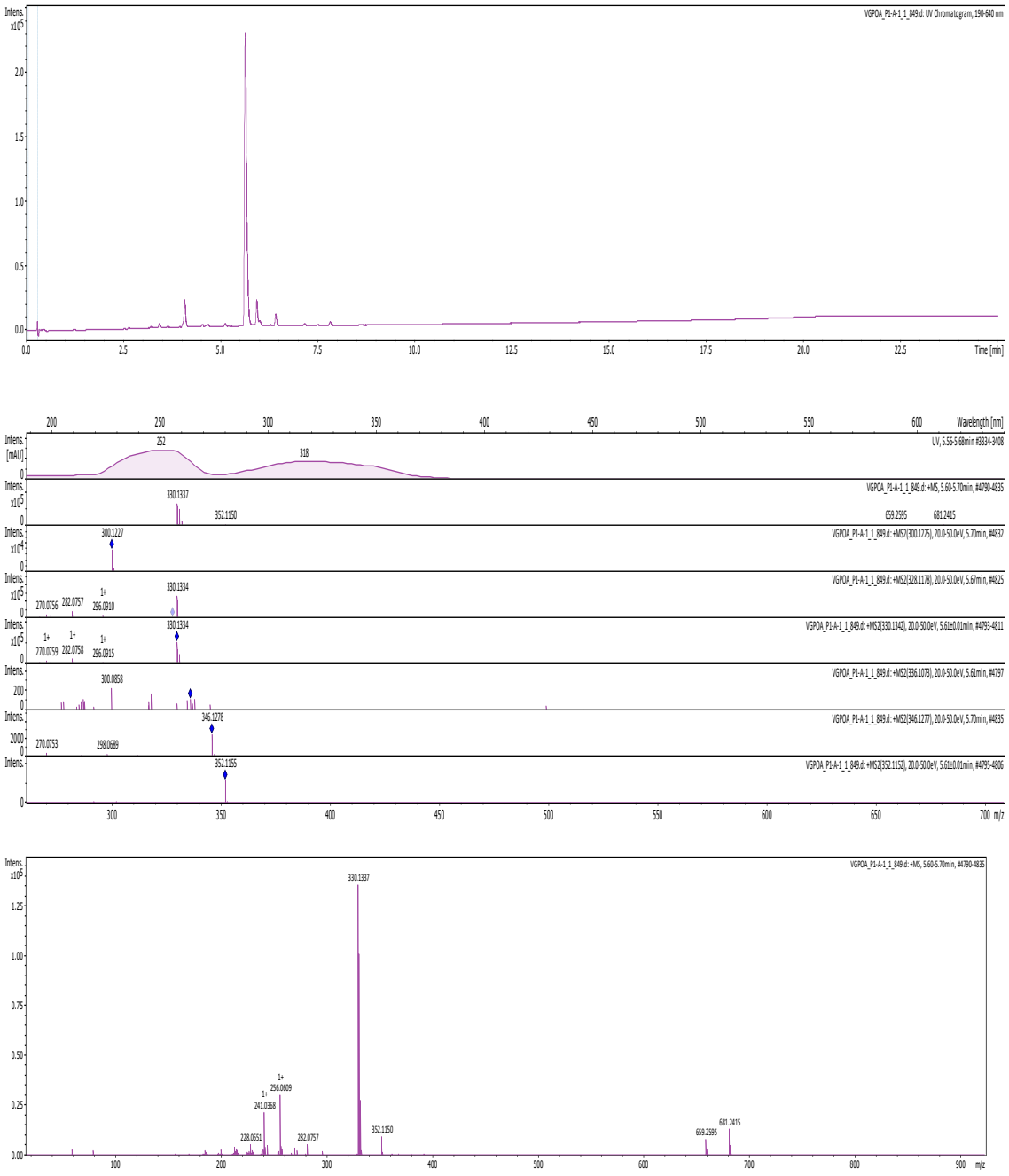

Appendix B2: ^{13}C NMR spectrum (150 MHz, $CDCl_3$) of compound 30

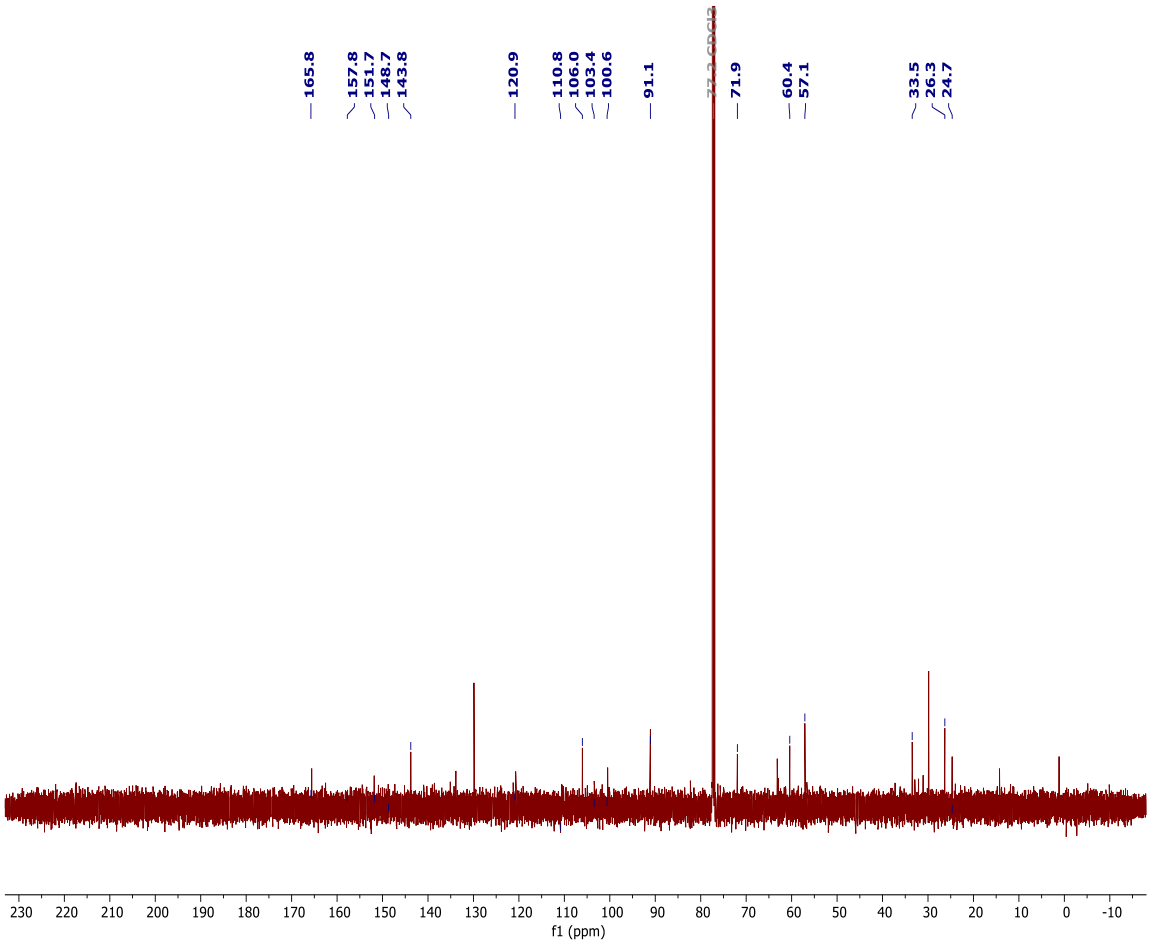

Appendix B3: ^{1}H NMR spectrum (600 MHz, $CDCl_3$) of compound 30

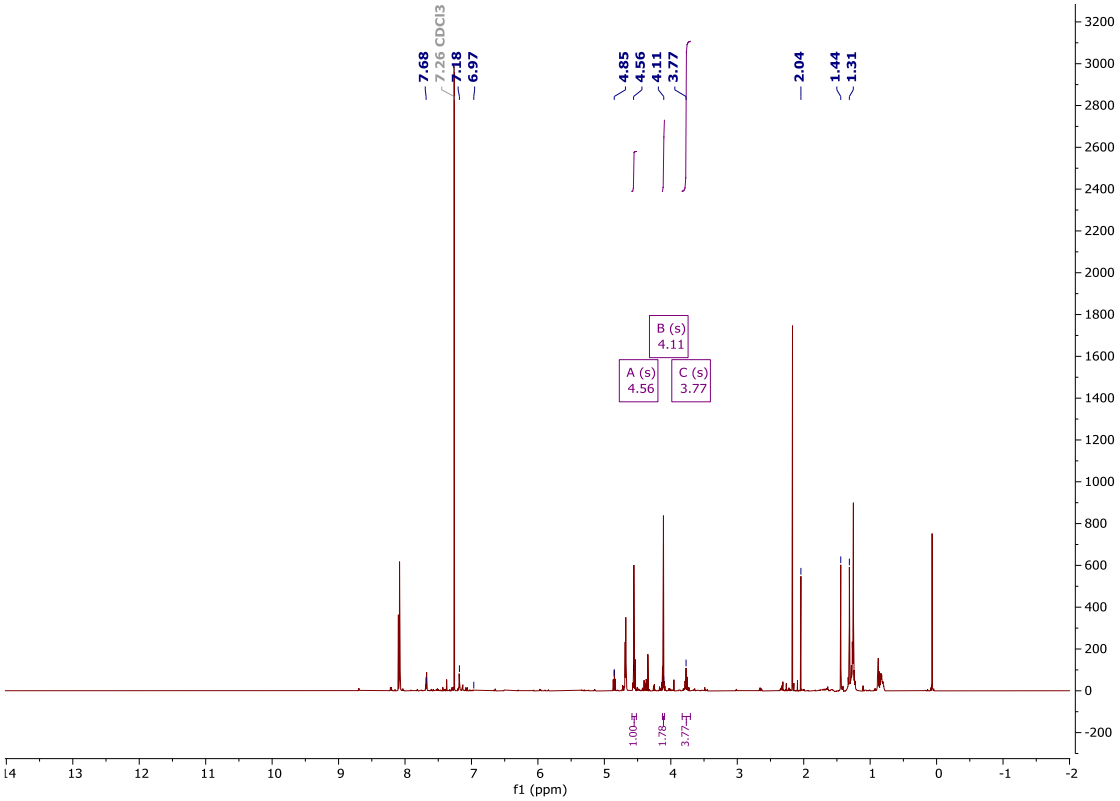

Appendix B4: HSQC spectrum ($CDCl_3$) of compound 30

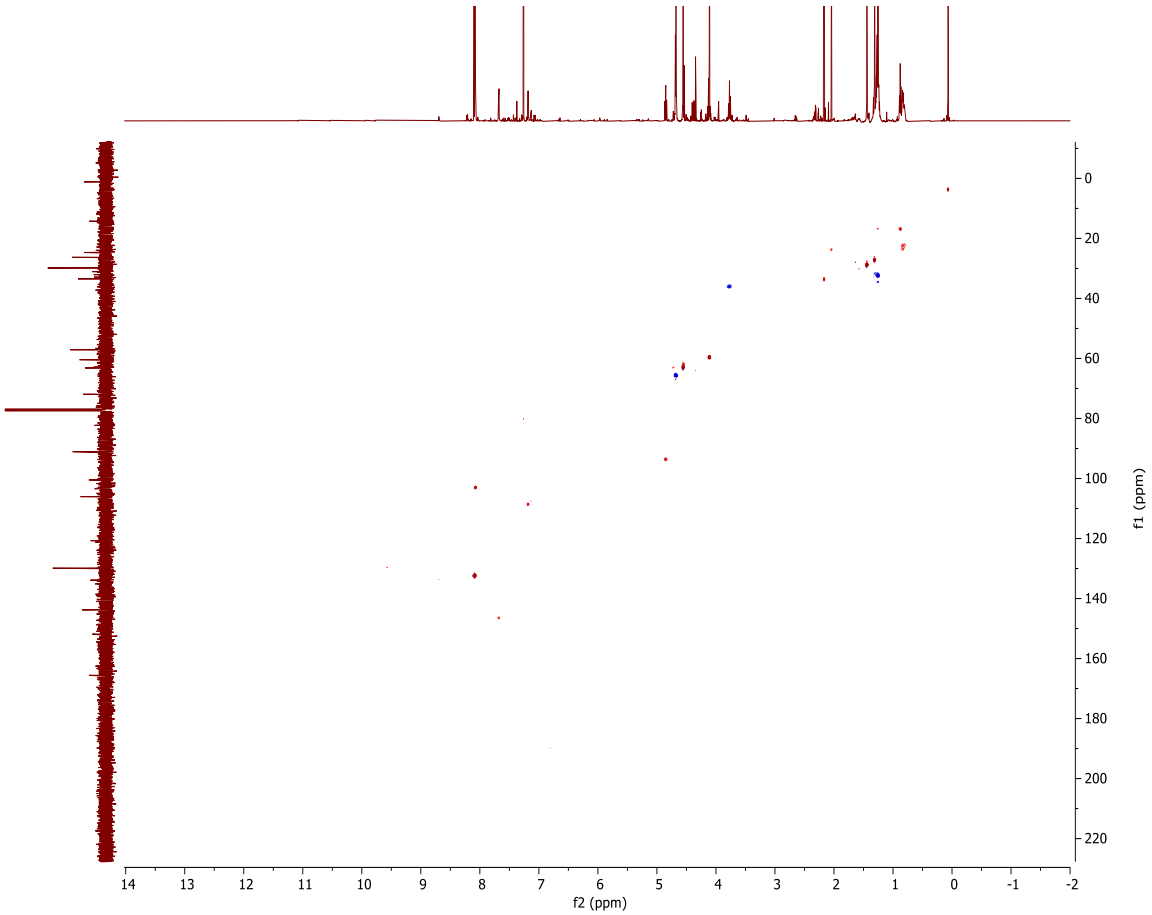

Appendix B5: ^{1}H-^{1}H COSY spectrum ($CDCl_3$) of compound 30

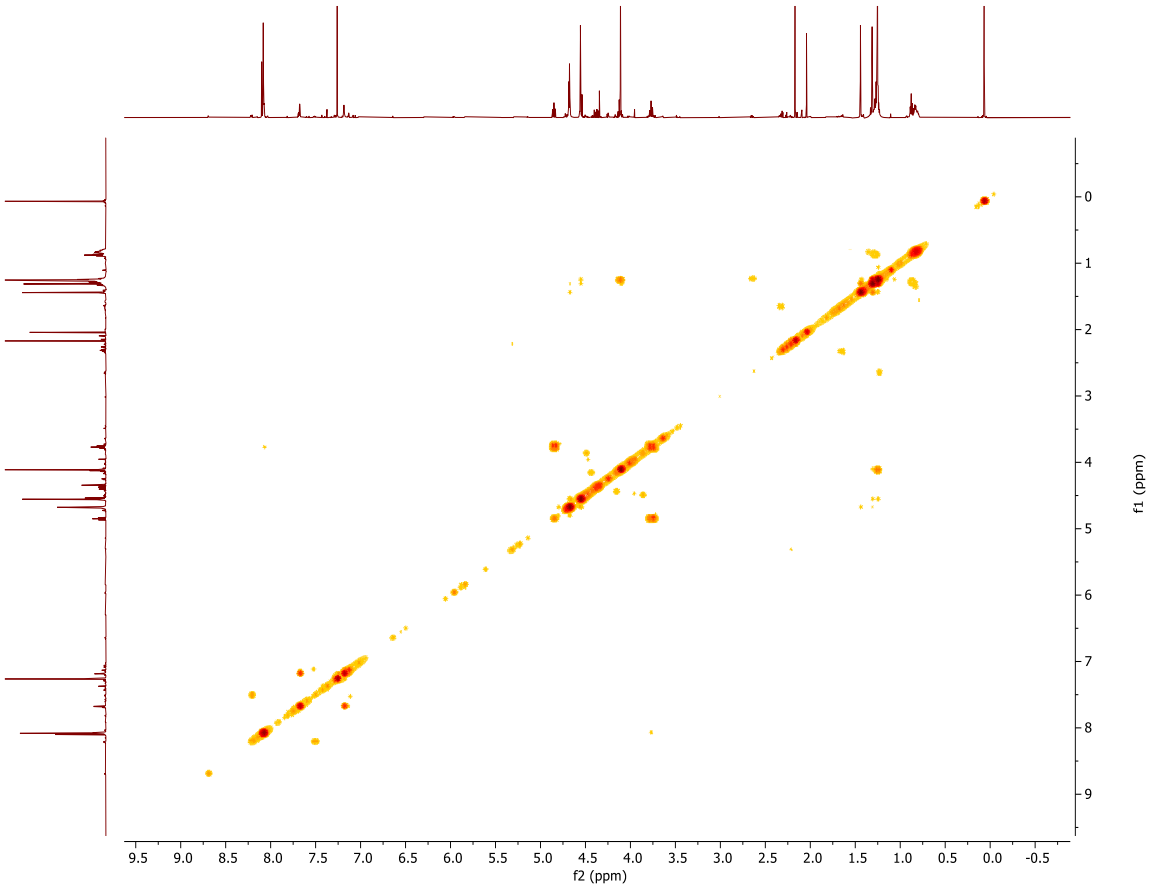

Appendix B6: HMBC spectrum ($CDCl_3$) of compound 30

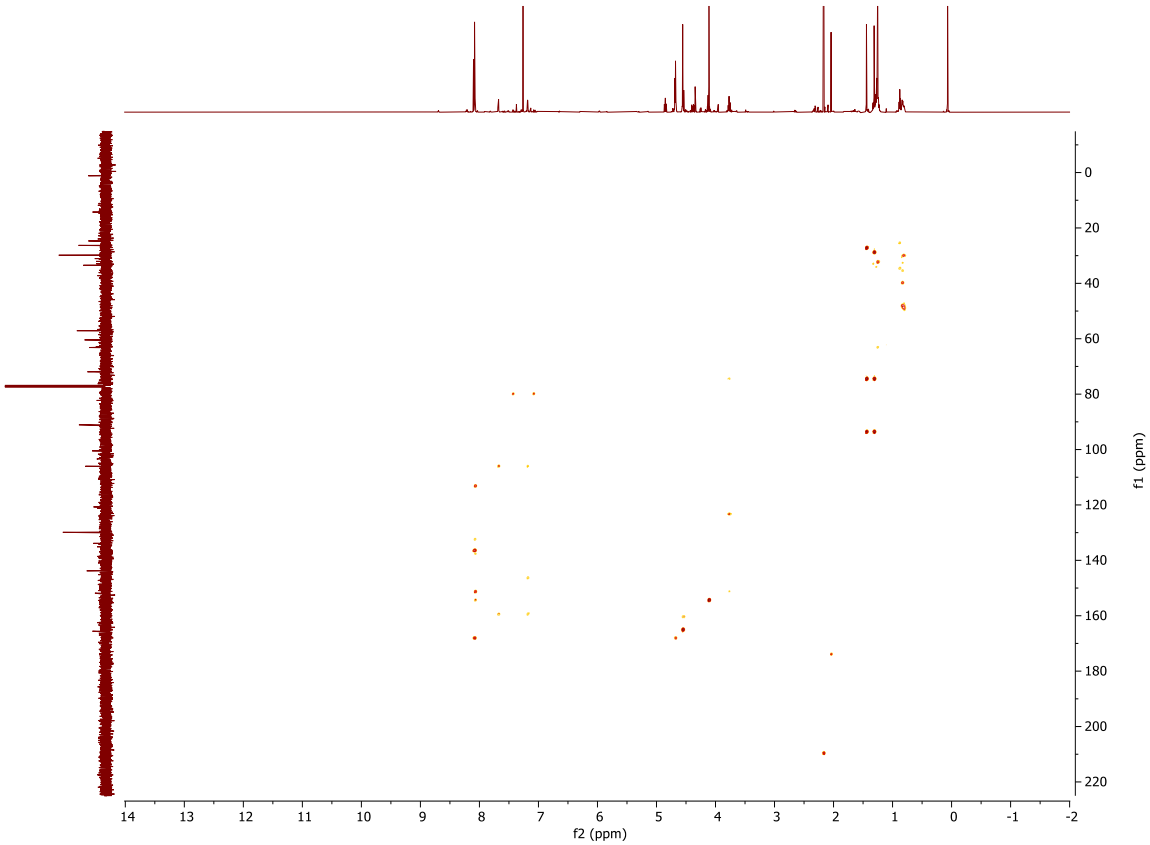

Appendix B7: NOESY spectrum ($CDCl_3$) of compound 30